Title
Microfluidic Frameworks for Immunoanalysis of Multiple Proteins

Permalink
https://escholarship.org/uc/item/7s62b771

Author
Tia, Samuel

Publication Date
2012

Peer reviewed|Thesis/dissertation

Microfluidic Frameworks for Immunoanalysis of Multiple Proteins

by

Samuel Tia

DISSERTATION

Submitted in partial satisfaction of the requirements for the degree of

DOCTOR OF PHILOSOPHY

in

Bioengineering

in the

GRADUATE DIVISION

of the

UNIVERSITY OF CALIFORNIA, SAN FRANCISCO

AND

UNIVERSITY OF CALIFORNIA, BERKELEY

Acknowledgements

In a 2010 piece in *Lab on a Chip*, my advisor contributed an editorial titled "Intimidating yet Inspiring" which outlined some of the current challenges facing bioanalytical technology development. This same title could be applied to my graduate school experience, although at this point looking back, I am so grateful for the many friends and mentors who have supported me along the way. First of all, I thank Professor Amy Herr who welcomed me into her group when there were very few of us around the laboratory. From that point forward, I have been inspired by how Amy works tirelessly as an advocate on behalf of all her students, while holding us to the highest standards as researchers and communicators. I know that I have become a better engineer and teacher because of her influence and her example of dedication, analytical rigor and warm outreach - towards lab members, as well as the broader community.

I would like to thank Professor Dorian Liepmann who has taken me under his wing since my time as a first year student in the UC Berkeley/UCSF Joint Graduate Group in Bioengineering. From serving as a mentor for our Management of Technology/United Nations International Development Organization project in East Africa, to participating in skype quals, and now to this final step, Dorian has always supported me with his advice, his love for teaching and his sense of humor. I would also like to thank Professor Joe Wong, who served on my quals committee and provided feedback on this dissertation. Joe's warmth and willingness to serve as advisor were truly appreciated.

Many other educators helped me along the path to become the engineer I am today: Jenni Buckley inspired me with her love for research and mentorship, while Joe DeRisi

Abstract

Immunoassays are workhorse laboratory tools for detecting protein targets based on highly specific antibody-antigen binding interactions. Greater confidence can be ascribed to an immunoassay when the specific binding interaction is coupled with a separation process based upon some characteristic physicochemical property of the analyte. This dissertation describes the maturation and optimization of microfluidic immunoassay technology to enable the simultaneous detection of multiple targets.

A multi-analytical immunoblotting technique is reported which integrates electrophoretic protein separation with antibody-mediated target capture in a two dimensional microgel. This immunoassay overcomes challenges to traditional multi-analytical protein blotting, which involves repeated cycles of antibody stripping and reprobing, exacerbating the laborious nature of conventional Western Blots. In contrast, an automated and integrated blotting workflow is made possible through a novel multi-stage photolithography process to pattern antigen capture gels at adjacent regions with zero dead volume. The blotting assay completes within 5 minutes, and exhibits a linear dynamic range from 8-800 nM. A label free detection strategy is also introduced to enable simultaneous and quantitative multiplexed measurements without the need for sample prelabeling.

The challenge of separating a post-translationally modified protein target from its unmodified counterpart motivated the development of an immunoprobed isoelectric focusing (IEF) separation within a polyacrylamide gel. Charge separated proteins are immobilized via covalent attachment to polyacrylamide gel, followed by multispectral

antibody-based detection, allowing for correlation of probed post-translational modifications to matching protein targets as well as characteristic pI shifts. Device performance was characterized through analysis of phosphorylated and acetylated proteins forms of heat shock protein 27 and superoxide dismutase 2, respectively. The assay reported protein isoforms in immune purified sample and raw cell lysate in two hours with sample volume requirements of 2 μL.

An analytical model based upon Langmuir immunoaffinity interactions is described to inform the rational design and operation of both immunoassays. The non-dimensional Damkohler number serves as an instructive measure of device performance for each application. 2D immunoblotting requires operation within a mass transport limited regime for effective target capture, whereas the design of the IEF immunoprobe system is specified to be reaction-limited to enable rapid and sensitive fluorescence probe measurements.

Table of Contents

List of Tables

List of Figures

List of Symbols and Abbreviations

Symbol	Definition	Units (if applicable)
E	Electric field strength	Volts/cm
η	Dynamic viscosity of sieving medium	Pa sec
μ	Electrophoretic Mobility	cm^2 / (Volt sec)
σ	Characteristic band width	μm
k_{on}	On binding constants	1 / (M sec)
k_{off}	off binding constant	1 / sec
b_m	Density of antibody binding sites	μM
L	Width of antibody functionalized gel	μm
U	Characteristic migration speed	Distance/time
Da	Damkohler number	Non-dimensional
SR	Separation resolution	Non-dimensional
α-	Anti-(target), denoting antibody specificity	
*	Asterisk indicating a fluorescent conjugate	
AceK	Acetylated Lysine	
AP	Alkaline Phosphatase	
BSA	Bovine Serum Albumin	
CRP	C-Reactive Protein	
GFP	Green Fluorescent Protein	
HSP27	Heat Shock Protein 27	
MS	Mass Spectrometry	
PAGE	Polyacrylamide Gel Electrophoresis	
PG	Protein G	
PhoS	Phosphorylated Serine	
PMT	Photomultiplier Tube	
PSA	Prostate Specific Antigen	
PTM	Post-translational Modification	
ROI	Region of Interest	
SDS	Sodium Dodecyl Sulfate	
SOD2	Superoxide Dismutase 2	
SNR	Signal to Noise Ratio	
TI	Trypsin Inhibitor	

1. Background and Motivation

In this chapter we describe the motivation for developing sensitive and highly specific protein immunoassays. The ability to quantitatively identify multiple protein targets within a system is of critical importance for medical and life science applications. Some important physical mechanisms employed in standard protein analysis are described along with an introduction to microfluidic systems for biological analysis. A brief overview of the dissertation structure is provided.

Proteins are the remarkable biomolecular machines that serve as a foundation for the hierarchical organization of cells and tissues which make up all living organisms. Proteins are composed of amino acid sequences encoded from genes, and are responsible for all functions of life, from musculoskeletal structure, to homeostatic regulatory mechanisms and neurological activity. Recent studies have identified ~21,000 protein-coding sequences in the human genome alone [1], but the diversity of the proteome is even greater when one considers post-translational modifications, cleavage sites or multi-protein complexes which regulate cellular activity [2]. In the framework of modern molecular biology, the ability to measure different proteins within a complex system has become increasingly important. Therefore, it is critical for scientists and clinicians to have access to accurate, efficient and quantitative tools for measuring multiple proteins within a single biological system.

Protein assays are able to identify and quantify specific biomolecular targets based on known physicochemical and/or functional characteristics of the protein of interest.

Physicochemical characteristics may include properties such as protein size and charge, whereas functional characteristics may include enzymatic activities or the ability of a protein to bind against a matched partner molecule. A high degree of measurement specificity can be attained when two physical, chemical or functional characteristics are known and used in tandem to identify a targeted protein.

Immunological systems have naturally developed physical binding mechanisms which serve to recognize specific target molecules. Throughout evolutionary history, immune systems developed feedback regulated abilities to identify and neutralize foreign threats while differentiating between self and non-self molecules. These immunological binding activities are regulated through a combination of steric, electrostatic and hydrophilic-hydrophobic interactions [3]. Assays have been developed to leverage binding components of the immune system (antibodies) and exploit their natural ability to recognize specific target molecules [4]. These immunoassays are not limited to the study of proteins, as antibodies have also been raised against compounds such as TNT and THC, as well as inorganic molecules [5-7]. Antibody mediated binding specificity is often combined with a physicochemical separation process and a reporter mechanism to result in powerful immunoassays used in medical diagnostic and life science applications [8].

1.1 Western Blot

Western blotting is one of the most powerful and ubiquitous techniques for proteomic analysis, yielding electrophoretic resolution of multiple species and providing specific immuno-identification of targets from a complex sample background [9]. The workflow

of a standard Western Blot is outlined in Figure 1.1, where sodium dodecyl sulfate polyacrylamide gel electrophoresis (SDS-PAGE) serves as a first step [10]. In electrophoresis, a small molecule within a conducting buffer medium is mobilized under the influence of an external electric field.

The migration speed of the molecule (u) is given by the equation: $u = E\mu$, where E represents the magnitude of the electric field strength and μ represents the characteristic electrophoretic mobility of the analyte molecule [11, 12]. μ can be represented by $\mu = \frac{z}{6\pi\eta a}$, where z represents the charge of the analyte, η represents the dynamic viscosity of the medium and a is the assumed size of the analyte molecule (modeled as a sphere). The term $6\pi\eta a$ represents the Stokes drag, or the drag force derived for a small spherical particle moving through a continuous and viscous medium at low Reynolds number [13]. Therefore, constant electrophoretic velocity (μ) represents a point where the Coulomb force on the molecule (exerted by the external field) is balanced by the Stokes drag force ($F_{coulomb} = F_{drag}$), so that $\Sigma F = F_{coulomb} - F_{drag} = 0$, and the analyte migrates at a constant velocity.

| Sample Preparation | SDS-PAGE | Membrane Transfer | Antibody Incubation | Blotting Detection |
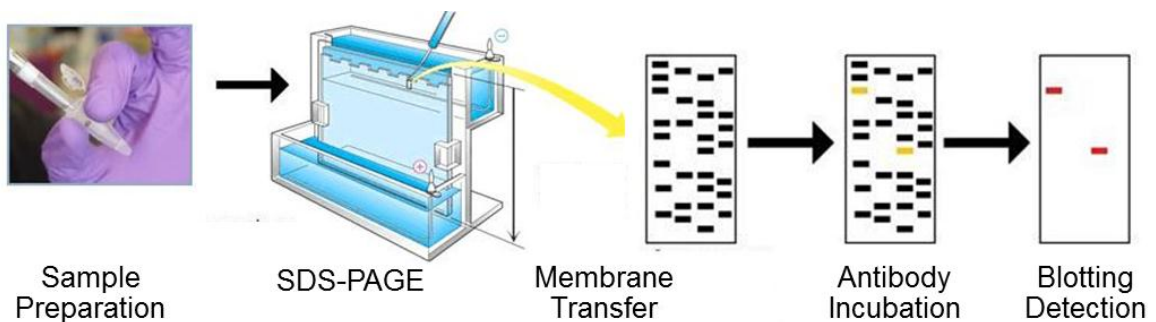
Figure 1.1: Major steps of Western Blotting are outlined. Protein samples are first separated through gel electrophoresis, then transferred to a blotting membrane for subsequent immunodetection of a specific target. Modified from [14].

In Figure 1.1, the polyacrylamide gel of the SDS-PAGE step serves as a porous sieving network which alters the electrophoretic mobility of protein analytes. Larger protein molecules experience greater retardation within a polyacrylamide gel matrix and these characteristic differences in electrophoretic mobility are observed as various proteins separate out of a complex mixture into distinct zones or "bands" under the influence of an electric field [15]. By unraveling native proteins into an elongated chain conformation and designating all analytes with a uniform charge-to-mass ratio, SDS-PAGE works to differentiate protein analytes on the basis of size [16]. The gel retardation experienced by protein analytes can be tuned for specific sizing applications by adjusting the density of the polyacrylamide matrices [17].

Following SDS-PAGE, separated protein bands are electrophoretically transferred onto a membrane which serves as a solid support for subsequent immunoblotting steps. Primary detection antibodies (specific for designated targets of interest) are applied to the membrane paper, and multiple incubation and wash steps with repeated manual interventions are necessary [18]. A secondary detection antibody is also usually required, with similar demands of time and manual intervention, before a detectable signal can be finally developed and observed upon the blotting membrane.

The versatility of the Western Blot technique has made it one of the most popular tools in molecular biology, with diverse biomedical applications including clinical diagnostics and biomarker validation studies. However, the preparation of a Western Blot, from SDS-PAGE separation through immunoblotting and detection can be laborious and time consuming (on the order of ~20 hours), leading to bottlenecks in cost and analytical throughput [18]. The technique also suffers from problems of

reproducibility (due to the inconsistency of membrane transfer) and is only semi-quantitative [19].

1.2 Isoelectric Focusing

Polyacrylamide gel electrophoresis is often performed in conjunction with an initial isoelectric focusing step [20, 21]. This integrated technique, known as two dimensional polyacrylamide gel electrophoresis (2D-PAGE), separates proteins based upon two physicochemical properties: charge (1st dimension) and molecular weight (2nd dimension) [22]. Isoelectric focusing works to separate protein analytes based upon isoelectric point: a characteristic charge which consists of charge contributions from each protein's constituent amino acids.
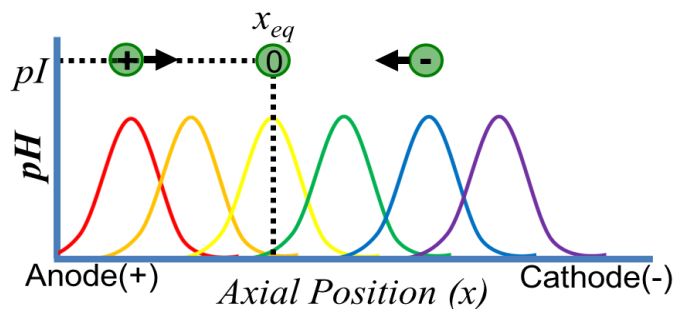
Figure 1.2: Isoelectric focusing establishes a stable pH gradient through a mixture of ampholyte buffers.

The isoelectric focusing (IEF) process employs a mixture of poly-buffers known as ampholytes. Upon the application of an external electric field, these ampholyte species focus into distinct zones, forming a spatial pH gradient at equilibrium [23]. When a protein analyte is located in a pH zone below its own isoelectric point (pI), the protein

assumes a positive charge and migrates towards the cathode. Similarly, an analyte molecule located at some pH above its own pI will assume a negative charge and migrate towards the anodic terminal. Eventually, in a stable pH gradient, all protein analytes will reach some spatial equilibrium where no net charge exists upon the molecule. This equilibrium position corresponds to the protein's pI, and spatial distribution of focused analytes then can be correlated against reference markers to identify proteins based upon characteristic charge. Unfortunately, the isoelectric focusing process can also be laborious and time consuming; preparatory IEF for 2D-PAGE is often performed overnight and requires the application of high electric fields (up to 10,000V, [23]).

1.3 Challenges to Multianalyte Immunodetection

Cellular signaling cascades are composed of complex networks of protein interactions. With over 4000 classified mammalian signaling proteins [24], information regarding the relationships and relative expression levels between different proteins is critical for the study of physiological processes. However, the problems of traditional Western Blotting become multiplied when a Western Blot must yield several antigen targets [18]. A common protocol for multianalyte detection is to apply "stripping" processes which employ heat, chaotropic agents and extreme pH conditions to remove previously-bound antibodies from the transfer membrane [25]. This stripping process allows a second or third set of incubation steps to be applied towards the same membrane - an approach known as "re-blotting".

The harsh stripping protocols can remove significant amounts of all proteins from the blotting membranes and damage membranes, rendering subsequent quantitative

comparisons of protein expression impossible. Stripping and incubation cycles may only be repeated a few times before further probing becomes impossible due to protein loss and membrane degradation [26]. Thus, reblotted membranes can only be used to confirm the presence of a protein and are not a reliable source for determining a protein's absence. Multianalyte reprobing results in a considerable increase of assay time, as each step has to be repeated - from washing and blocking to blotting, incubation and target detection. Nevertheless, re-blotting is often the only method that can be applied for analyzing multiple targets from the same sample.

Other antibody-based techniques which have been employed for simultaneous multi-protein measurement include protein microarrays [27], dot blot assays [28], and color encoded fluorescent microbeads [29]. However, these immunoassays (like ELISA) provide less information and less confidence in measurement due to cross-reactivity concerns because antibody binding serves the reporter of protein identity. Having additional layers of characteristic information to be correlated with protein identity is important, as it has been estimated that as many as 80% of commercially available antibodies display some cross-reactivity or may be impotent against their intended target [30].

Alternatively, aliquots sourced from an identical or similar biological sample can be used to perform multiple assays for individual protein targets, either sequentially or in parallel. The long timescales and laborious manual interventions associated with these multiple assays can inhibit experimental throughput [31]. Multiple separate assays are also accompanied by problems of measurement reproducibility, which represent a barrier to the understanding of sophisticated protein signaling networks. Therefore, the

7

development of efficient and quantitative tools for the simultaneous measurement of multiple targets from a single sample is critical for proteomic science in the 21st century [32, 33].

1.4 Microfluidic Tools for Protein Analysis

Micro-electromechanical systems (MEMS) have recently emerged at the intersection of mechanical and electrical engineering applications. The development of MEMS devices for efficient and precise sensing and actuation has been made possible through advancements in microfabrication [34, 35]. As part of this trend, many MEMS devices have also been applied towards biological analysis (BioMEMS) in areas such as genomics, proteomics and analytical chemistry [36-38]. Microscale integration presents the opportunity to perform multiplexed biological measurements while benefitting from ultra-low sample volume requirements and efficient assay capabilities [39]. For example, microfluidic PAGE at high electric field strength has been demonstrated to separate proteins and DNA on a timescale of seconds, and some commercial miniaturized systems for protein measurement are already available [12, 15, 40, 41].

Some forms of immunoassay have also been demonstrated on microfluidic chips [36, 42-45]. Because physical binding forces are intrinsically important in molecular analysis, microscale technologies are useful due to their ability to probe a different range of physical forces which may not be accessible using conventional laboratory techniques [46, 47]. Similarly, the development of new forms of microfluidic immunoassay requires further understanding and exploration of how antigen-antibody binding interactions will function in the physical context of an integrated microdevice.

1.5 Organizational Overview

This dissertation describes how two microfluidic immunoassays were adapted and optimized to meet the multi-analyte detection needs of modern proteomic science. These assays take advantage of known immunoaffinity interactions to enable novel measurements of multiple targets in a rapid microscale format. A non-dimensionalized model of device physics is presented along with a numerical simulation which informs system design.

**Antigen-Antibody Interactions
in Electrophoresis**

↓

Damkohler Analysis

Design and Fabrication
of a Multianalytical
Native Protein Blotting Chip

↓

Demonstration of
Multianalyte Blotting

Optimized
Immunoprobe
Loading

↓

Probed IEF for
PTM Analysis

Multi-target Detection
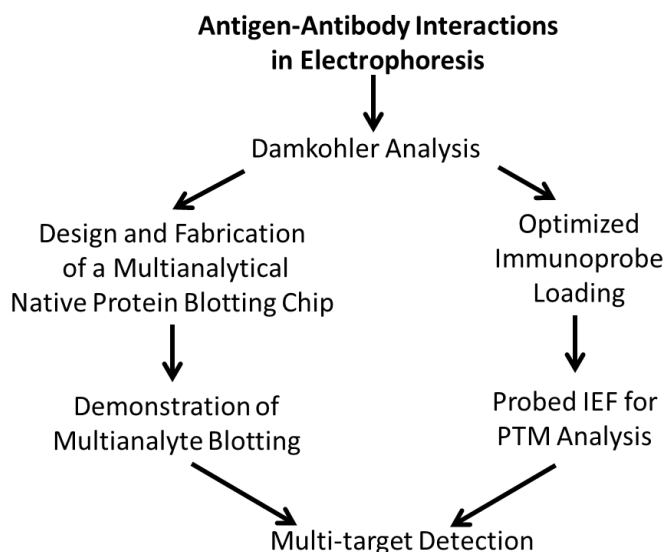
Figure 1.3: Antigen-antibody interactions within a microscale electrophoretic system allow optimized immunoassays to be applied towards multi-analyte blotting and probed analysis of post-translationally modified protein targets.

Dynamics of antibody probe introduction and signal development are explored, with an application of non-dimensional Damkohler analysis. Finally, some immunoassay detection strategies are proposed with the goal of driving measurement limits of detection down into the picomolar range. A unifying theme of this work is the maturation of microfluidic immunoassay technology towards multi-target proteomic analysis.

2. Antigen-Antibody Interactions in Electrophoresis

Antigen-antibody binding interactions serve as the characteristic foundation for all forms of immunoassay. In this chapter, we describe a platform for on-chip immunoblotting and present a model to describe the competing effects of electrophoretic and molecular binding forces. Results from numerical simulation are compared against experimental observation. In design and evaluation of an electrophoretically driven microfluidic immunoassay, it is critical to understand how electrokinetic mass transport can influence antigen-antibody interactions. A non-dimensional approach to binding analysis is discussed, which also forms a basis for understanding the dynamics of on-chip immunodetection. Finally, a comparison of the two immunoassay formats described in this work is provided.

BioMEMS devices for protein separation usually employ a networked channel layout [36, 38, 41]. However, microfluidic chips with planar separation formats have also been developed, opening up new possibilities for multidimensional protein analysis [48-50]. A planar separation format (such as that of field flow fractionation) provides a continuous space for high throughput sample processing and dynamic versatility in directing analyte migration towards subsequent analysis [51]. A continuous separation zone is preferable to a discretized separation zone, because the discretization of separation space results in a loss of measurement resolution [52].

A two-dimensional immunoassay was developed [53] wherein the vertical dimension of a microfluidic chamber (approximately 1 mm × 1mm × 20 μm) contains a

polyacrylamide matrix and the second (horizontal) span of the device contains an antibody functionalized capture gel (*Ab1*) as illustrated in Figure 2.1. Protein migration (indicated by the green band, *Ag1*) is electrophoretically directed through the application of an external electric field (*E*), just as electromigration occurs within traditional slab gel PAGE. The vertical polyacrylamide gel within the microdevice is used as a sieving matrix to separate proteins based upon charge-to-mass ratio, while the horizontal span of the device contains a gel to immobilize target proteins as they are subsequently directed through this lateral blotting region to form the immune complex: *Ag1-Ab1*.
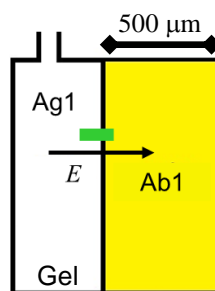
Figure 2.1: A target band (Ag1) is electrophoretically transferred to an antibody functionalized blotting gel region (Ab1), as specified for target capture. Ag1 and Ab1 represent matched binding partners which form the immune complex Ag1-Ab1. Lateral band transfer of the protein target into the blotting gel is directed by applying an external electric field (E), as indicated by the arrow.

The role of the blotting gel is analogous to that of the transfer membrane in standard Western Blots – it captures the separated antigen protein and serves as a solid support for subsequent target detection [54]. However, one key difference here is that a traditional blotting membrane (usually nitrocellulose paper or PVDF) is pan-specific for protein immobilization. All transferred proteins are assumed to bind with blotting paper, based on a combination of hydrophobic and electrostatic interactions. In contrast,

immobilization of a target protein within the microfluidic blotting gel depends on a specific binding interaction between the antigen target and a matched antibody. If the capture antibody within the gel exhibits no cross-reactivity with other proteins in the sample, only the matching target will be retained upon the blotting matrix. Thus, understanding the interaction of target proteins as they migrate through the antibody functionalized region is critical to ensure effective analyte capture and to inform system design.

Examining the behavior of a protein electromigrating through a matched antibody gel is not a unique to the study of 2D microfluidic blotting. In macro-format "rocket" and "crossed" immunoelectrophoresis, proteins from a complex mixture such as blood serum are electrophoresed through an agarose gel containing antibodies raised against specific analytes in the sample [55-57]. The resulting gel precipitate is subjected to Coomassie stain and the size and shape of these immunoprecipitates are analyzed for quantitative identification of matching protein targets. In 2D microfluidic blotting, the intensity and spatial distribution of the immobilized target also provides information regarding protein concentration and immunoaffinity. However, microfluidic blotting analyses can be performed in an automated format to detect protein samples in the picogram range [58]. For characterization of migration behavior, a protein target is fluorescently labeled (usually with AlexaFluor dye, Life Technologies Inc.) and its movement is tracked through fluorescence microscopy. Thus, a fluorescent protein can serve as a model target for studying the dynamic and competing effects of electrophoretic mass transport and antibody binding within a microfluidic blotting system.

Imaging of our microfluidic blotting systems were performed with a charge coupled device (CCD) camera (CoolSNAP HQ2, Roper Scientific) and a 10× objective (UPlanFL, N.A. = 0.3, Olympus) using an inverted epifluorescence microscope (IX-70, Olympus) equipped with a mechanical shutter to reduce photobleaching effects (Sutter Instruments). The standard camera exposure time was 300 ms and 2×2 pixel binning was employed, resulting in a full field image representing a 1 mm × 1.34 mm field of view. Emission from the mercury arc lamp was filtered through XF100-3 or XF111-2 filter sets (Omega Optical) for illumination of AlexaFluor 488 and 568 labeled proteins, respectively.
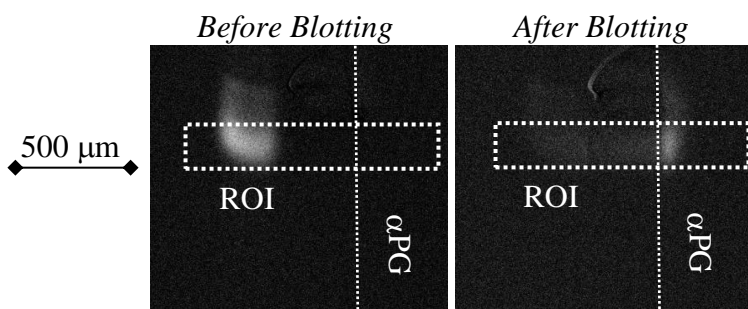
Figure 2.2: A sample ROI is used to measure spatial distribution of the fluorescent protein band as it migrates from the separation zone (L) and eventually becomes immobilized in a corresponding blotting gel (R).

Image analyses were performed with ImageJ software (National Institutes of Health) and regions of interest (ROI) were selected to correspond with the separations and blotting regions. These ROI were consistently applied, and line sections across the ROI were averaged for the calculation of spatial distribution and fluorescence signal. One example of an experimental ROI is shown in Figure 2.2, both before and after the immobilization of a target band, where the ROI corresponds with the blotting gel interface. Full field imaging allows for comparison of experimental blotting results

13

against a theoretical model to understand dynamics of electrophoretic migration through an immunoaffinity gel.

2.1 Model: On-chip Immunoaffinity Interactions

A one-dimensional model of a blotting system can aid in forming a mathematical description of binding kinetics, coupled to mass transport for an antigen moving through a matched antibody gel. If we imagine an infinitesimal, homogeneous slice of the blotting region (in Figure 2.3 as *dX*), we can assume that binding kinetics within that control volume are described by the following Langmuir first order linear differential equation [59]:

$$\frac{dC_{bound}}{dt} = k_{on}C(b_m - C_{bound}) - k_{off}C_{bound}$$

Here, C_{bound} represents the concentration of protein molecules captured at the control volume. The concentration of the free antigen *C* at any given time point is given by *C(t)*, and this protein band is assumed to follow a Gaussian distribution as it migrates through the control volume. A discussion of system design and modeling must begin by identifying the critical variables which affect device performance (Tables 2.1 and 2.2).
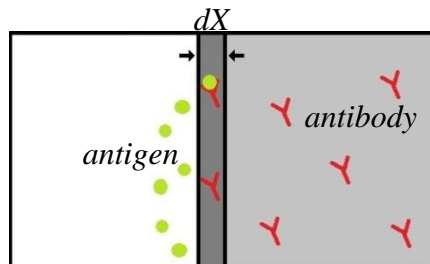
Figure 2.3: A numerical simulation of antigen-antibody binding kinetics is modeled upon the targeted binding activity of an infinitesimal gel element.

14

Variable	Description
b_m	Density of antibody binding sites
L	Width of antibody functionalized gel
E	Electric field Strength

Table 2.1: Several parameters which influence antigen-antibody binding efficiency can be specified by the design of the microfluidic system.

Sample properties	Description
k_{on}, k_{off}	On, off binding constants
C	Concentration of target molecules
σ	Spatial distribution of Gaussian target band
μ_o	Electrophoretic mobility of antigen

Table 2.2: Other parameters which dictate system performance are intrinsic properties of the analyte.

Some of these variables are parameters that can be specified through assay design (b_m, C, E, L), while some are intrinsic physical constants of the chosen system (μ_o, k_{on}, k_{off}), and yet other variables such as σ and μ_o are influenced (but not completely determined) by design parameters such as gel density. Integrating across the time span of band migration and the total length of the binding region describes the entirety of the protein captured by the blotting gel:

$$total_{bound} = \int\limits_{0}^{L} \int\limits_{0}^{t_{res}} \frac{dC_{bound}}{dt} dt dx$$

The relevant time interval (residence time = t_{res}) corresponds to the full width of the protein band divided by the average protein migration speed. If the length (L) and the

lateral field strength (E) are properly specified, *total*$_{bound}$ will approximate the total number of target molecules within the injected band and capture efficiency (efficiency = *total*$_{bound}$ / *total # of target molecules*) approaches 100%.

The concentration of target molecules bound to the blotting membrane cannot exceed the original density of antigen binding sites. The concentration of free target molecules will decrease as the band moves along the length of the blotting region, as binding sites closest to the interface (at $x = 0$) are filled in first. Our model assumes that the Péclet number (describing relative contributions of advective versus diffusive transport) for the system is high [60]. Therefore, band diffusion does not play an important role when compared against the rate of target molecule migration.

Each of the parameters which govern system performance will fall between some physical and practical limitations, described in Table 2.3:

Variable	Limits
b_m	Dictated by the maximum antibody concentration within the gel
L	Maximum width of the microdevice and limits of fabrication resolution
E	Assay speed (on the low end) Gel breakdown (on the high end)
k_{on}, k_{off}	Natural limits of antigen/antibody interactions
μ_o	Determined by gel density and protein charge-to-mass ratio
C	Physiologically and experimentally relevant target concentrations

Table 2.3: Physical and practical limitations of governing parameters for Langmuir binding kinetics within an antibody functionalized blotting gel.

For our purposes, these limits are estimated as:

Sample properties	Estimated Range
k_{on}	$10^4 - 10^8$ $M^{-1}S^{-1}$
C	$10 - 500$ nM
σ	$10 - 100$ mm
μ_o	$1-7 \times 10^{-5}$ cm^2/V s

Table 2.4: Estimated working ranges for the governing parameters of a computational model simulating Langmuir antigen-antibody binding kinetics.

Performance and analysis of a Langmuir binding system will be heavily dependent upon the values from Table 2.4. Values for k_{on} are especially important, but the reported range for these affinity values also spans the widest degree of variation [61]. Forward binding reaction rates would be dependent upon the specified antigen/antibody pair, and k_{on} may vary across several orders of magnitude. Here, we have little control over the affinity for a desired target other than trying to select and apply a capture antibody having the strongest possible binding affinity. Reaction rates can be difficult to predict as these are dependent upon the local gel and buffer conditions - values reported in literature are usually determined from studies performed in free solution [62, 63].

2.2 Computational Model

To simulate the dynamics of antigen-antibody binding interactions within our system, the full length of the blotting region was modeled as a series of finite gel elements. Values from Table 2.5 were input to the model and the subsequent protein band

migration speed was used to set the length of a residence time step (Δt) wherein each target band element was co-localized or "incubated" against a matching gel element.

Variable	Value	Units
b_m	1×10^{-6}	M
L	200	μm
E	50	V/cm
C	5×10^{-5}	M
σ	50	μm
k_{on}	5×10^{5}	1/(M s)
k_{off}	1×10^{-3}	1/s

Table 2.5: Assumed parameters for antigen-antibody binding kinetics simulation

Protein concentration values for the target band and for the blotting gel elements were recorded as arrays. Initial conditions were set so that all binding sites were unoccupied and the concentration of the target band assumed a Gaussian distribution. A Langmuir binding function was used to update all array elements as they proceeded through a series of simulated incubation periods. The numerical simulation was performed in a step-wise fashion until all targeted protein molecules had either immobilized to the blotting region or moved out of the blotting gel limits.
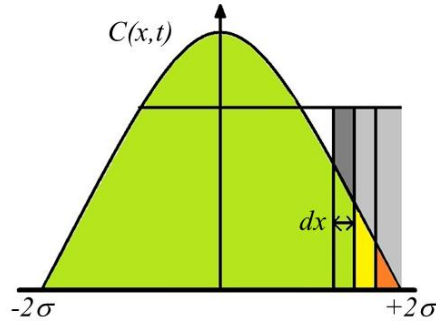
Figure 2.4: The target protein band is modeled as a 1D series of finite elements of width dX, where dX is matched to the width of corresponding blotting gel elements. The concentration of the protein band is modeled as a Gaussian distribution with full band width 4σ.

Complete and annotated MATLAB (MathWorks) source code for simulating in-gel electrophoretic antigen-antibody binding kinetics has been reproduced in Appendix D. This model can be used to predict how changes to a single variable would affect binding performance, and is useful in providing guidelines for device design such as specifying the applied lateral field strength and requisite blotting gel width.

2.3 Damkohler Analysis for Understanding System Dynamics

More generally speaking, the Damkohler number (Da) is a dimensionless value used in chemical engineering to relate a reaction timescale with other relevant processes which may simultaneously occur within a fluid flow [64]. In a simplified model, the antigen binding process can be considered a finite incubation step in which the residence time is described by the electromigration time scale ($t_{res} = L_o/U_o$). The characteristic reaction time is described by the binding constants ($t_{rxn} = (Ck_{on})^{-1}$), where k_{on} is a rate constant specific to the gel. Thus:

19

$$Da = \frac{t_{res}}{t_{rxn}} = \frac{L_o k_{on} C}{U_o}$$

In the case of electrophoresis, $U_o = \mu E$. A large Damkohler number translates into high binding efficiency, while a low Da number would be associated with shorter transport time for the assay [59, 65].

A simple "rule of thumb" for the design of capture gels is based upon the Damkohler number wherein the aim is to operate within a mass-transport limited regime ($Da > 10$). In our case, a high Da means that the required binding time is shorter than transport time through the blotting gel – leading to high capture efficiency. When reasonable estimates of k_{on}, μ_o, E and b_m are available, the requisite blotting gel width L can be selected to ensure high target capture. Values for E and b_m (and to some degree μ_o) can be specified through system design, while other values need to be calculated or assumed on a case-by-case basis depending upon the antigen target.

2.4 Requisite Blotting Length: Antigen Concentration

An experiment was performed wherein a blotting gel functionalized with anti-protein G at 1.6 μM was blotted with fluorescently labeled protein G at concentrations ranging from 50 to 1250 nM. In this system, the strength of the lateral transfer field is $E = 50$ V/cm, resulting in an estimated Damkohler number of 9.3. Fluorescence micrographs and distribution plots from this dilution series are illustrated in Figure 2.5.
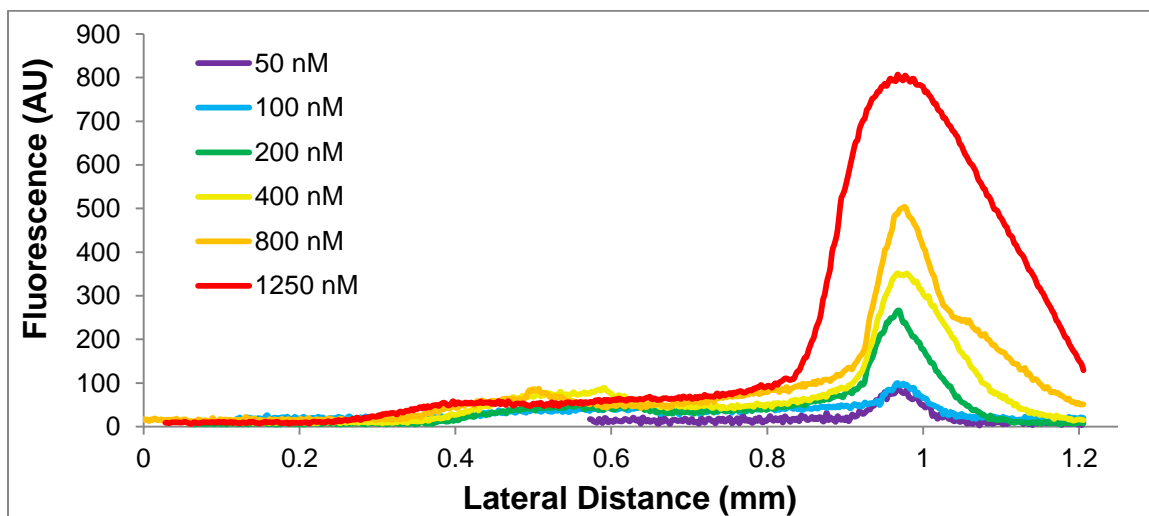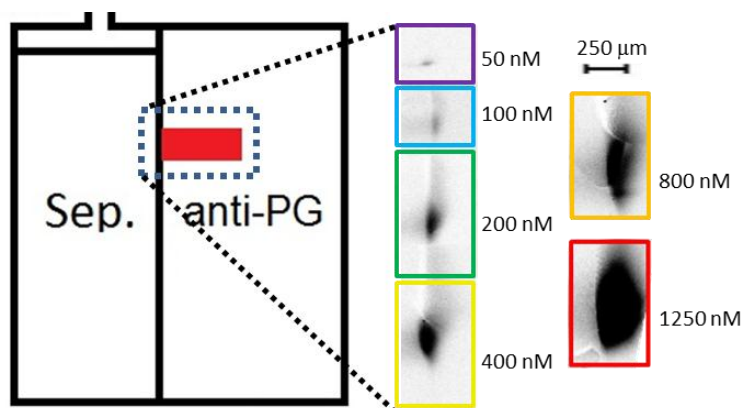
Figure 2.5: Fluorescent micrographs (top) and lateral fluorescence distribution plots (bottom) illustrating blotted green fluorescent protein bands of varying concentration (50-1250 nM).

Figure 2.5 demonstrates that for most assayed concentrations, 200 μm of blotting gel was sufficient for capture of the targeted band. Even at high concentrations (800-1250 nM), the majority of the immobilized target band was captured within the first 200 μm of blotting length. Bands of lower protein concentration are more likely to be captured within the first 100 μm of the blotting gel. The peak fluorescence intensity increased as a function of concentration, along with total band width (Figure 2.6).
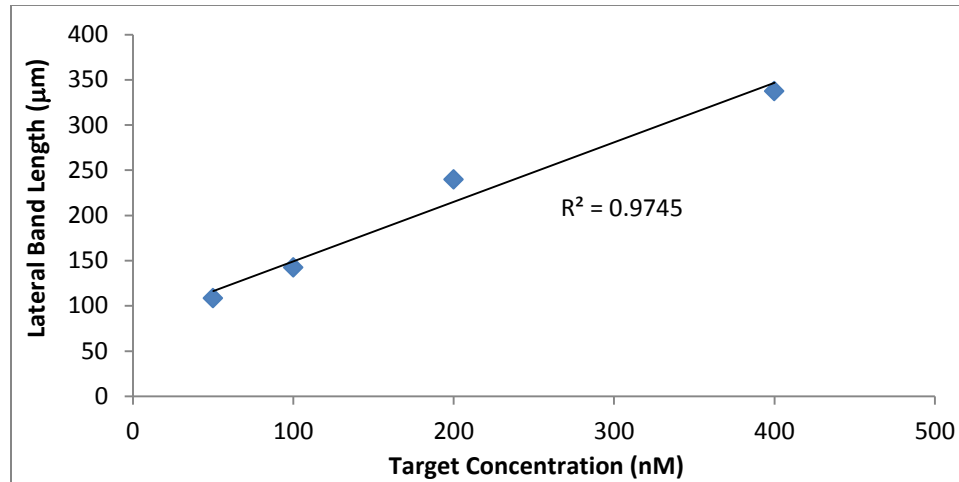
Figure 2.6:   Requisite lateral transfer lengths for full antigen capture increase with higher target concentrations, based upon experimental data.

In Figure 2.5, a set of representative post-blotting fluorescence distribution plots was superimposed across a range of sample concentrations. The spatial distribution of bound target fluorescence was asymmetric, as immobilized bands display a local maximum at the blotting gel interface, followed by a more gradual decrease in fluorescence intensity moving away from this interface. This shape resembles the spatial distribution of the immobilized band predicted by the computational model (Figure 2.7). Thus, the model can also be used to curve-fit experimental data and to estimate k_{on} or other parameters for an antigen/antibody pair based upon the immobilized target distribution across an antibody functionalized gel [66].
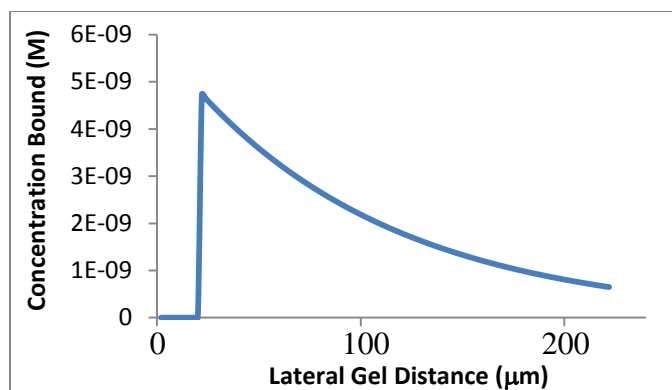
Figure 2.7: From computational model – the occupied binding site density falls off sharply away from the maximum antigen concentration at the blotting gel interface.

2.5 Requisite Blotting Length: Applied Field Strength

Another set of experiments was performed wherein an anti-protein G antibody functionalized region was repeatedly blotted with fluorescently labeled protein G (100 nM). In this case, the magnitude of the electric field strength for the lateral transfer process was varied from 33 to 200 V/cm. The spatial distribution of the target antigen as it was immobilized against the antibody functionalized region is plotted in Figure 2.8, where the red dashed line indicates the approximate location of the blotting gel boundary. Each fluorescence distribution plot was normalized to the intensity of the corresponding transfer band. When the lateral transfer field was increased, the spatial distribution of the immobilized target bands appeared to be more disperse (Figure 2.8).
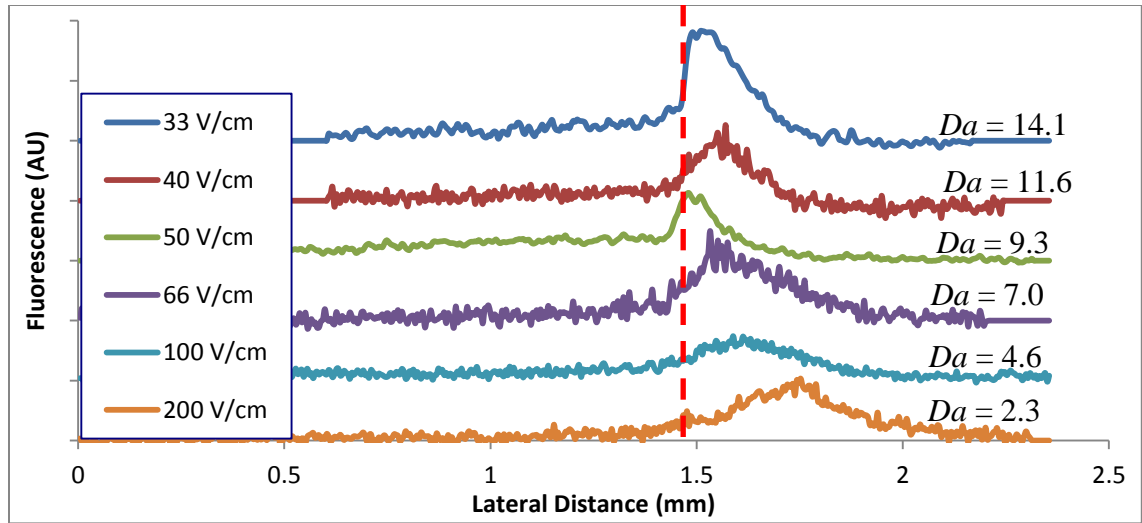
Figure 2.8: Spatial distribution of immobilized protein G target bands (100 nM) across an anti-protein G blotting gel at multiple transfer field strengths

Numerical simulation suggests that for a given set of experimental conditions, the assay capture efficiency will increase with blotting gel width (Figure 2.9). This improvement in capture efficiency is due to the fact that spatial distribution of the bound antigen follows an exponential decay pattern, with the highest concentration of bound molecules located at the gel interface.
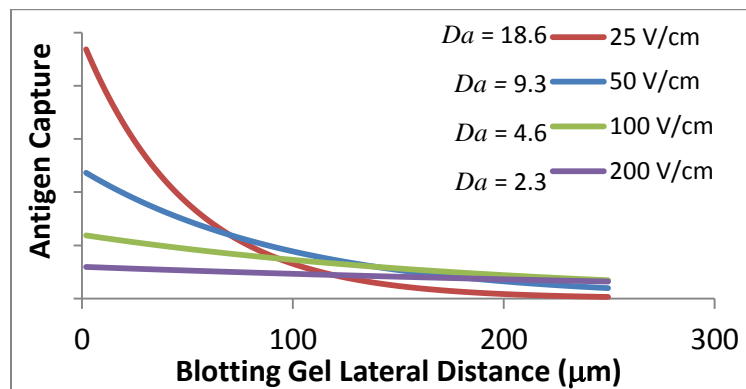
Figure 2.9: From simulation – the spatial distribution of target molecules immobilized across a 250 μm blotting region is plotted for a range of transfer field strengths.

24
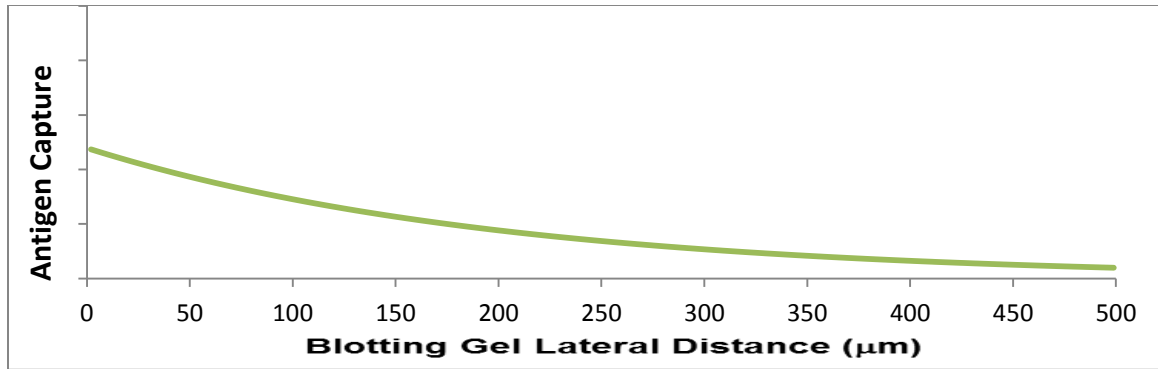
Figure 2.10: From simulation – immobilized antigen spatial distribution demonstrates full tailing across a 500 μm capture length at 100 V/cm (Da = 4.6).

At higher transfer speeds, captured antigen molecules form a longer and more disperse "tail" which requires longer blotting regions if full antigen capture is desired. When the binding gel is not long enough, the tail end of the target distribution becomes cut off. Thus, the length of the blotting gel is important because capture efficiency is not only dependent on binding site availability, but also upon the spatial distribution of immobilized target molecules. The elongated spatial distribution of the protein band at high field strengths (Figure 2.10 and Figure 2.11) was consistent with experimental observation.

This tailing distribution can also be described in terms of the Damkohler number, which is inversely proportional to the applied electric field strength ($Da = L_o k_{on} C / \mu E$). A higher transfer field will result in a lower Damkohler number, indicating a bias towards a reaction limited operating regime. Thus, the elongated distribution of the immobilized antigen points to the need for a wider blotting gel (width = L_o) when a high transfer field strength is employed.

25
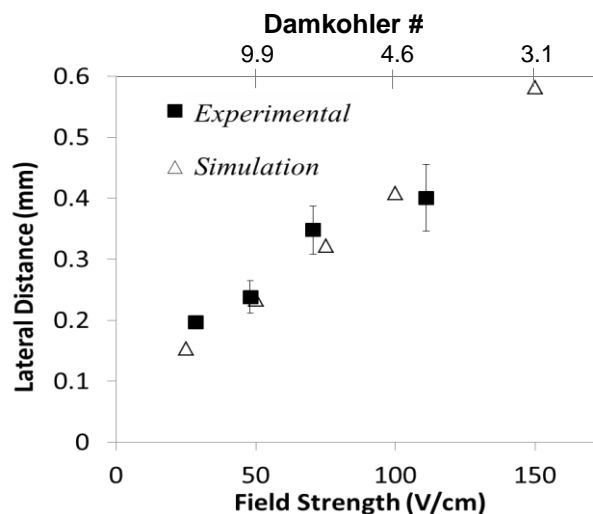
Figure 2.11: Antigen distribution plots for varying electric field conditions demonstrate that requisite blotting distances increase with the magnitude of the lateral field. Results from simulation are compared against experimental results (n=3).

The efficiency of antigen binding can be expressed in terms of the Damkohler number. In Figure 2.12, the *x*-axis is plotted based upon the non-dimensional *Da* rather than any individual component variable. Results from an experiment where *L* was limited to 100 μm and the gel binding site density was 1.6 μM were superimposed upon results from simulation, demonstrating close correlation.
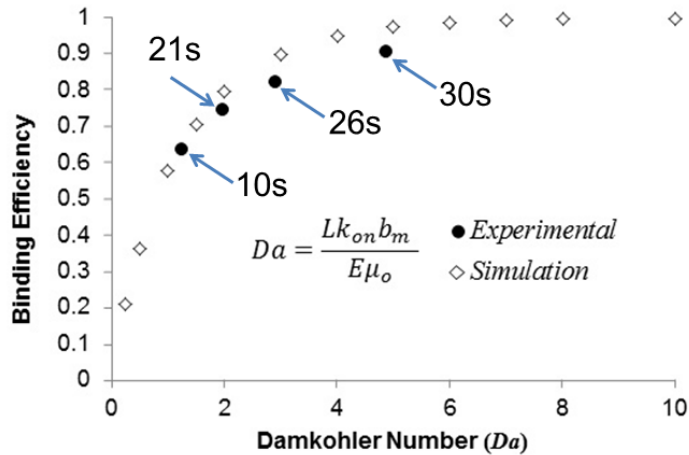
Figure 2.12: Antigenic capture efficiency increases as a function of Da. Results from simulation are compared against experimental results, with corresponding blotting times as indicated.

Experimentally, an increase in *Da* from 1 to 5 resulted in an increase of blotting transfer time from 10 seconds to 30 seconds (Figure 2.12). This increased transfer time resulted in a much higher binding efficiency within the first 100 μm of blotting gel. The Damkohler number here is situated within an intermediate range (1 < *Da* < 10) which balances efficient blotting performance with reasonable transfer times. When results are compiled within a single data set, these points collapse into a single performance curve describing the interrelationship between five distinct design variables. Thus, the Langmuir-based computational model serves as a useful tool designing an electrophoretic blotting system with antibody-mediated target capture.

2.6 Multi-target On-chip Immunoassays: Format Constraints and Goals

In the first half of this dissertation, I develop a novel multi-stage photolithography process for patterning a series of blotting zones within a microfluidic device for efficient, multi-analytical target capture. These blotting zones are located within a planar two-

27

dimensional chamber and consist of regions of polyacrylamide gel decorated with matching capture antibodies. Multiple native proteins can be separated and immunoblotted simultaneously within this microdevice, which overcomes many obstacles to multi-protein detection in the traditional slab gel blotting format.

The challenge of an acetylated superoxide dismutase 2 assay leads to the second half of this dissertation, which integrates immunoprobe analysis with on-chip isoelectric focusing to detect the charge shift behavior that is characteristic of protein post-translational modification (PTM). A pan-specific immobilization strategy is used to capture a percentage of all proteins within the sample following isoelectric focusing in a single channel. Here, multi-spectral antibody probes were used in tandem to identify target proteins bearing specifically modified residues. Co-localization of antibody probes specific for target proteins and PTMs provided a quantitative basis for measuring the relative abundance of modified target proteins.

Isoforms or post-translationally modified protein forms often share the same molecular weight as their non-modified counterparts - although isoforms can exhibit significant differences in charge [65, 67]. Those charge differences would be masked under SDS-PAGE examination, which separates proteins solely on the basis of size [68]. Native PAGE differentiates proteins based upon a characteristic charge-to-mass ratio. Still, native PAGE separations would probably be less sensitive to charge differences compared against isoelectric focusing, which resolves analytes purely upon the basis of isoelectric point.

No single assay format is ideal for every type of protein measurement. Functionalized blotting gels provide an effective mechanism for immunoassay when the

target is known and when a strong binding partner has already been established. Antibodies naturally exhibit wide variations in binding affinity [3], and so the identification of an appropriate capture antibody can be challenging. In some cases, the target protein may be unknown and a panel of antibodies must be screened against the entirety of the sample. Cross-reactivity concerns can be avoided by screening antibodies prior to on-chip use, but some experiments will intentionally search for targets which exhibit multiple epitopes of interest (*e.g.* co-IP, pull-downs, and analysis of post-translational modification).

In contrast to using an antibody functionalized gel, in probed IEF, pan-specific protein capture techniques immobilize a portion of all proteins in the sample for subsequent screening purposes. In the case of acetylation analysis, antibodies to acetylated lysine are known to display weaker binding affinities when compared against other primary detection antibodies [69]. Therefore, having the flexibility to screen multiple antibodies or to attempt extended antibody incubation periods can be desirable.

Both the 2D blotting assay and the probed IEF strategy employ antigen-antibody interactions in a microdevice format under the influence of an electric field. However, the protein separation which occurs in these two cases is based upon different physical mechanisms. In 2D multi-protein blotting, analyte proteins are separated based upon charge-to-mass ratio. Because the immobilized target signals are spatially resolved upon discrete capture zones, the ability to performed multiplexed protein measurement is conferred by the geometry of the device. More protein targets can be accommodated by using a wider chip layout and therefore we describe the 2D blotting device as being spatially multiplexed (Figure 2.13). In the case of probed isoelectric focusing, proteins

are first separated on the basis of charge and multiple targets are identified using a spectrally multiplexed detection strategy. When multiple proteins are immobilized within the same region, co-localized targets can be detected through the application of color encoded fluorescence probes, an approach which is further described in Chapter 7.

Spatial Multiplex   Spectral Multiplex
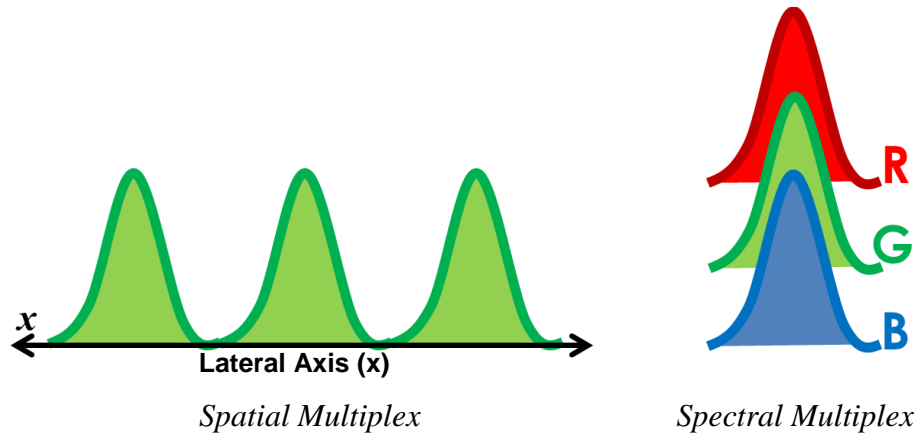
Figure 2.13: Fluorescence signals arising from multiple protein targets may be spatially multiplexed (as in the case of the 2D blotting device, L) or spectrally multiplexed (in the case of a single channel IEF device, R).

3. 2D Microgels for Multianalytical Native Protein Blotting

A native protein blotting chip is proposed which integrates an electrophoretic protein separation region with multiple antibody functionalized blotting zones through multi-stage photolithography. The design rationale for applying a planar microfluidic device for simultaneous protein immunoblotting is described, and corresponding metrics of assay performance are discussed. Targeted specifications are informed by theoretical models, known device physics, and existing work within the field.

3.1 Design of a Planar Microdevice for Multianalyte Protein Blotting

Given the constraints of traditional multianalyte blotting, we propose an application of the 2D microfluidic blotting technique towards simultaneous analysis of multiple protein targets [70]. This design goal requires an expansion of the blotting region to include multiple blotting gels functionalized with a diverse, spatially discretized panel of capture antibodies. The planar layout of the central chamber provides two geometric dimensions to yield multiple layers of information. Specifically, a 2D configuration yields the charge-to-mass ratio of the protein along the vertical axis, and specific, antibody-mediated target recognition from sequential blotting zones along the horizontal axis. A schematic which illustrates the general operation of the proposed two-dimensional immunoassay is given in Figure 3.1:
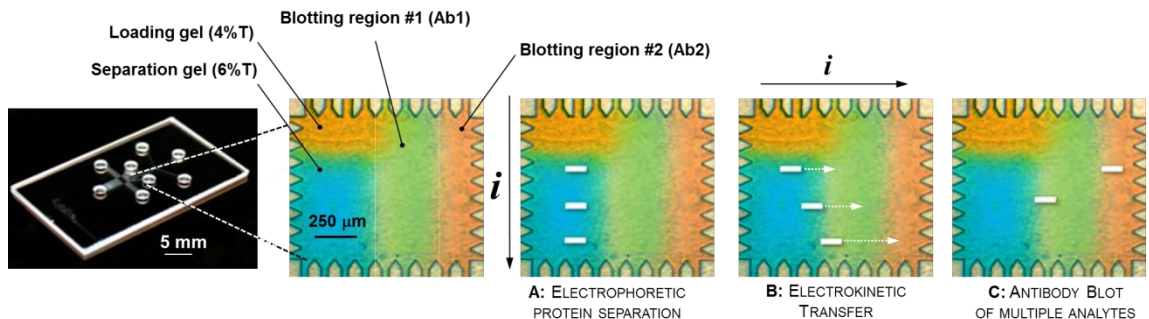
Figure 3.1: The separation region of the two dimensional gel reports protein charge-to-mass ratio, whereas the second blotting dimension reports protein identity. Green and orange false colorings demarcate IgG functionalized blotting regions which specifically target two different antigens.

Figure 3.1 demonstrates the three major steps involved in multianalyte 2D immunoassay, proceeding from protein separation (A) to blotting transfer (B) and detection (C). A plug of sample material (approximately 0.5 nL) is first electrophoretically loaded and injected to the central chamber, where the sample constituents travel along the length of a polyacrylamide sieving matrix (A). These analytes separate into a series of distinct bands according to their intrinsic charge-to-mass ratio. The separated protein bands are then transferred (B) across a series of blotting gel regions by switching the direction of the electric field into the lateral direction. Finally, proteins of interest are immobilized to distinct blotting regions corresponding to their matched antibody pairs (C). The device is then imaged to determine target protein quantification and identity.

In contrast to traditional SDS-PAGE, protein analytes within our microfluidic 2D blotting system are not subjected to SDS, DTT or heat treatments to denature proteins and break disulfide bonds. Native protein confirmation is conserved and detergent treatments are omitted, so as not to interfere with natural antigen-antibody binding

interactions [71]. All microchannel and chamber structures are contained in a wet-etched soda-lime glass chip (approximately 2.5 cm × 1.5 cm), consisting of two thermally bonded glass faces. The compact footprint of the planar central chamber (approximately 1 mm × 1mm) requires fine control of electric field line distribution, as well as precise placement of blotting gel boundaries during device fabrication.

Photolithography emerged during the latter half of the 20th century to become an indispensable manufacturing tool for the microelectronics industry [34]. Advances in photolithography have enabled the formation of structures upon silicon wafers with sub-micrometer resolution [72]. Furthermore, gel photopolymerization using light sensitive free radical initiators (such as riboflavin) has been a well-established technique to form sieving matrices for applications in molecular biology [73]. Thus, the adoption of multi-step photolithography as a gel fabrication tool and the integration of photolithography with UV-activated photoinitiator chemistry hold promise for the fabrication of multi-gel structures having zero dead volume.

Several microfluidic chip layouts were designed and tested for two dimensional blotting, with a selected subset of designs shown in Figure 3.2:

5 mm
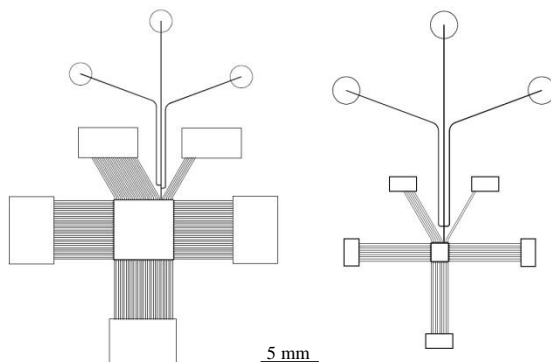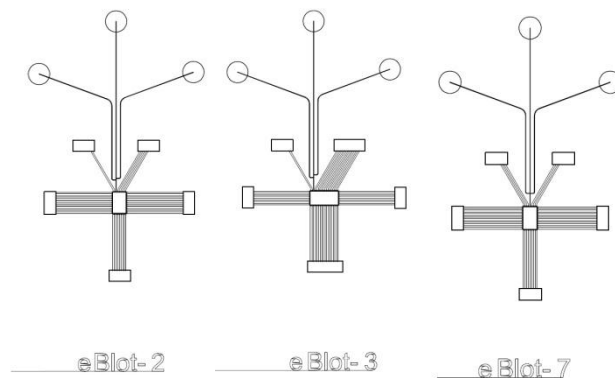
Figure 3.2: Various layouts of microfluidic blotting devices, with eBlot-2, eBlot-3 and eBlot-7 designs shown in the bottom row.

These microfluidic devices vary in the dimensions of their central chamber, ranging from 0.7 mm × 0.7 mm to 5 mm × 5 mm, where the separation and blotting transfer steps occur. The primary chip layout chosen for two dimensional microfluidic blotting was the eBlot-2 design, due to its compact footprint and the availability of an offset space to house multiple blotting regions (Figure 3.3).
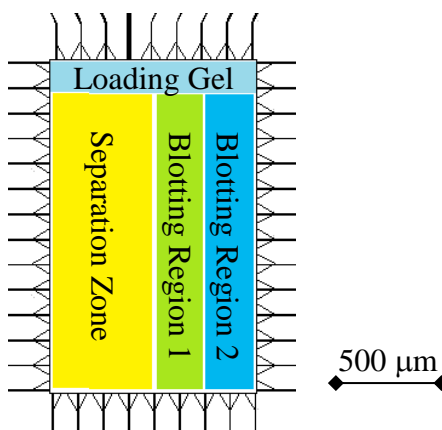
Figure 3.3: eBlot-2 two-dimensional protein analysis device contains multiple functionalized regions for protein separation and blotting, as well as an additional loading-to-separation gel stacking interface.

The eBlot-2 chip design allocates 600 μm of lateral transfer length, so multiple antigen binding zones can fit comfortably within this device footprint. The question regarding maximum analytical capacity (or how many blotting zones may be fit into a single device) involves previously discussed theoretical limits for efficient sample capture as well as some more practical considerations – such as fabrication technique and limits of device geometry. All antigen binding zones do not necessarily need to be the same width, as there will be some minimum value required for efficient target capture depending on the strength of the antigen-antibody binding interaction. Analytical modeling and empirical observations suggest that most antigenic targets can be completely immobilized within the first 100 μm of lateral blotting gel if the antigen concentration is on the order of 100 nM or less. Based upon a scaled-up sequential photopolymerization process using a microdevice with a 4 mm lateral span, 15 to 20 analyte capture zones contained within a single device should be possible. Increasing the number of antigen-binding zones also increases the number of sequential UV exposures, so that the separation zone could become densely polymerized to the point where undesired gel exclusion effects may be observed.

3.2 Metrics of Performance

In addition to seeking to maximize the number of available blotting zones, other key metrics of system performance include:

Separation resolution

Separation resolution (SR) between protein analytes is one of the most critical metrics of system performance, defined as $SR = \Delta L/4\sigma$, where ΔL is the distance between adjacent band centers and σ represents the average characteristic band width (assuming a Gaussian spatial distribution) [11]. Two analyte bands are said to be successfully separated or "resolved" when $SR > 1$. Although native protein electrophoresis does not separate proteins purely on the basis of size, a protein of interest can still be resolved from a complex sample background based on characteristic charge-to-mass ratio. Previous work [53] with on-chip 2D native protein separations indicate that SR values ranging from 1.25 to 1.93 can be achieved between isoforms of prostate specific antigen (PSA) within a 1.6 cm separation length. This length scale is approximately equal to the separation length of the eBlot-2 device, and so a similar degree of resolving power is expected of the 2D multianalyte blotting chip.

Assay Time

Looking at the denominator of the expression $SR = \Delta L/4\sigma$, separation resolution is clearly proportional to the initial width of the sample band. Microfluidic length scales of on-chip separation mechanisms enable the injection of a compact plug, resulting in smaller values for band width (σ) and shorter times towards analyte resolution. The high surface area to volume ratio of microscale electrophoresis works to counteract joule heating, and high electrical field strengths can be applied to expedite electrophoretic protein migration. Higher field strength (100's of V/cm rather than 10's of V/cm in standard PAGE) is advantageous, as ΔL is directly proportional to the applied field strength: $\Delta L = E(\mu_1 - \mu_2)t$.

Microfluidic devices with polyacrylamide matrices have demonstrated full electrophoretic resolution of multiple proteins from a complex sample within timescales on the order of seconds [74]. Following the analyte separation process, target proteins are directly transferred to adjacent blotting gels by simply redirecting the applied electric field. Sample transfer and detection stages are integrated to a streamlined and automated format, precluding the need for manual intervention steps. Thus, multianalyte blotting time is expected to be on the order of minutes, as opposed to the hours or even days required for slab gel multi-analyte blotting.

Measurement Specificity

Immunoassays are dependent upon the functional activity of antibodies which will not exhibit binding affinity for anything other than their intended targets. Determining the presence of a specific protein target via immunoassay usually depends upon the interpretation of some localized antibody signal. In designing and testing a novel immunoassay, one must validate that the physical mechanism of the working assay does not contribute additional cross-reactivity beyond the behavior of the antibody itself. Antibody functionalized blotting gels have shown that they are capable of specific target immobilization without also capturing or excluding non-target proteins [75]. In some instances, the pore size of the gel may need to be tuned to avoid size-based exclusion, and non-specific protein interactions with the antibody functionalized gels will also be screened.

<u>Measurement Sensitivity</u>

Previous results for single analyte 2D microfluidic Western blotting indicated a signal-to-noise ratio of 40 for a fluorescent antigen assayed at 500 nM [53]. Therefore, limits of detection in the low nanomolar range are anticipated when validating a labeled target in the on-chip multi-analyte blotting format. Detection of an unlabeled antigen through application of a fluorescent antibody probe is also investigated as a part of this work – with similar expectations of measurement sensitivity. Of course, hardware limitations are intertwined with limits of measurement sensitivity and so optical system design considerations for fluorescence detection are discussed. Enzyme linked immunodetection strategies which employ a secondary antibody to amplify a targeted signal are also presented to enable effective protein detection into the sub-nM range.

4. Multianalytical Blotting Device Fabrication and Operation

In this chapter, we describe the fabrication process as well as the basic operation of the two dimensional multi-blot microdevice. A novel multi-step photolithography process enables disparate polyacrylamide zones to be photopatterned within the device at high spatial resolution and with zero dead volume. Problems which occurred during the process of assay development and troubleshooting (such as gel shifting) are characterized, and solutions to these problems are described.

Etched soda-lime glass devices were received from a commercial supplier (Caliper Life Sciences), while the drilling and bonding steps were performed in-house. Drilling of glass chips was performed on a variable speed microdrill press (Cameron Micro Drill Presses) using Triple Ripple 2.1 mm diameter drill bits (Abrasive Technology, Inc.). One point of emphasis here is that drill bits should be frequently replaced, as working with dulled bits increases the risk of cracking the glass due to high pressure and frictional forces. Drilled chips are washed using acetone, followed by a piranha soak, then washed and rinsed thoroughly prior to mating surfaces together and pressure bonding within a furnace. During the pressure bonding process, both faces of the glass device are pressed together between two flat Macor ceramic discs underneath a 1 kg steel mass. Soda lime glass devices are fused together over a 7.5 hour furnace heating process which approaches 600°C.

One challenge to device fabrication was the low yield of the drilling and bonding process. Only about half of all microfluidic devices were able to fully bond without

leakage between surfaces or without exhibiting newton ring formation. The inability to consistently achieve clean glass-on-glass contact following the piranha soak and wash steps represented a major obstacle. It can be helpful to perform glass bonding steps within a true clean room environment to ensure higher fabrication throughput. Reservoir wells drilled into the surface of the glass chip allow samples and reagents to be introduced to the device and these reservoirs serve as an interface between the external platinum electrodes and the interior of the polyacrylamide gel.

A Caliper high voltage supply can be operated under current feedback or voltage feedback control settings and is used to direct electromigration processes throughout the two dimensional microfluidic device. Resolution of current control was ± 0.01 μA and resolution of voltage control was ± 1V, with a dynamic operating range of 4000V. The Caliper 605 HV power supply was adapted from an AMS90SE DNA electrophoresis system, and computer controlled through the AMSRecorder software package, which allows real-time monitoring of applied currents and voltages on eight independent channels. One sample program sequence for voltage control is given in Table 4.1, with a corresponding electrode map in Figure 4.1.

	Electrode Terminal Applied Voltage / Current							
	1	**2**	**3**	**4**	**5**	**6**	**7**	**8**
Sample loading	*0 μA*	*-400 V*	*-0.1μA*	*-200 V*	*0 μA*	*0 μA*	*-0.05 μA*	*0 μA*
Injection / separation	*-290 V*	*0.1 μA*	*-400 V*	*0.1 μA*	*-295 V*	*0 μA*	*-220 V*	*0 μA*
Transfer & blotting	*0 μA*	*0.05 μA*	*0 μA*	*0.05 μA*	*0 μA*	*-50 V*	*0 μA*	*-120 V*

Table 4.1: On-chip immunoblotting voltage control program (see Figure 4.1 for electrode map).
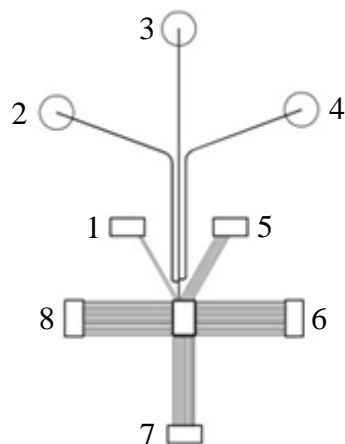
Figure 4.1: Electrode layout for a two dimensional electrophoresis process mapped upon the reservoir wells of an eBlot-2 device.

4.1 Gel Components and Multi-Stage Photolithography

The interior of the microfluidic device contained three types of polyacrylamide gels photopatterned in various regions of the central chamber. These include: large pore-size loading (3%T), separation (6%T) and antibody functionalized (4%T, 3.8 μM streptavidin-acrylamide) gels. A commercially available streptavidin acrylamide conjugate (Life Technologies) enables versatile functionalization of the blotting gel, which makes use of the high affinity biotin-streptavidin binding pair [76]. A suite of well characterized technologies is readily available for attachment of biotin groups to antibodies through lysine conjugation [77]. Biotinylated antibodies were included at a standard concentration of 1.6 μM within the blotting gel precursor solution and incubated for 1 hour at room temperature (25°C) prior to photopolymerization. The streptavidin acrylamide to biotinylated antibody ratio dictates the maximum binding site density, and streptavidin content can be adjusted relative to antibody concentration to tune the spatial distribution of antigen capture.

Commercially available antibodies were sometimes received at concentrations below 1 mg/mL, which posed challenges to the biotinylation process. Most biotin conjugation protocols require starting antibody concentrations of ~1 mg/mL, and the biotinylated antibody yielded from this process is directly mixed to streptavidin polyacrylamide in order to form the blotting gel precursor solution. Low concentrations of biotinylated antibodies can place limits upon capture antibody density within the blotting gel. A spin filtration step using a >100 kDa molecular weight cut-off filter can be used to preconcentrate antibodies before biotinylation in order to circumvent these limitations.

Polyacrylamide gels were prepared from a 30% acrylamide (29:1 acrylamide/bisacrylamide ratio) stock solution from Sigma-Aldrich. All gel precursors used in photopolymerization contained 0.2% (w/v) 2,2'-Azobis-[2-methyl-N-(2-hydroxyethyl) propionamide] (VA-086) from Wako Chemicals as a photoinitiator. The gel electrophoresis buffer was Tris-glycine (25 mM Tris, 192 mM Glycine at pH 8.3) from BioRad which was also utilized as a sample and run buffer. Functional gels were fabricated within the two-dimensional glass structure through multi-step photolithography as described in Figure 4.2.

500 μm

Glass Chip Chamber

4%T, Ab1

Antibody functionalized precursors
are wicked through the central chamber

4%T, Ab2

Photomask

UV

Define antibody functionalized
blotting region

Photomask

UV

Define blotting region 2

nask

UV

Polymerize separation gel

UV

Flood UV Illumination
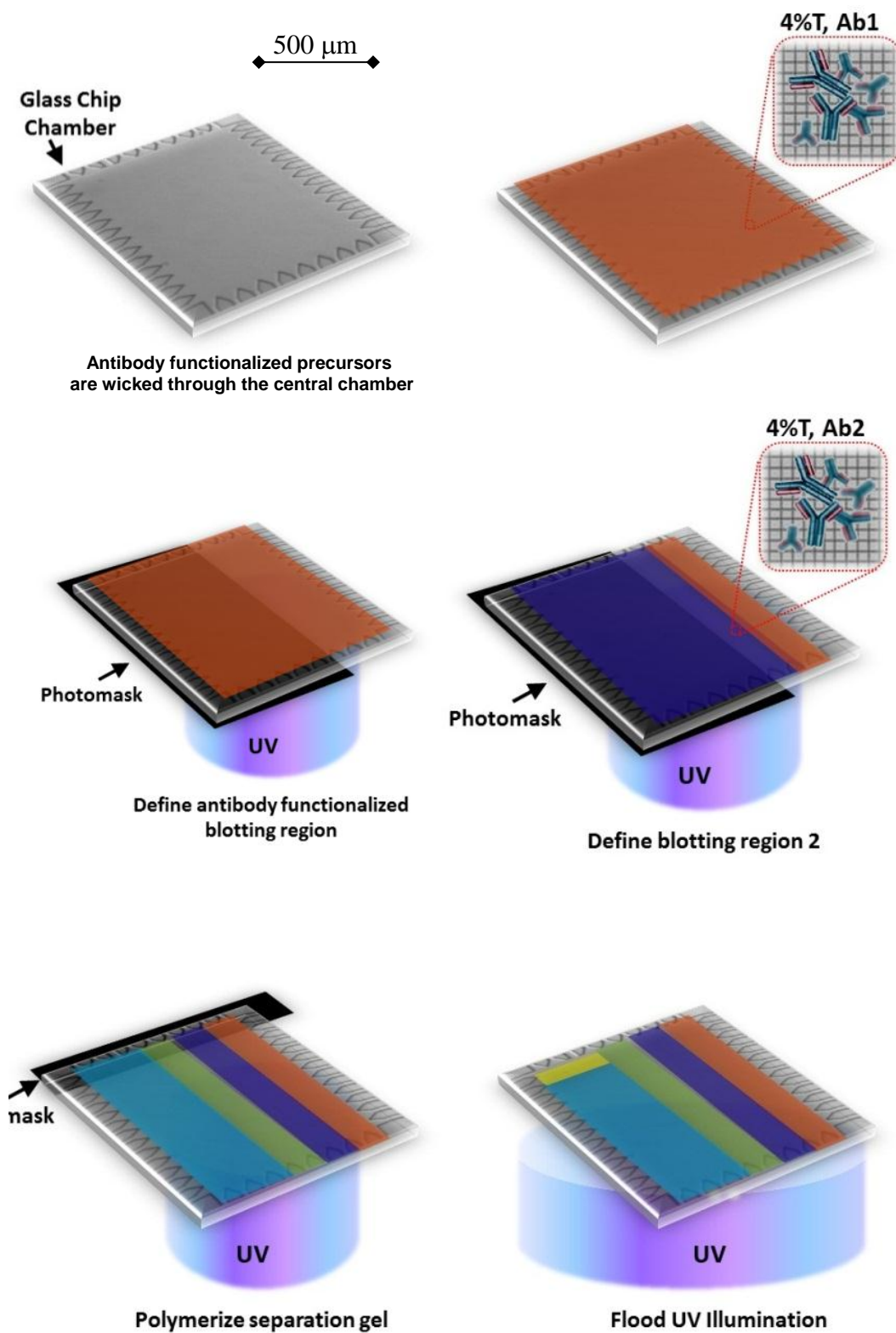
Figure 4.2: Multistep photolithography defines multiple, spatially distinct functionalized gel regions.

43

A Hamamatsu LightningCure LC5 with variable intensity control was used as a UV light source. The UV beam from the LC5 was directed along the light path of a Nikon Diaphot 200 inverted microscope through a UV-transmission objective lens (UPLANS-APO 4×, Olympus). Prior to each polymerization step, the desired gel precursor solution was loaded into adjacent reservoirs and flushed using vacuum pressure throughout the device. The chip was then placed upon the microscope stage and manually aligned within the field of view with respect to a photomask to selectively define different gel regions through a multi-step photolithography process. Between each UV exposure step, all unpolymerized precursor solutions were evacuated and replaced by applying a vacuum at adjacent reservoirs. Visual inspection of the device channels and chamber was performed before each photopolymerization step to avoid introduction of air bubbles. If observed, bubbles within the channels or chamber could be readily flushed out with a buffer solution via application of vacuum pressure and fresh PA gel precursor could then be flushed in.

When all requisite blotting regions were complete, the separation gel was photopolymerized in the region directly below the injection channel. The lower density loading gel precursor solution was finally flushed throughout the uppermost loading channels and the entire chip was then exposed to a filtered mercury lamp (B100-AP, UVP) with cooling fan. This multistep lithography process resulted in a device with discrete loading and separation gel zones as well as n blotting gel regions fabricated within $n + 2$ UV exposure steps (where n corresponds to the desired number of protein targets to be identified). Although the blotting regions were designed for single use,

interior gels could be dissolved by immersing chips overnight in an acid bath, allowing the glass chips to be reused.

One major challenge to repeatable device fabrication was that gel features could only be photopatterned within about ± 50 μm spatial resolution. This limitation could be related to the orientation of the mask and the device relative to the UV objective if UV light strikes the mask at an angle. Manual manipulation of the device relative to the mask could be imprecise and so a wider, rectangular blotting region such as that of the eBlot-3 device provides more tolerance for blotting gel fabrication to accommodate the challenges of limited spatial resolution. Use of a mask aligner photolithography system can also improve the spatial resolution and repeatability of gel fabrication.

4.2 Gel Displacement

The relative size and position of gels located within the device was found to change considerably over the course of experimentation. This "gel shift" phenomenon was usually observed after extended application of electric field strengths at magnitudes higher than 150 V/cm. Gel shifting seemed to be especially problematic in the lateral transfer direction. Distorted gel boundaries pose an obstacle to data interpretation. For example, Figure 4.3 illustrates the displacement of a previously straight blotting gel boundary, which shifts towards the left as a lateral electric field is applied over the course of 15 minutes. The streptavidin acrylamide blotting gel exhibits a different charge density from the 6%T polyacrylamide separation gel and shifts in response to the application of an external electric field. The shifted gel boundary obstructs the separation path length and subsequent visual interpretation of the blotting gel becomes compromised.
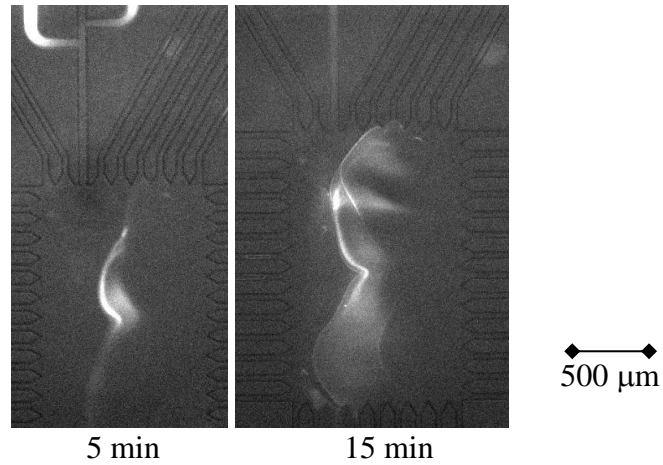
Figure 4.3: Lateral displacement of a blotting gel boundary after extended electric field exposure (150 V/cm for 5 minutes and 15 minutes)

Warped gel boundaries of the blotting region were also visible under brighfield illumination, as illustrated in Figure 4.4. Although two straight and clearly delineated membrane boundaries were photopatterned at intervals of 300 μm, these blotting membranes rapidly expanded and deformed under influence of the lateral field.
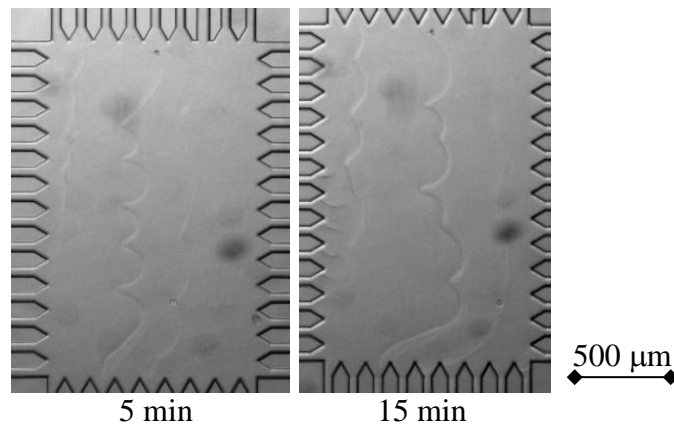
Figure 4.4: Brightfield images of the blotting gel interface upon initial and extended exposure to a lateral electric field (150 V/cm for 5 minutes and 15 minutes).

46

This same gel shifting behavior was also observed at the stacking interface near the top of the separation reservoir. Figure 4.5 depicts an eBlot-2 device containing a 4% to 8%T polyacrylamide gel stacking interface. Some distortion of the stacking gel interface occurs during separation and injection, as these field strengths are in the range of 100-200 V/cm. A distorted or slanted stacking interface will result in an elongated sample band and subsequent loss of separation resolution.
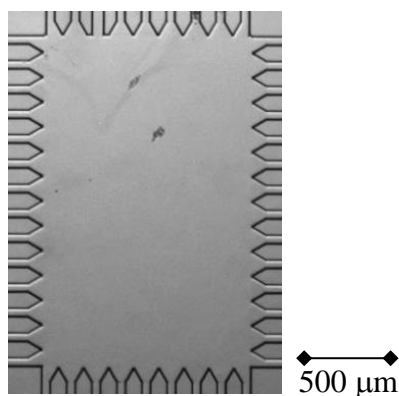
Figure 4.5: The stacking interface of a 4%T loading gel and an 8%T separation gel results in displacement of the function under extended application of an electric field, as visible under brightfield illumination.

One approach for avoiding the gel shift effect was to utilize a lower lateral field strength. No shifting of the analyte band was observed when electric field strengths were in the range of 50 V/cm ($Da \approx 9.3$), although low field strengths resulted in slow electromigration of analytes and assay reagents. As a result, reagent coverage throughout the device was poor and the length of time required to complete the assay became extended. Alternatively, silanization steps have often been employed within glass microfluidic devices to facilitate adhesion of polyacrylamide to glass surfaces [78]. A silanization process was applied by first treating the glass with sodium hydroxide for 10

minutes followed by a 30 minute incubation with a silane (3-(trimethoxysilyl) propyl methacrylate, Sigma-Aldrich), acetic acid, methanol and water mixture at a 2:2:3:3 ratio. Silane incubation was concluded with a series of water and methanol flushing steps. This surface treatment left a self assembled organosilane monolayer upon the glass which attached to the polymer chains of the acrylamide gel matrix and prevented subsequent gel shifting. After the silanization process, an electric field of 300 V/cm ($Da < 1.6$) could be applied to the gels for over two hours without observing any shifting of gel boundaries.

4.3 Electric Field Shaping

The central chamber of the two dimensional blotting device is bordered by an array of parallel microfluidic channels. These side channel arrays serve the dual purposes of enabling reagent transport from the chamber boundaries while allowing for uniform shaping of electric field lines throughout the central chamber [79]. Electrodes placed at reservoir wells act as point sources of charge [50] and therefore exhibit the field distribution shown on the left side of Figure 4.6.
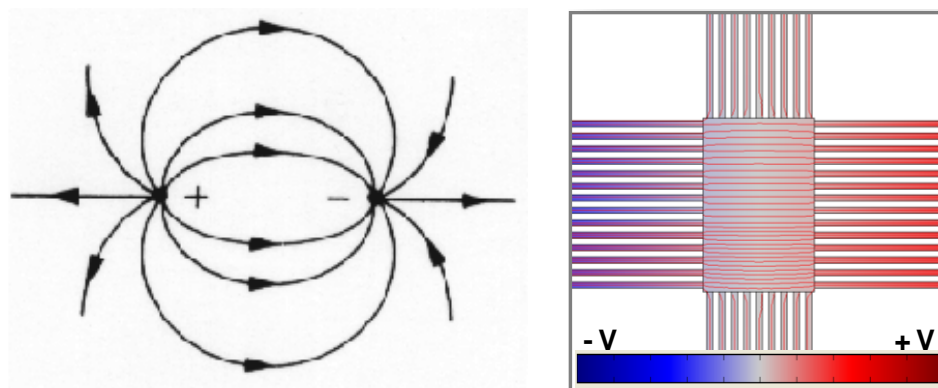
Figure 4.6: Electric field lines distributed across two point charges will demonstrate fringing effects (L, adapted from [80]) whereas side channel arrays work to redistribute unidirectional field lines across the central chamber (R, results from Comsol simulation adapted from [53])

Placing parallel sets of microchannels along the boundary of the central chamber prevents electric field line fringing which would result in heterogenous electrophoretic migration and subsequent warping of protein bands [53]. Electrode terminals 6 and 8 (on the sides of the device) were used for applying lateral electric fields, while electrode terminals 1, 5 and 7 (top and bottom, Figure 4.1) were employed to shape the electric field surrounding the injection channel and separation length. Electrodes which were inactive during a particular process were generally set to 'float' (at 0 μA) so that they would not negatively impact protein migration (Table 4.1).

4.4 Sample Stacking and Destacking

A plug of protein is initially confined within a 400 μm junction in the loading channel network before it is electrokinetically injected to the separation gel (Figure 4.7). Current control was used to shape the plug during the loading and injection process [81]. Application of "pull back" or "pinching" currents at the sample loading and sample waste

reservoirs prevent excess proteins from leaking into the separation and blotting regions [82].

Sample Loading   Sample Injection
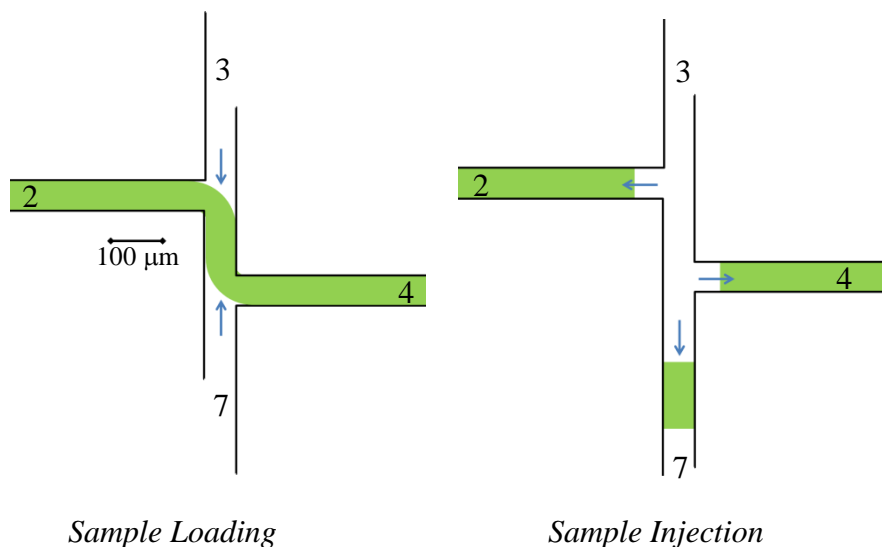
Figure 4.7: Illustration of current and analyte direction as a sample plug is loaded through the upper channel network and then injected towards the central chamber. Electrode reservoirs are numbered (see Figure 4.1 map), while arrows indicate the direction of applied pinching and pull-back currents during sample loading and injection, respectively.

When the injected protein plug enters the planar region of the device, the distribution of electric field lines within the central chamber shapes the protein plug into a band before it encounters a transition from a large pore size gel to a small pore size gel. The change in gel density results in a sample stacking effect as proteins migrate more slowly through the smaller pore gel (typically a 3% to 6%T transition). This change in electrophoretic velocity results in accumulation of the protein bolus into a tighter band, similar to the effect at a stacking gel interface for slab gel SDS-PAGE [68]. As proteins moved away from the interface, a "sample destacking" phenomenon was often observed as bands broadened over time (Figure 4.8).
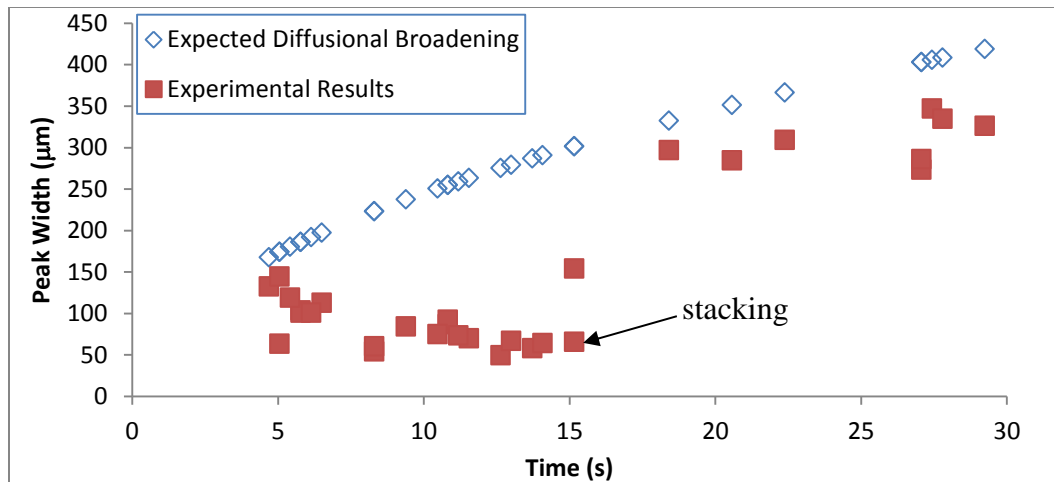
Figure 4.8: Average band width increases as a function of separation time after leaving the stacking interface. The full width of the band (prostate specific antigen, 400 nM) passes through the stacking gel at t = 15 seconds. Experimental results are compared against anticipated results from theoretical band broadening under the influence of diffusion (where $\sigma = \sqrt{2Dt}$).

Figure 4.8 shows that the width of the sample band changes from $t = 15$ seconds to $t = 30$ seconds, representing an approximate 7× increase in band width. The increase in peak width was also correlated with a loss of detection sensitivity as bands dispersed within the gel (Figure 4.8 and Figure 4.9 showing fluorescent prostate specific antigen at 400 nM).
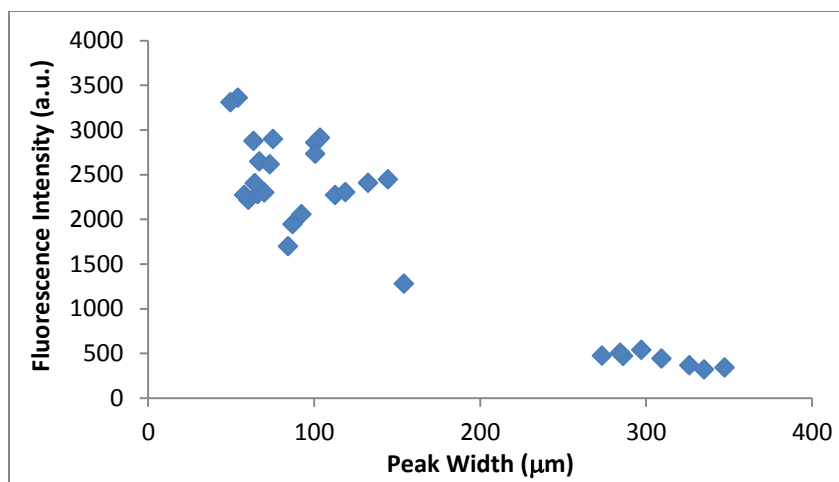
Figure 4.9: The maximum fluorescence intensity of a protein band decreases as band dispersion results in an increase of peak width.

The subsequent loss of measurement sensitivity can also be expressed in terms of the separation length. A plot of average peak intensity at various separation distances for seven experimental runs is shown in Figure 4.10.
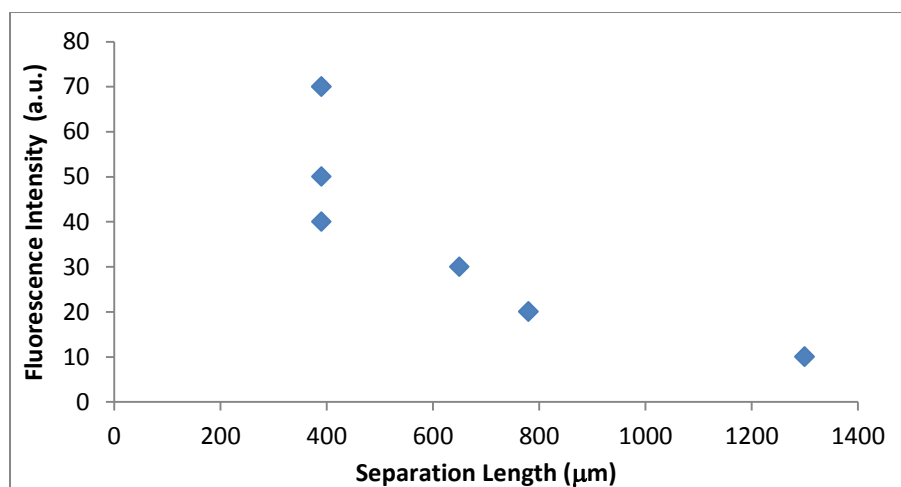
Figure 4.10: Protein bands demonstrate a decrease in average peak fluorescence intensity as bands disperse along the length of the separation gel (eBlot-2 device, PSA at 400 nM)

These results highlight the time sensitive nature of band transfer into the lateral blotting regions in order to reduce dispersive losses in measurement sensitivity. In a system where molecular diffusion is assumed to be the main source of protein dispersion, long separation times are advantageous for high separation resolution - as diffusion scales to $\sqrt{time}$ whereas the distance between bands scales linearly with time. Some band dispersion is caused by heterogeneity of the separation gel, which causes proteins on the leading edge of the band to assume a higher electrophoretic mobility. Gel interfaces that are fabricated via photopolymerization are known to exhibit a higher gel density due to free radical scavenging effects and increased monomer consumption at polymerization boundaries [83]. More uniform gel conditions can be implemented by decreasing the intensity of the UV exposure step to reduce the degree of monomer diffusion at the polymerization interface [74].

5. Demonstration and Assessment of 2D Blotting Device Performance

The performance of the two dimensional multi-blotting device is described through model experiments which allow metrics of performance (such as antigenic capture efficiency) to be characterized. Some key components of the integrated assay process include protein separation through a sieving matrix and subsequent selective target transfer to antibody functionalized blotting regions. A label-free target detection strategy is presented which employs a matched fluorescent antibody probe, and off-chip screening methods are used to validate antigen capture and detection antibodies. Fluorescence measurement characteristics of the system (such as lower limits of detection) are also described, along with on-chip enrichment membranes that can be applied to increase measurement sensitivity.

5.1 Antibody Functionalized Blotting Gels

The ability to bind a target protein by moving the protein through an antibody functionized polyacrylamide gel was assessed by drawing a stream of fluorescent protein across the full length of a separation gel. This elongated protein stream was then transferred towards an adjacent blotting membrane by applying a lateral electric field. Initial experiments of an alpha-actinin negative control (100 kDa) migrating across a 8%T anti-C-reactive protein blotting gel resulted in retention of alpha-actinin, suggesting nonspecific exclusion of high molecular weight proteins (Figure 5.1).
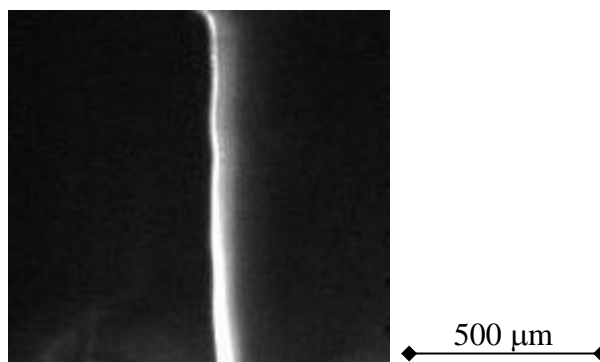
Figure 5.1: Alpha-actinin (100 kDa) is immobilized to the blotting/separation gel interface as protein is transferred laterally across the width of the central chamber.

The pore size of the blotting gel was enlarged by reducing the formulation of the blotting region from 8% down to a 6%T density gel. The ability of this 6%T gel to bind against a matching target protein was assessed by drawing an elongated stream of C-reactive protein (CRP, 500 nM) and transferring it across to the 6%T anti-CRP blotting membrane (Figure 5.2). This lateral transfer process resulted in a high affinity interaction with CRP immobilized to the blotting gel at >90% efficiency.
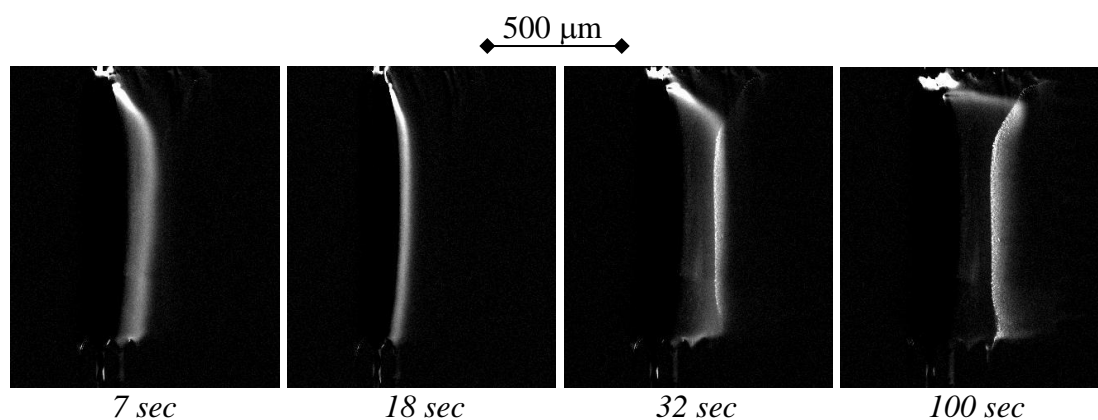
Figure 5.2: Lateral CRP transfer from left to right, shown at 7, 18, 32 and 100 sec.

To test the influence of size-based exclusion upon the 6%T anti-CRP blotting gel, an elongated stream of alpha-actinin was drawn across the separation region and transferred

55

towards the anti-CRP region. This time, there was no interaction between the alpha-actinin and the anti-CRP membrane. A side-by-side image comparison of the two experiment (post-blot) is shown in Figure 5.3. The fact that the 6%T blotting gel is able to bind the 115 kDa pentameric CRP without retaining the 100 kDa alpha-actinin molecule suggests that the anti-CRP is effective in binding its intended target and that a 6%T pore structure is large enough to prevent non-specific size-based protein exclusion.

L: alpha-actinin   R: CRP
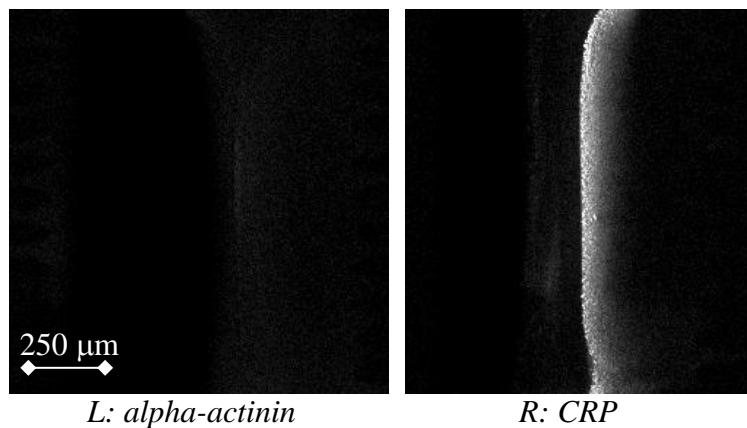
Figure 5.3: Blotting gel interface after lateral protein transfer (t = 40 sec).

Protein G Binding:

A stream of protein G (125 nM) was transferred laterally to an anti-protein G functionalized blotting membrane, yielding a signal to noise ratio (SNR) of ~90 (Figure 5.4). This value was higher than a previously reported SNR of ~40 for fluorescent prostate specific antigen at 500 nM [53]. Part of the reason for this increased sensitivity is attributed to the strong binding affinity of the protein G antigen-antibody pair, which is exceptionally high.
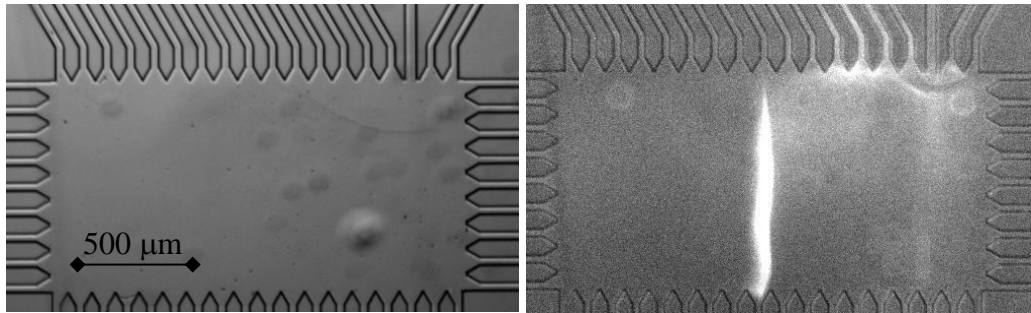
Figure 5.4: Pre- and post-blot fluorescence images of protein G binding (125 nM) to the blotting membrane of an anti-protein G device (eBlot-3).

C-Reactive Protein Binding:

CRP and PSA (as a negative control) were assayed across an anti-CRP blotting membrane at 500 nM each. The anti-CRP blotting membrane exhibited a strong affinity for its target, and non-target proteins (PSA) were not retained following lateral transfer. The fluorescence intensity profile of Figure 5.5 is measured at a ROI which corresponds to the anti-CRP blotting region as a function of time.
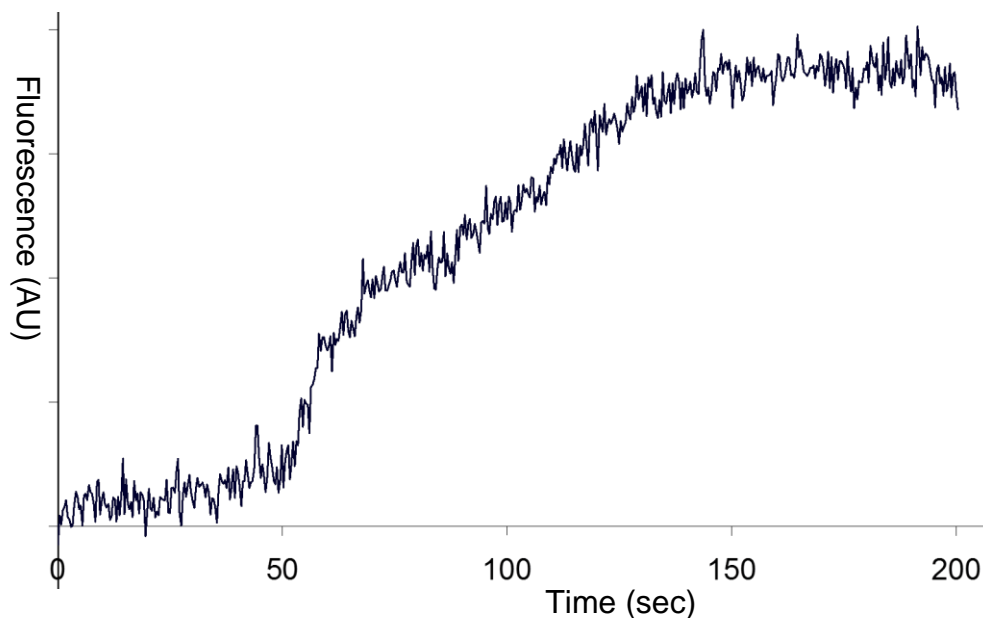
Figure 5.5: Fluorescence signal from a CRP target is retained upon lateral transfer to the anti-CRP blotting gel.

Average fluorescence intensity at the ROI increases as the protein target migrates into the blotting region, eventually reaching a plateau value in which all of the target molecules are immobilized within the blotting region. SNR of antigen binding detection was ~30 when CRP was assayed at 500 nM, and ~12 when binding of the same sample was assayed at 333 nM. When the corresponding intensity-versus-time measurement is plotted for the negative control PSA passing through an anti-CRP functionalized region, we observe that the bulk of the protein band passes through the blotting region without hindrance and that the fluorescence signal approaches its previous baseline value as the target band moves out of the blotting gel (Figure 5.6).
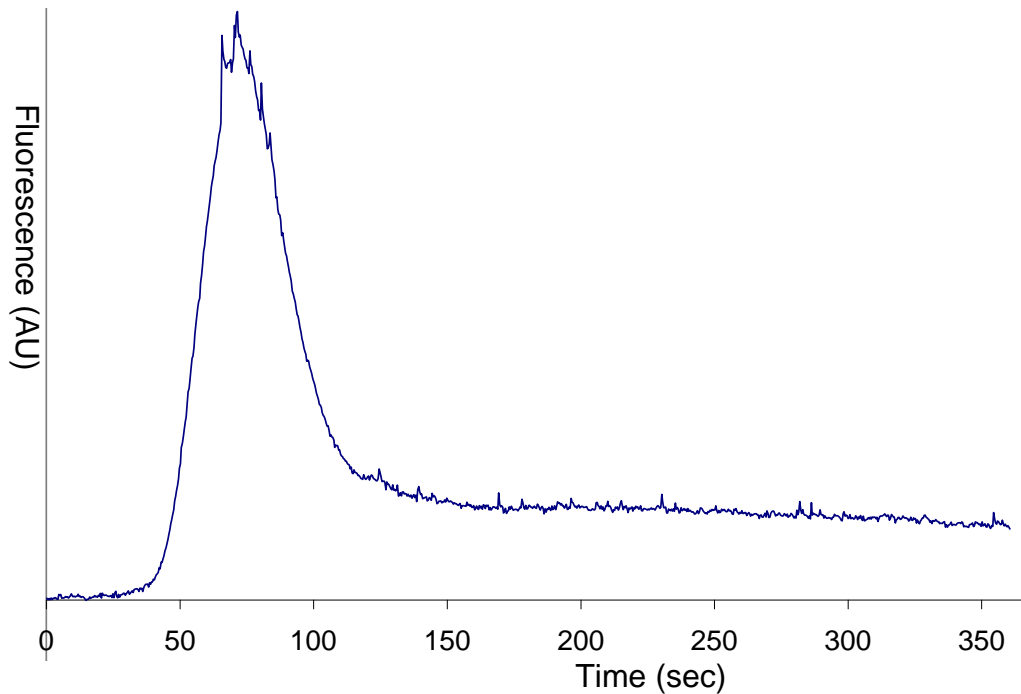
Figure 5.6: Fluorescence signal from PSA at the anti-CRP blotting region is transient, as the PSA band is able to pass through the anti-CRP gel without being retained.

5.2 Separation Resolution & Blotting Transfer

C-reactive protein (CRP, 770 nM), protein G (PG, 550 nM) and trypsin inhibitor (TI, 133 nM) was used to demonstrate separation and capture of selected targets from a multi-component mixture. CRP and PG served as target antigens, while TI served as a high mobility negative control. Fluorescent conjugates of PG and TI were obtained from commercial sources (Invitrogen), while CRP (EMD Chemicals, Inc.) was labeled with AlexaFluor 488 according to manufacturer's instructions. Figure 5.7 displays a CCD fluorescence imaging sequence from sample injection to electrophoretic separation. Separation resolution values were calculated by applying a Gaussian peak fitting algorithm through OriginPro (OriginLab) to find band width (σ), while ΔL was defined as the distance between peak centers.
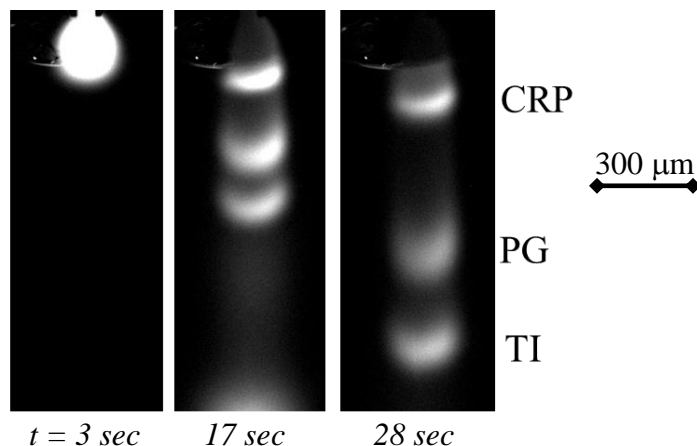
Figure 5.7: Trypsin inhibitor (TI), protein G (PG), and C-reactive protein (CRP) are separated to baseline resolution within 30 seconds, E = 95 V/cm.

After sample injection, the injected plug entered the large 2D chamber and native PAGE separation was initiated at 95 V/cm (Figure 5.7). At the top of the chamber, the protein sample encountered a 3%-to-6%T stacking interface and became baseline

59

separated into constituent bands within 17 seconds. During native PAGE, the average

band width (σ) for PG, TI and CRP was 122 μm, 96 μm and 68 μm respectively

(measured at 17 seconds within the separation gel). The stacking interface reduced

injection dispersion by 75%, from 117 μm ($\sigma_{injected}$) to 29 μm ($\sigma_{stacked}$), resulting in a 41%

$\pm$ 19% ($n = 6$) increase in maximum fluorescence signal.
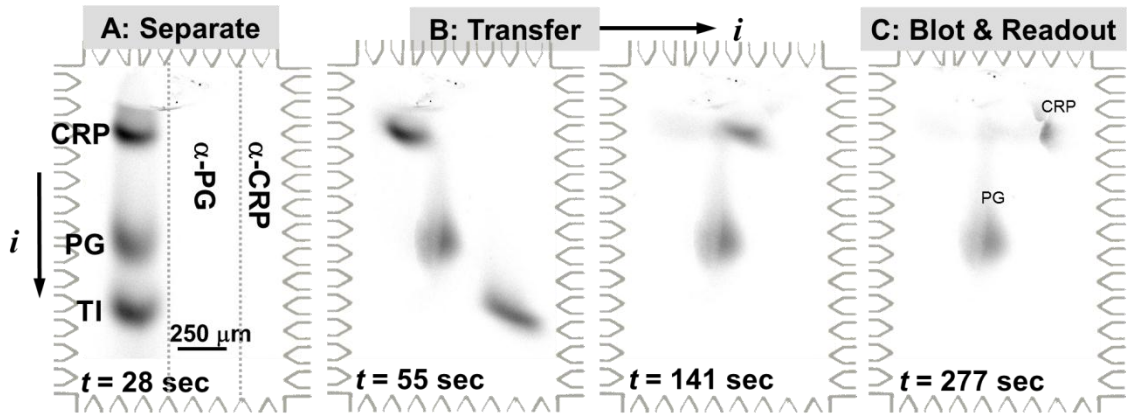
Figure 5.8: Simultaneous transfer and immunoblotting of protein G (PG) and C-reactive protein (CRP). Trypsin inhibitor (TI), the negative control, does not interact with the antibody functionalized blotting regions. E = 50 V/cm.

The 2D microfluidic blotting device employed two distinct antibody regions

containing anti-PG and anti-CRP (denoted by α-PG and α-CRP in Figure 5.8). At $t = 28$

seconds, electrophoretic transfer of resolved peaks from the separation gel towards the

blotting regions was initiated by switching off the separation field. Subsequent

application of a transfer field perpendicular to the separation axis drove all protein bands

out of the separation gel and into the blotting regions (E = 50 V/cm, Figure 5.8). SR was

maintained throughout the transfer process (Table 5.1) with average variations of 18%

and 6% for separations between TI/PG and PG/CRP peaks, respectively. Full band

transfer to the blotting regions was completed within 250 seconds, resulting in detection

of each immobilized protein target at a corresponding blotting zone. Uniform lateral transfer fields result in excellent fidelity of spatial mapping between resolved bands in the separation gel and the final position of those target bands as they are immobilized in the blotting regions (Table 5.2).

Analyte Pair	Separation Resolution	Variation
PG/TI	2.5 (Before lateral transfer)	18%
	3.0 (After lateral transfer)	
CRP/PG	4.6 (Before lateral transfer)	2%
	4.5 (After lateral transfer)	

Table 5.1: Separation resolution is maintained throughout lateral transfer.

Analyte	Bandwidth (µm)		Peak Center Shift (µm)	Variation
TI	Before lateral transfer	127	14	3%
	After lateral transfer	123		
PG	Before lateral transfer	171	29	7%
	After lateral transfer	182		
CRP	Before lateral transfer	89	53	14%
	After lateral transfer	101		

Table 5.2: Band widths and central peak positions are maintained throughout lateral transfer.

At the point of lateral transfer, the fastest moving protein bands were located near the bottom of the separation region. As these are analytes of highest electrophoretic mobility, they also display the fastest lateral migration, resulting in the diagonal arrangement of bands during transfer illustrated in Figure 5.8. Proteins which are not specific to the antibody functionalized gels moved through and out of the blotting regions without experiencing a change in electrophoretic mobility (Figure 5.9). The negative control TI band was able to migrate out of the blotting region within 50 seconds. Total measured lateral migration time of 250 seconds was consistent with the speed of the slowest CRP band, based upon applied field strength and the electrophoretic mobility of CRP. Total assay time consists of sample loading, electrophoretic separation and lateral

transfer time. Specifically, the lateral transfer time depends upon migration speed and the requisite length of travel to the corresponding blotting region. Lateral transfer is complete when the slowest component has been given enough time to clear the lateral span of the central chamber (t = distance/speed).
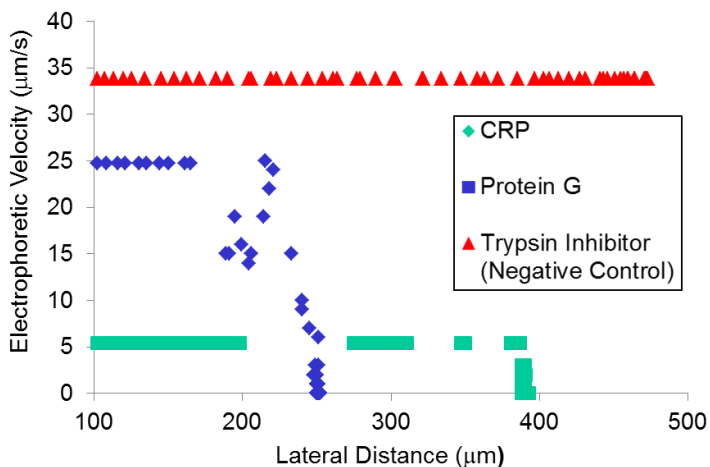
Figure 5.9: An anti-protein G functionalized membrane is located at 250 μm whereas an anti-CRP membrane is located at 400 μm. Plotting electrophoretic migration velocity as a function of lateral distance demonstrates that target molecules become immobilized (velocity = 0) at their specific matched blotting interface, while nonspecific negative control molecules maintain a consistent velocity as the move across the capture gels.

Image analysis was performed with ImageJ and regions of interest corresponding to the separation and blotting regions were consistently applied. Line sections across the ROI were averaged to calculate the spatial distribution of the fluorescence signal. To assess non-specific exclusion or retention at the blotting gel interfaces (i.e., separation-to-blotting region, blotting region 1-to-2) and within each blotting region, negative control proteins not specific to the antibody functionalized gel were monitored. In the dual analyte assays, negligible change in electrophoretic mobility was observed (μ_{TI} along

separation axis: 4.93×10^{-5} cm^2/(V s), μ_{TI} in α-CRP region: 4.93×10^{-5} cm^2/(V s); μ_{TI} in α-PG region: 4.95×10^{-5} cm^2/(V s)). Negligible stacking or de-stacking was observed at either of the gel interfaces (separation to blotting gel or between the two blotting regions) due to the closely matched pore-sizes within the regions and at the interface. Figure 5.9 plots the velocity of target and non-target molecules as they migrate across the lateral span of the central chamber. Specifically targeted molecules slow to zero velocity as they encounter their corresponding antibody capture zone, whereas non-target molecules continue electrophoretic migration at constant velocity. Comparisons of the band fluorescence of PG and CRP before and after blotting demonstrate that 85-95% of each target is captured upon the matching blotting membrane.

5.3 Measurement Linearity and Lower Limits of Detection

Protein G (20 kDa) was observed to bind with the anti-protein G functionalized membrane with extremely high affinity. A sequence of images demonstrating protein G injections followed by transfer to the lateral membrane is shown in Figure 5.10. Protein G bands of width ~150 μm could be consistently immobilized to the blotting gel and did not dissipate after 60 seconds of extended field exposure at 100 V/cm. The high binding affinity of protein G to the anti-protein G membrane makes this antigen/antibody pair an excellent model for demonstrating operation of the two dimensional multianalyte blotting device.
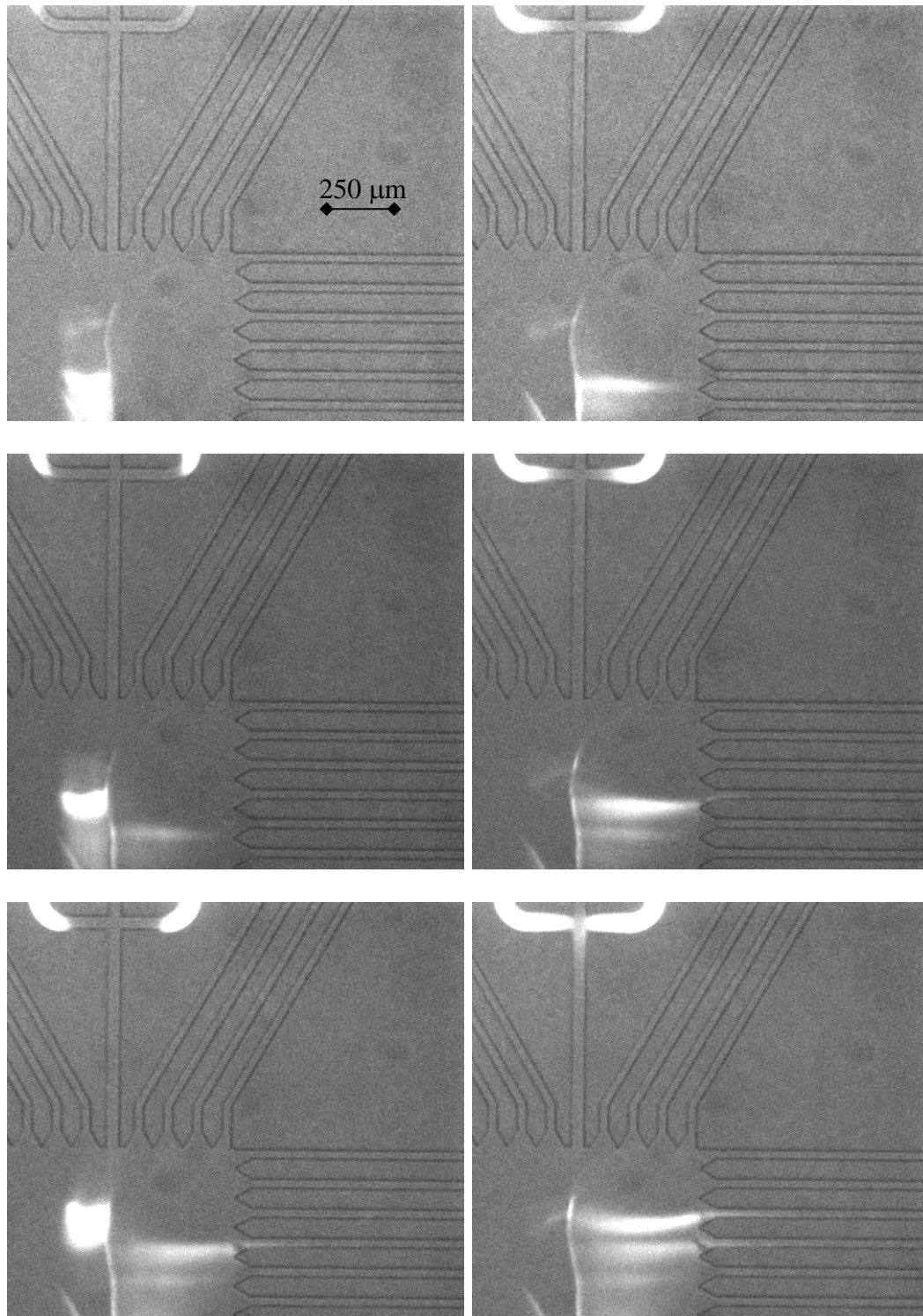
Figure 5.10: From top to bottom, left to right, sequential blotting of protein G bands against an anti-protein G functionalized membrane. Estimated binding efficiencies are >90%.

The dose response curve of Figure 5.11 was generated by testing a dilution series of fluorescent protein G at 50, 100, 200, 400, 800 and 1250 nM against an anti-PG blotting gel. Area under the curve was measured based upon the spatial distribution of each immobilized fluorescent protein band and plotted as a function of target concentration. Figure 5.12 provides an example of typical spatial distribution for fluorescent signal across the axis of the central chamber for protein G antigen blots at 50 and 200 nM. The resulting fits exhibit excellent linearity across a range from 50-1250 nM, demonstrating that fluorescence observations from immobilized targets are capable of producing quantitative and linear measurements of initial protein concentration.
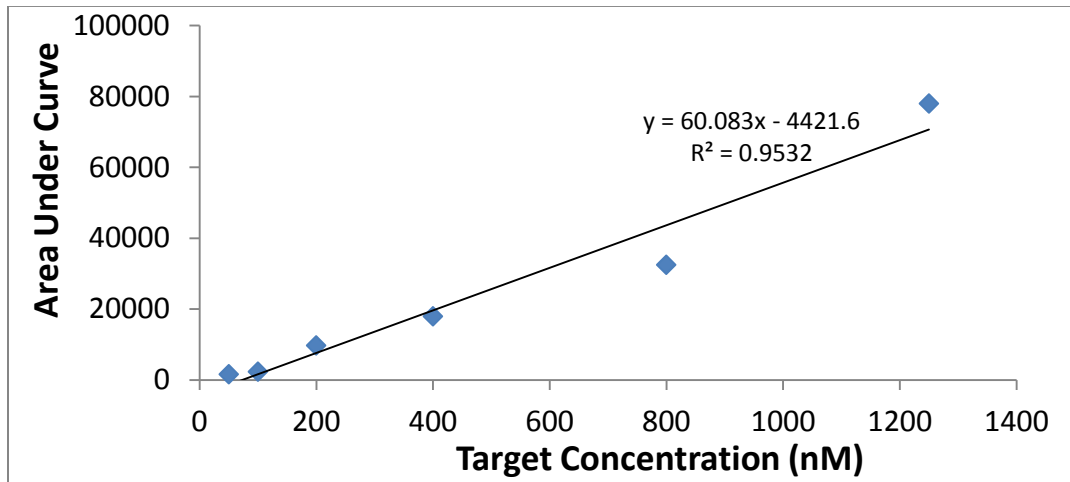
Figure 5.11: When fluorescence intensities for immobilized bands are plotted spatially, the resulting area-under-the-curve for each immobilized protein band can be linearly correlated to the starting concentration of the sample.
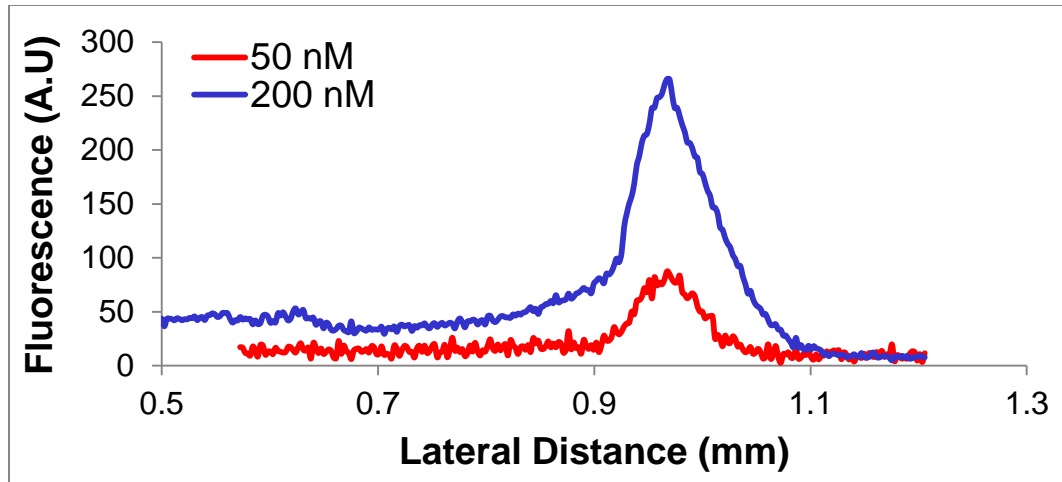
Figure 5.12: Fluorescence distribution plots of fluorescent protein G, immobilized across the lateral span of a blotting gel.

A dilution series of AlexaFluor 488 labeled protein G ranging from 1-10 nM was utilized to investigate the lower limit of detection for an antigen target. Figure 5.13 shows SNR for a series of measurements taken across this dilution series. The signal measured here was the peak fluorescence intensity across the ROI, while noise was defined as the standard deviation of pixel intensity across the span of the chip. The LLOD for the system under fluorescence microscopy with CCD imaging is approximately 2.5 nM, based upon a threshold of SNR = 3.
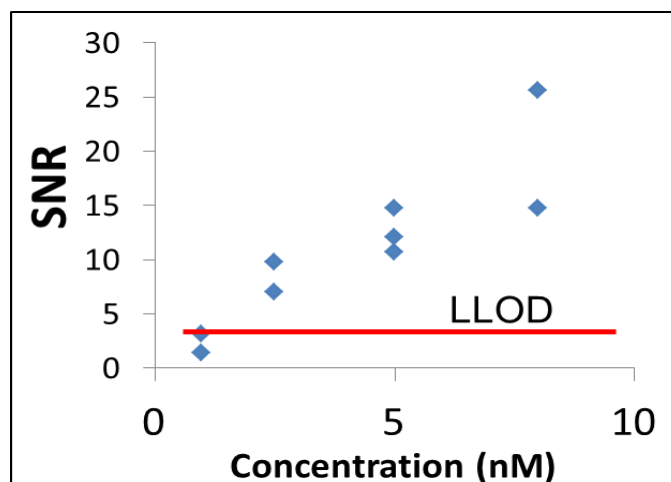
Figure 5.13: SNR readings for a series of immobilized protein measurements ranging from 1-10 nM demonstrate a lower limit of detection at ~2.5 nM, based upon a SNR threshold of 3.

Two major factors contribute to noise in these experiments – spatial variations in illumination across the field of view and lamp flickering. SNR results were based upon observations using a 10× objective and 300 ms CCD exposure time settings. Multiple measurements of the blotted bands were performed using various exposure times and objective lenses. Longer camera exposure times produced brighter fluorescence signals, but did not result in higher SNR under the conditions employed, as the noise also tended to increase. However, use of higher NA objectives did result in higher SNRs.

5.4 Label Free Detection

A protocol was designed to perform analyte separation and detection to obviate the need for a fluorescently labeled target by using a separate matched fluorescent probe antibody. An unlabeled protein sample was included in Figure 5.14 as a model target protein along with a ladder mixture of larger and smaller proteins. The sequence of events is similar to a sandwich ELISA:

- Step 1: Loading, stacking and separation of multi-protein sample mixture.

- Step 2: Transfer of separated proteins through a specific antibody functionalized region, retaining the unlabeled target.

- Step 3: Introduction of dye-labeled antibody probe through blotting and separation regions to bind with immobilized targets.

- Step 4: Clearance of unbound probe molecules from the central chamber and subsequent identification of the probed and immobilized target band.
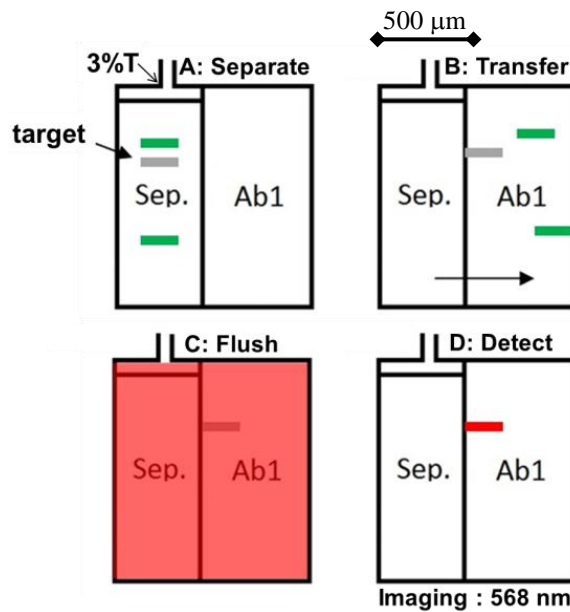
Figure 5.14: General operating protocol for fluorescent sandwich probe detection of an unlabeled target protein.

Two-dimensional blotting devices were used to study the process of antibody introduction to the central chamber. Fluorescently labeled IgG (6 μM) was introduced from the right side channel array to test the uniformity of antibody introduction under an electric field of 40-50 V/cm for 20 minutes. Gel regions of higher density within the device retained a higher antibody concentration, and the final antibody distribution within the central chamber was non-uniform. Antibody concentrations on the side of the device

where antibody loading was initiated tended to be higher than that of the opposing side, as would be expected (Figure 5.15).

250 μm

Antibody Introduction: Series 1   *Antibody Introduction: Series 2*
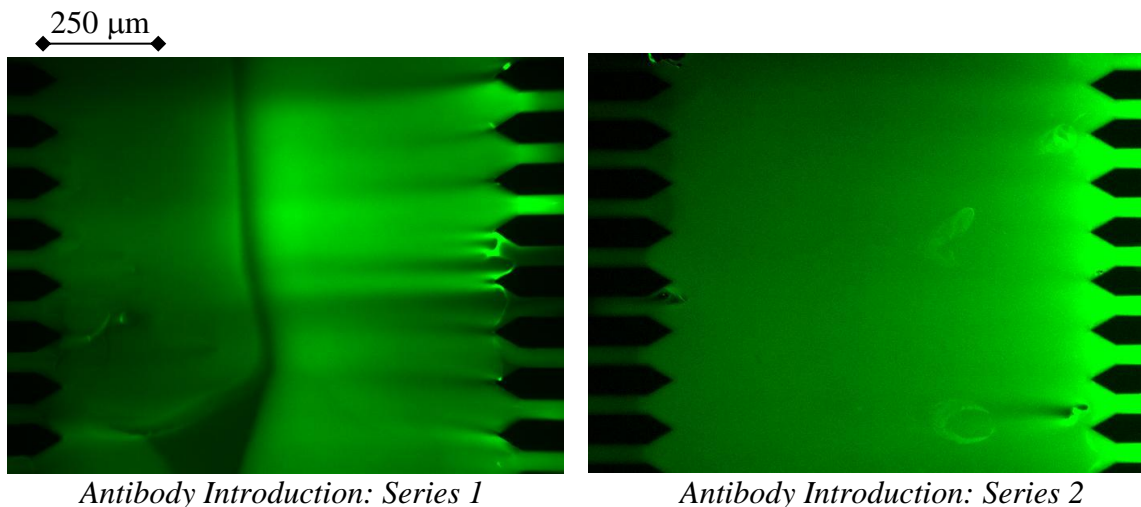
Figure 5.15: Two examples of the distribution of green fluorescent-labeled antibodies after being introduced across the central chamber of a 1 mm × 1.5 mm blotting chamber at 50 V/cm for 20 minutes.

Higher antibody concentrations at the point of incubation will result in more sensitive measurements. In seeking to define an adequate antibody introduction procedure, the most important metrics will be:

- <u>Time to equilibrium</u>: Antibody introduction time should be rapid (preferably less than 20 minutes), but applied electric fields should not strip away bound antibodies.

- <u>Antibody concentration</u>: Local concentration of antibodies within the central chamber can be measured from fluorescent intensity levels and will directly influence measurement sensitivity.

- <u>Spatial homogeneity of antibody distribution</u>: Deviation across the span of the central chamber should not differ by more than 30% to ensure comparable blotting analyses in disparate gel regions.

- Repeatability: Comparable antibody concentrations within the central chamber should be observed from experiment to experiment and from chip-to-chip by applying a standard loading procedure

Mass transport of blotting antibodies into the central chamber does not occur at a constant rate. When voltage control is employed and the current is monitored as a function of time, the current reading illustrated in Figure 5.16 is often observed. Currents 6 and 8 refer to the current monitored at electrodes 6 and 8 on the left and right sides of the device.
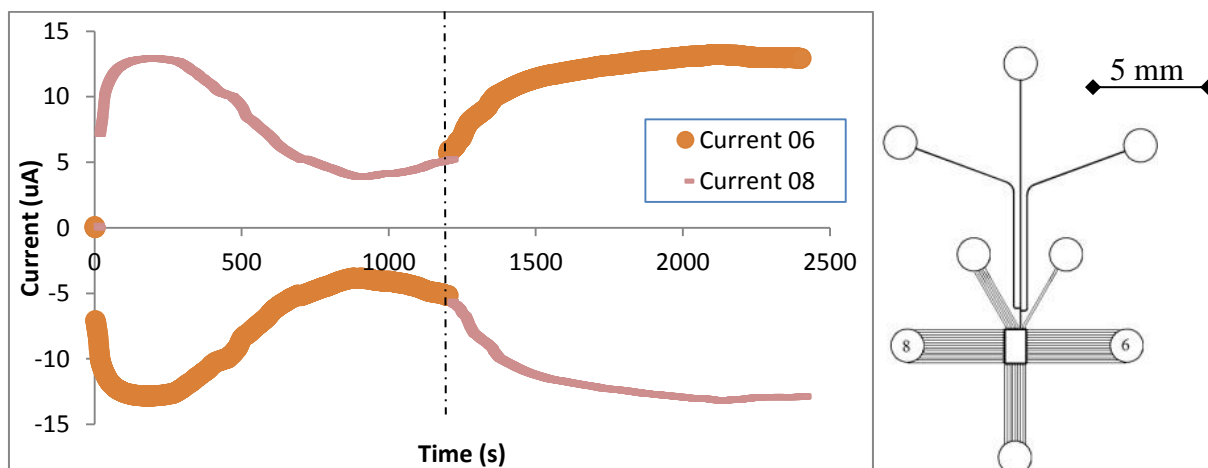
Figure 5.16: Lateral transport current is monitored as a function of time during the antibody introduction process, as proteins migrate from Electrode 6 towards Electrode 8. Dashed line indicates reversal of polarity after 20 minutes of probe introduction.

Figure 5.16 illustrates a typical experiment in which the current gradually decreases while a constant voltage is maintained across the central chamber. The graph plots a time course of 2400 seconds (40 minutes) where the polarity is reversed at $t = 20$ minutes, indicated by the dashed line. As the direction of the electric field is reversed, the transport current eventually returns to original levels.

71

Rather than a hardware limitation, time dependent changes in current may reflect a physical limit to the electrokinetic system wherein fewer charge carrying ions become available. If the magnitude of the transport current cannot be maintained due to a lack of charge carrying ions, the mass transport rate will decrease, even as the applied electric field strength remains constant. Current monitoring during the antibody introduction process provides an additional piece of information regarding the efficiency of antibody migration. It can be helpful to reduce the length of the control channels bordering the central chamber and to increase well volume to avoid this charge depletion effect.

As an example of the label free detection strategy, a 1 μM protein G sample labeled with AlexaFluor 488 was injected and immobilized upon an eBlot-7 device containing an antibody functionalized region against protein G. The final location of immobilized band is shown in Figure 5.17 (center) using a green fluorescent protein (GFP) filter set.

568 filter cube (pre-blot)   *488 filter cube*   *568 filter cube (post-blot)*
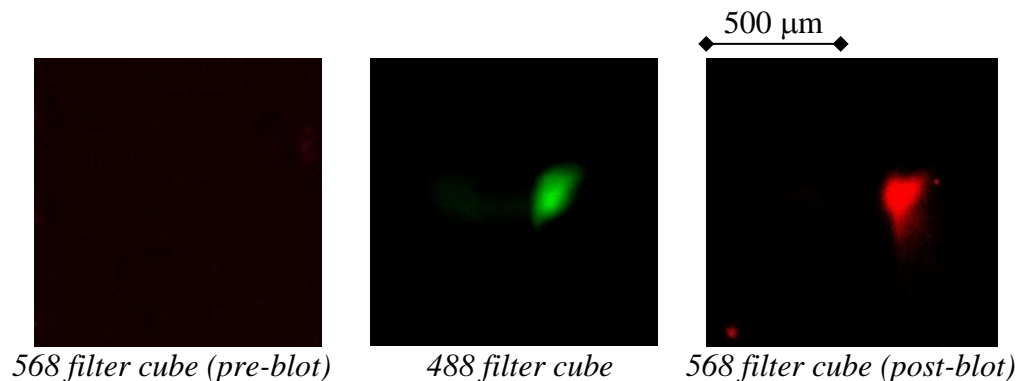
Figure 5.17: AlexaFluor 488 green labeled immobilized protein G target (center) is initially invisible at the red wavelength (left) until it is incubated with a Texas Red labeled anti-protein G probe (right).

After a 30 minute bovine serum albumin (BSA) blocking step, sandwich probe immunodetection of the Protein G band under the 568 nm filter cube was carried out by

introducing a Texas Red-labeled antibody solution (α-PG, AbCam 500 nM) at the side channel reservoir and applying a high E-field (150 V/cm) across the central chamber for 25 minutes. The antibody solution was incubated within the gel for 30 minutes and then flushed away from the central chamber leaving behind the fluorescent immunoprobed target (Figure 5.17, right). SNR for this label free measurement was ~39, which was comparable with the original labeled fluorescence signal measurement (SNR ~53).

As with any immunoassay, the ability to detect a target of interest depends upon the availability of a matched, working antibody component. In many cases, antibodies tested via on-chip immunoassay were incapable of binding with their intended target, even when those same antigen-antibody pairs demonstrated binding affinity in manufacturer's reports, published accounts or off-chip blotting validation formats. Several mechanisms are hypothesized as reasons for this differing behavior. For example, a binding epitope for a SDS-treated protein target may not be readily available in the folded native conformation due to steric hindrance, or the binding association constant (K_a) may become significantly reduced within a polyacrylamide matrix. Electrophoretic transport of the antigen may not allow enough time for binding interaction to occur when compared against conventional diffusive antibody transport, and the presence of an electric field could alter electrostatic charge-based affinity interactions.

5.5 Off-Chip Antibody Validation

While the on-chip separation and blotting processes are relatively rapid, preparation of a two dimensional microfluidic blotting device may require several hours when each chamber interior is fabricated through multistage photopolymerization of disparate gel

elements. Furthermore - once a blotting assay has been performed, an overnight soak within an acid bath is necessary before the glass chip can be reused. The availability of high-affinity antibody partners is of critical importance in performing on-chip immunoassay, but not all antibodies compatible with SDS-PAGE Western Blotting will be equally compatible with our electrophoretic on-chip immunoassay format. Practical considerations of time and labor make it difficult to screen large numbers of potential antibodies to find the highest affinity pair. Therefore, off-chip antibody screening strategies were necessary to increase experimental throughput.

It is possible that the capture and detection antibodies will exhibit competitive binding interactions for the same target epitopes, even when both capture and detection antibodies are polyclonal. Because the gel-based immunoblot works as a sandwich assay (Figure 5.18), the antibody functionalized immobilization matrix may reduce the protein target affinity for the detection antibody by occupying some of the same binding sites. This competitive interaction could therefore decrease measurement sensitivity.
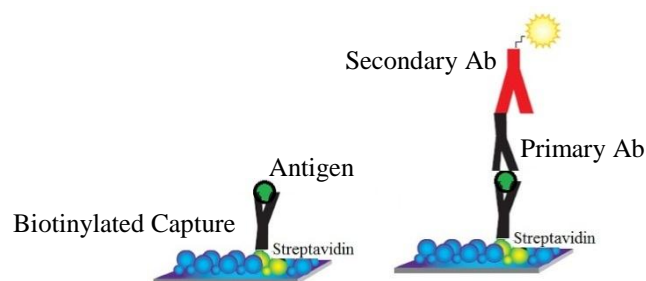
Figure 5.18: Biotinylated capture antibodies and detection antibodies may exhibit competitive binding interactions for the same targeted epitopes, thus reducing measurement sensitivity (Adapted from Thermo Scientific).

A glass slide dot blot experiment was performed to assess the effects of competitive binding interactions on antigen detection. Dot blotting on a glass surface provides a high throughput screening ability with excellent measurement linearity and sensitivity, as fluorescent antibodies can be directly imaged via high power laser scanning (Axon 4000B, Molecular Devices). Protein G samples at 500 and 250 nM were spotted on an Array-It SuperEpoxy microarray substrate slide using a handheld MicroCaster array tool. Spots on the left half of Figure 5.19 were incubated with Texas Red-labeled, rabbit polyclonal anti-PG for one hour. Spots on the right side of Figure 5.19 were first incubated with biotin-conjugated rabbit polyclonal anti-PG at equal concentration for one additional hour prior to incubation with Texas Red fluorescent anti-PG detection antibody.
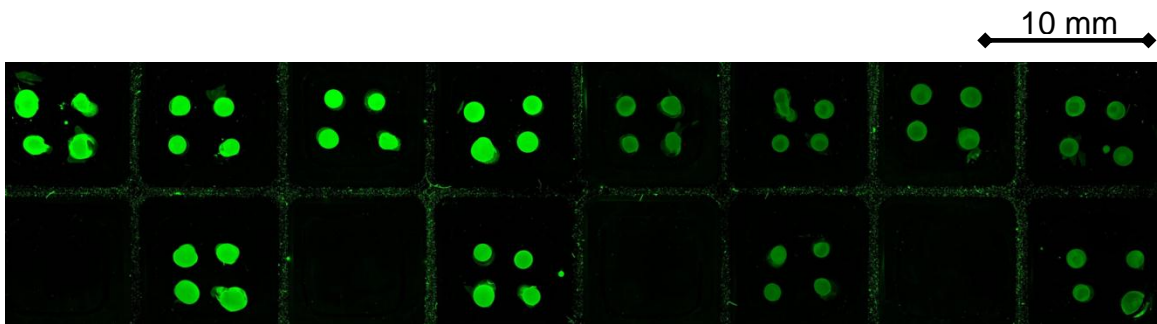
Figure 5.19: Laser scan at 532 nm of a protein G spotted microscope slide following incubation with anti-PG antibodies. Spots on the right half of the slide were first exposed to competitive binding interactions against a different form of non-fluorescent anti-PG prior to incubation with the detection antibody. Empty wells are negative controls.

Image analysis demonstrates that PG spots treated with the biotinylated anti-PG prior to incubation with the fluorescent antibody exhibit an average decrease of ~54% in intensity when compared against fluorescent detection antibody treatment alone (Figure

5.19). This result suggests a competitive interaction which could explain some of the low SNR values observed with the microfluidic label-free detection strategy.

5.6 Selectivity of Blotting Gel Capture

The selectivity of protein capture within the antibody functionalized gels allows one to utilize the blotting membrane for differentiating between targets of interest amongst a complex background - even if those targets are not completely resolved at the point of transfer. A two-dimensional blotting device with a 3% to 6%T stacking interface and an anti-PG blotting gel was used to demonstrate multianalyte separation and blotting in two colors (Figure 5.20).
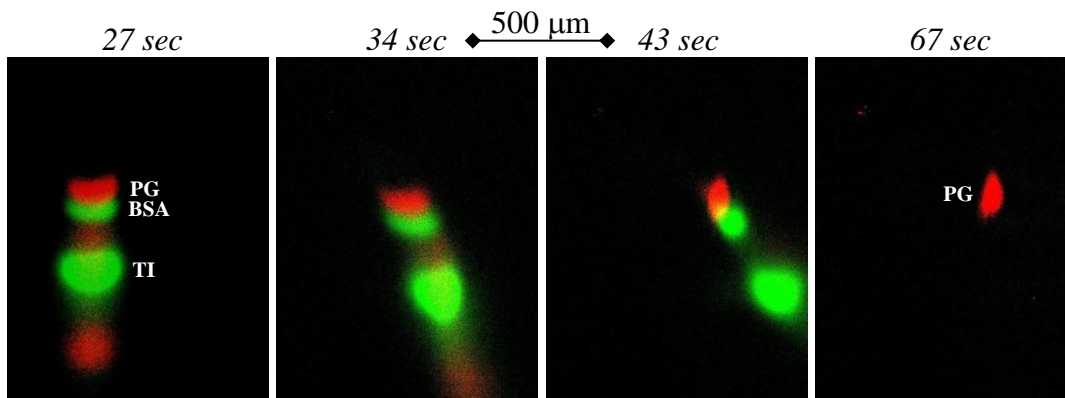
Figure 5.20: Green Channel: Trypsin inhibitor (TI) was included as a faster migrating internal standard at 110 nM along with BSA (330 nM). Red Channel: Protein G was included as the blotting target (330 nM).

Native Protein G and BSA migrate at similar velocities (6.6×10^{-5} cm^2 V^{-1} s^{-1} for PG versus 7.3×10^{-5} cm^2 V^{-1} s^{-1} for the electrophoretic mobility of BSA). Gaussian peak fitting analysis of the three proteins shows that PG and BSA could not be fully resolved at the point of sample transfer (Figure 5.21). However, the green labeled BSA and TI

were both able to pass through the anti-PG blotting gel, while the PG target became immobilized to the anti-PG region.
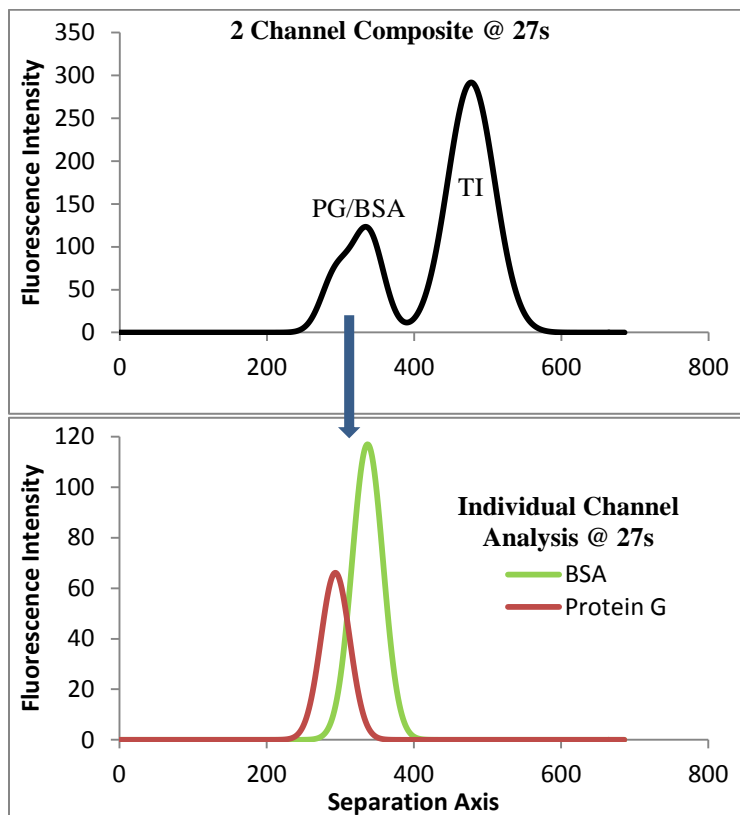
Figure 5.21:   Breaking down the multiband pattern into its individual spectral components indicates that BSA and Protein G bands are not completely resolved at the point of lateral band transfer (t = 27 seconds).

Non-target proteins which do not interact with the antibody gel simply pass through, leaving behind minimal background signal. Choosing a region of interest at the edge of the blotting interface and observing this ROI over the course of an experiment allows one to assess the capture specificity of each antibody functionalized region. ROIs were selected where protein entrapment and exclusion are most likely. Figure 5.22 represents post-blot fluorescence measurements performed for various combinations of analytes and

antibody functionalized gels. Each result was normalized to the maximum fluorescence observed at that ROI over the course of lateral transfer. Matched antibodies to protein G and CRP display high binding specificity for their partners and stronger fluorescence signals when compared against other combinations of antibodies and non-specific antigen targets. The analytes shown here are selected to demonstrate a range of protein sizes, ranging from 20-150 kDa.
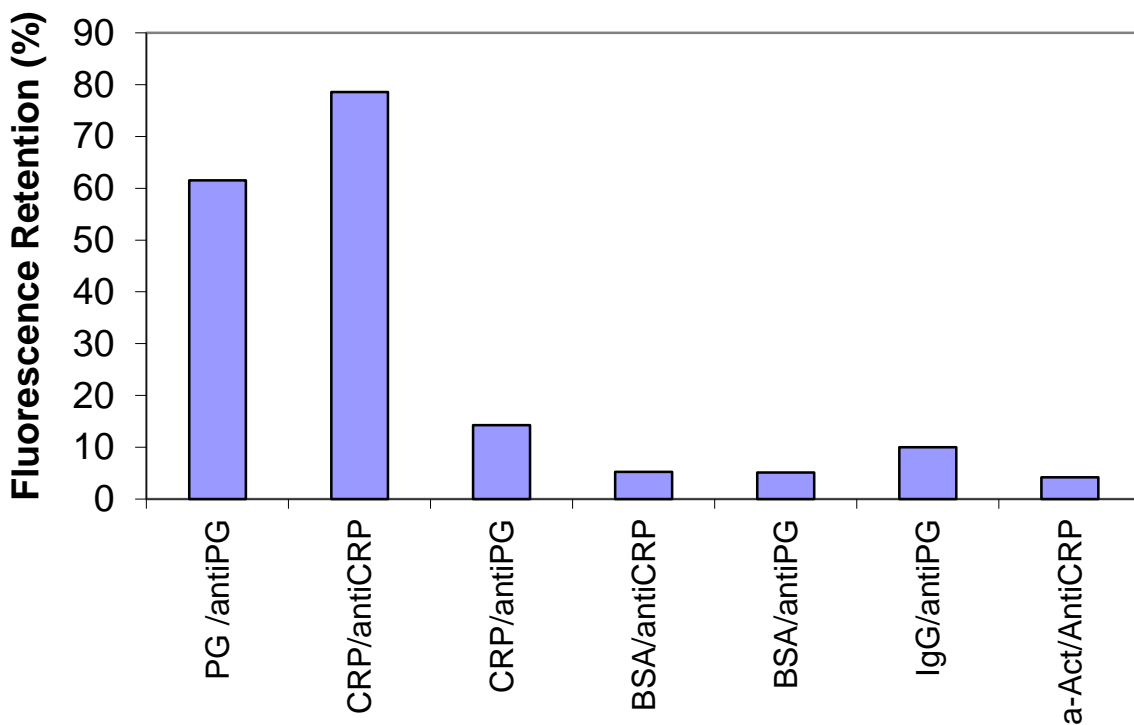
Figure 5.22: Antibody functionalized gels are specific for their matched binding partner and display minimal retention of off-target proteins. Antigen/antibody pairs are denoted by the y-axis label.

5.7 Membranes for On-Chip Enrichment

In a case where the initial target protein concentration within a sample may be low, an on-chip enrichment strategy can be utilized to enhance the sensitivity of detection [84].

The layout of the loading and injection channel ensures that a compact band of protein will be injected to the separation gel. However, the initial length of the injected protein plug is only about 500 μm and this represents only a tiny fraction of the sample volume available at the reservoir. A longer injection channel can provide more volume and thus, more sample mass for analysis. The layout and operation of the microfluidic blotting device places some practical limitations on injection volume, but gel-based enrichment membranes have been previously employed to boost the concentration of starting material in sample injections [85, 86]. These enrichment membranes work on the basis of size exclusion − similar to how a dialysis membrane sets a molecular weight cut-off limit. If a membrane composed of a high density gel (with a small pore network) can be used to exclude the target of interest based on its size, a continuous stream of material can be loaded against this filter, resulting in concurrent accumulation of target molecules. The enriched sample plug can then be eluted from the membrane where it is injected to the stacking interface/separation gel. A "virtually infinite" loading channel is theoretically possible when loading against an enrichment membrane − although practical considerations of loading time, fouling and gel breakdown must be taken into account.

Enrichment membranes were fabricated with a 2 kW 355 nm Nd:YAG laser (Teem Photonics) on a straight channel microfluidic chip. A polyacrylamide membrane was placed at the upper loading and separation channel network of the blotting device. The programming of the high voltage power supply was modified to include an on-chip enrichment step prior to sample separation. One potential concern was the possibility of target proteins passing through the enrichment membrane. A 40%T 6%C density membrane was chosen as a starting point and polymerized within the loading channel of a

two dimensional blotting device (Figure 5.23), and the UV laser exposure time was 60 seconds.

Brightfield   *t = 0 sec*   *t = 60 sec (loading)*

t = 62 sec (unloading)   *t = 64 sec (injection)*
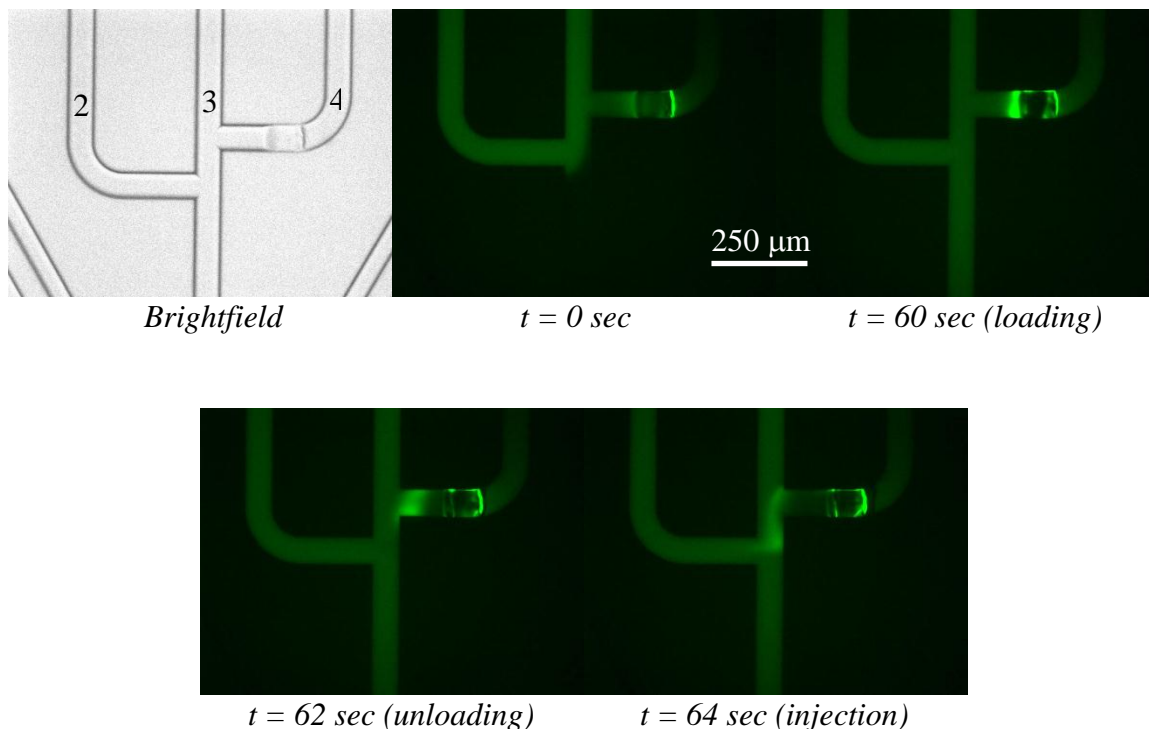
Figure 5.23: On-chip enrichment of GAPDH using a 40%T membrane proceeds over a one minute time course, with a concentrated protein band eluted at 63 seconds.

We tested the ability to preconcentrate analytes by loading against the 40%T membrane prior to sample separation and blotting. Figure 5.23 illustrates a typical experiment wherein the sample was primed across Reservoirs 2 and 3 (see brightfield for reference) before enrichment loading against the membrane (Reservoir 4) for 60 seconds. At $t = 60$ seconds, the electric field was momentarily reversed across Reservoirs 4 and 2 before the bolus was injected down the length of the separation channel ($t = 62$, 64 seconds).

Bands which resulted from these experiments demonstrated an average 3× increase in signal intensity after 60 seconds of enrichment when compared against baseline (non-enriched) bands, although several challenges were noted. For example, some fluorescent protein material leaked into the separation channel during the enrichment process and the high resistivity of the membrane causes a current drop at Reservoir 4 which inhibits protein enrichment. Protein leakage around the enrichment membrane could be minimized through careful current control at adjacent loading channels and by extending the UV polymerization process. A more compact injection profile could be achieved by polymerizing the enrichment membrane in-line with the separation channel (Figure 5.24).

250 μm
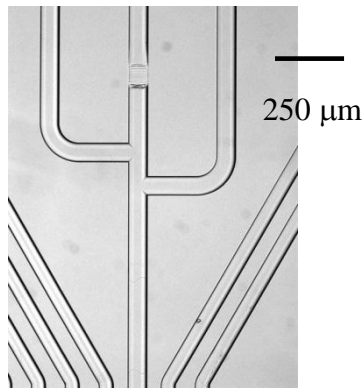
Figure 5.24: A 40%T enrichment membrane was placed at the central injection channel of a two dimensional blotting device.

A chrome-on-glass photomask was applied in conjunction with the UV laser to fabricate a 40%T 6%C enrichment membrane. Placement of the membrane within the central injection channel of a 2D blotting device (Figure 5.24) was made possible through the small aperture of the photomask. UV laser exposure time was extended to 90 seconds and the chip also contained 6%T separation and 3%T loading gels. GAPDH (37kDa, 40

nM prior to sample injection) was used as a model protein for sample preconcentration, and a sample image montage is shown in Figure 5.25.
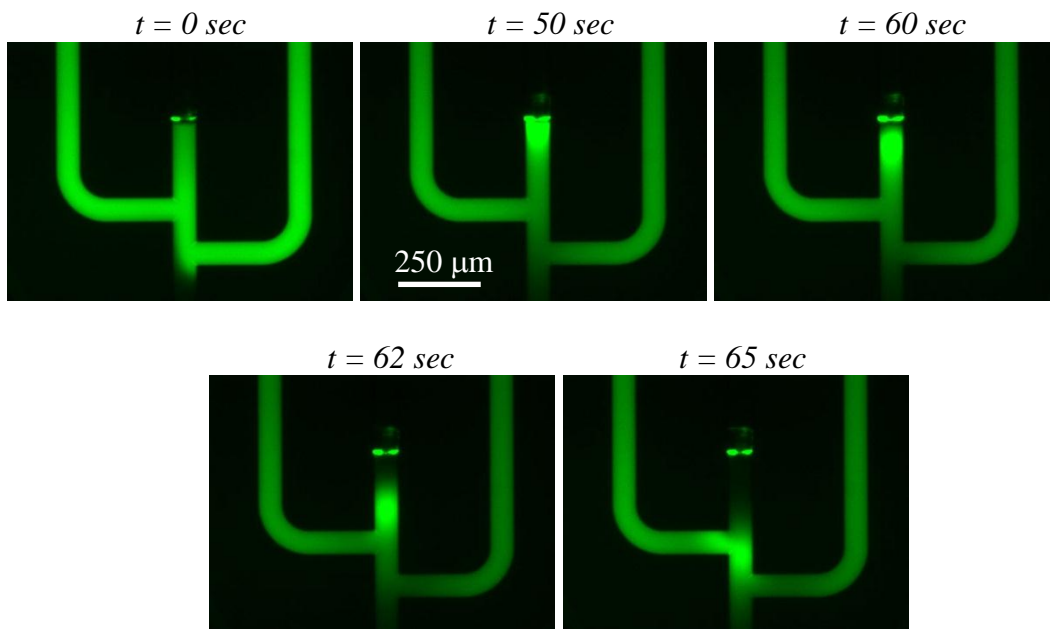
Figure 5.25: Enrichment of GAPDH (40 nM). The membrane enrichment process at the central injection channel begins at t = 0 sec, with commencement of band elution at t = 57 sec

The centrally located membrane was effective for sample enrichment, although the placement of the 40%T gel made it difficult to generate a sufficient electric field along the separation axis due to its high resistivity. Future designs seek to bypass this membrane by switching the separation field across two alternative electrode terminals when band elution from the membrane is complete. Some alternative chip designs with extra channels to bypass the preconcentration membrane and to increase the separation field strength are shown in Figure 5.26.
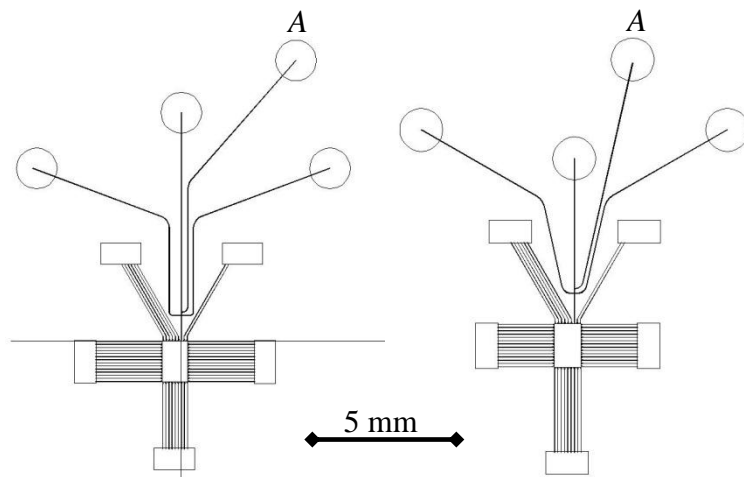
Figure 5.26: Sample devices featuring an additional injection reservoir ('A') which enable the separation field to bypass the centralized enrichment membrane.

6. 2D Native Immunoblot Analysis of Superoxide Dismutase 2

This chapter describes the application of the 2D native immunoblotting chip towards analysis of superoxide dismutase 2, an antioxidative mitochondrial enzyme of interest in studies of cellular metabolism. Performance requirements for a cell-based SOD2 assay and results from on-chip SOD2 immunoblotting are presented. The role of SOD2 acetylation is described in relation to its antioxidative activity and the charge shifted behavior of acetylated SOD2 is examined through isoelectric focusing experiments.

6.1 Overview of Superoxide Dismutase 2 Assay

To demonstrate the separative power of 2D microfluidic blotting and test the limits of the immunoassay, an eBlot-2 device was applied towards the analysis of superoxide dismutase 2 (SOD2), a 23 kDa mitochondrial enzyme. SOD2 is also known as manganese-fixing SOD (Mn-SOD) due to the presence of its manganese co-factor [87] which enables SOD2 to convert reactive oxygen species (O_2^-) into hydrogen peroxide (H_2O_2) and O_2 through the following half reactions:

$$(1) \qquad Mn^{+3}\text{-}SOD + O_2^- \rightarrow Mn^{+2}\text{-}SOD + O_2$$

$$(2) \quad Mn^{+2}\text{-}SOD + O_2^- + 2H^+ \rightarrow M^{+3}\text{-}SOD + H_2O_2.$$
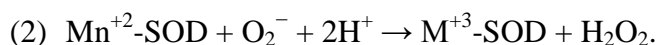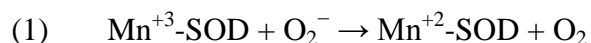
SOD2 is a prime target in studies of cellular metabolism due to its antioxidative activity. The free radical theory of aging posits that over time, the accumulation of intercellular reactive oxidative species (ROS) is responsible for damage to mitochondrial DNA,

causing mutations which result in cancer, age-related disease and loss of function [88]. Based on this paradigm, it becomes critical to understand the biochemical mechanisms underlying oxidative stress. Animal models such as genetic knockouts can be useful for investigating the cellular signaling pathways involved in regulating antioxidative activity. However, immunoassays can be challenging to work with when dealing with small animal models due to the poor sensitivity of antibody-based detection in dealing with limited sample volumes.

As an example, approximately 1×10^7 bone marrow cells are available from the tibial and femoral bones of a single mouse sacrifice. For an experiment requiring hematopoietic stem cells (HSCs), these bone marrow cells are sorted through a Fluorescence Activated Cell Sorter (FACS), isolating cells which bear surface markers indicating HSC lineage [89]. Therefore, it is estimated that the number of HSCs yielded from FACS would fall in the range of 10^3 to 10^4 cells per animal. Product literature for an SOD2 ELISA kit (DuoSet IC, R&D Systems) recommends loading 100μL of 6× diluted lysate initially containing 1×10^7 cells/mL. To accommodate this sensitivity requirement, HSC cells which are sourced from multiple animal specimens must be pooled together into a single sample. This process requires large numbers of animal sacrifices, while sample pooling causes a loss of data-point resolution which obscures subsequent interpretation of results.

The low end of this cell-based ELISA measurement falls at 10 ng of SOD2 per 10^7 cells, with a lower limit of detection at ~300 pg/mL (4 nM). Several challenges must be met in order to develop an on-chip blotting assay suitable for SOD2 study from a small cell population. These include:

- High resolution on-chip separation of SOD2 from a complex sample.

- Target binding at high efficiency.

- Primary/secondary antibody-based detection with appropriate sensitivity

6.2 Microfluidic SOD2 Blotting Assay

FLAG-tagged mouse SOD2 was expressed in HEK293T cells to serve as a model SOD2 sample. Transfected cells were either lysed with RIPA buffer to obtain raw cell lysate; or with immunopurification (IP) lysis buffer (50 mM Tris-Cl pH 7.5, 150 mM NaCl, 10% glycerol, 2 mM $MgCl_2$, 1 mM DTT and 1% NP40 supplemented with a complete protease inhibitor cocktail (Roche), trichostatin A, and nicotinamide). Immunopurification was achieved by incubating the IP lysate with FLAG antibodies for two hours, followed by extensive washing and free FLAG peptide elution.

The raw transfected SOD2 lysate was used to simulate SOD2 detection from a complex sample. A recombinant human form of SOD2 (rSOD2) was obtained from AbCam, and both the recombinant and transfected forms of SOD2 were labeled with AlexaFluor dyes. Two anti-SOD2 antibodies (B-1: mouse monoclonal, and FL-222: rabbit polyclonal) were obtained from Santa Cruz Biotechnology and biotinylated with the EZ-Link Sulfo-NHS-Biotinylation kit (Pierce) before incorporation to 6%T gel precursor solutions.

A colorimetric dot blot was used to assess the binding affinity of rabbit polyclonal anti-SOD2 for recombinant human SOD2 and 293T immunopurified SOD2 (Figure 6.1). The chromogenic detection mechanism uses a HRP-conjugated secondary antibody to produce a blue precipitate upon reaction with 3,3',5,5'-tetramethylbenzidine (TMB).

rSOD2 and transfected SOD2 (500 nM each) were both spotted in 0.2 µL droplets on a PVDF membrane and then incubated against a rabbit polyclonal anti-SOD2 primary antibody. The primary antibody incubation step was followed by a goat anti-rabbit HRP conjugate secondary antibody incubation and TMB substrate development (Figure 6.1). Results from the chromogenic dot blot demonstrate that the rabbit polyclonal antibody was immuno-compatible with both human recombinant SOD2 and transfected mouse SOD2 as well as enzyme linked detection methods. Thus, membrane-based dot blot experiments provided a quick and easy way to determine antigen-antibody compatibility.

Anti-Rabbit HRP-IgG   *rSOD2*   *Transfected SOD2*

5 mm
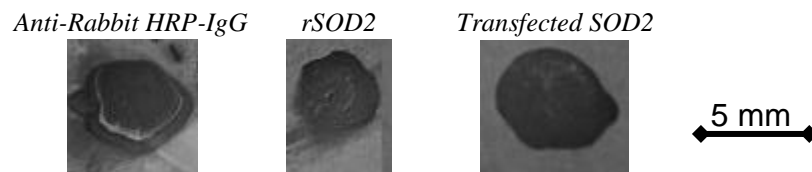
Figure 6.1: Colorimetric dot blot assay of rabbit polyclonal anti-SOD2 indicates binding affinity for recombinant human SOD2 and SOD2 from transfected 293T cells.

The two α-SOD2 capture antibodies were tested using labeled recombinant SOD2 (800 nM). Results suggest that that the binding affinity of the mouse monoclonal antibody is stronger than that of the rabbit polyclonal antibody (Figure 6.2), an observation which was compatible with results from dot blot validation experiments.
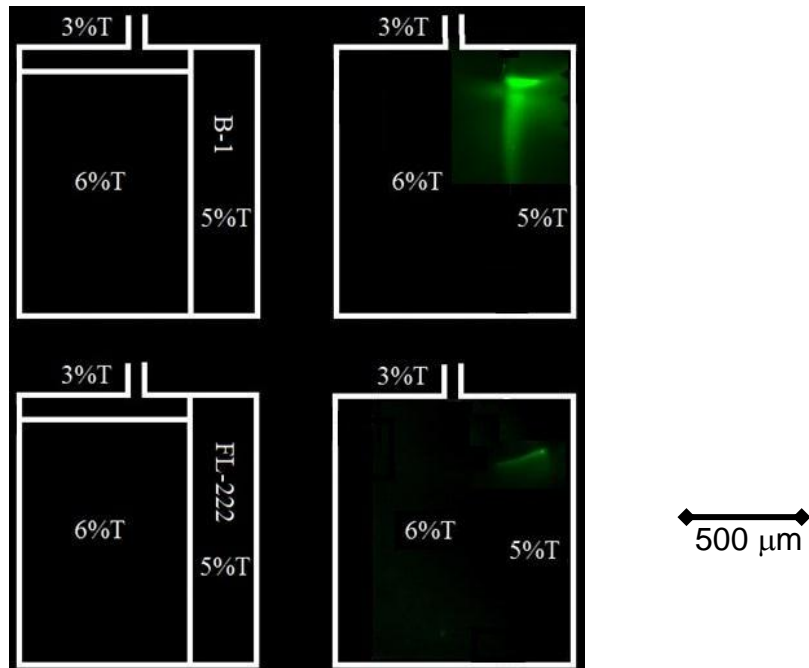
Figure 6.2: Blotting assessment of SOD2 on α-SOD2 gels. At right, post-blot fluorescence images of the central chamber are superimposed upon a chip schematic. Mouse monoclonal (B-1) capture antibody demonstrates a markedly higher binding affinity for SOD2 when compared against rabbit polyclonal FL-222

6.3 Acetylation of SOD2

The antioxidant activity of SOD2 has been linked to the presence of acetylated lysine groups surrounding its catalytic core [87]. Qiu *et al*. [69] demonstrate that substitution of the primary amine group with an acetyl group on lysine sites K53 and K89 of SOD2 has been correlated to decreased antioxidative activity in cells. The K53 and K89 lysine sites are critical residues adjacent to the active site on SOD2 and when exposed, may increase SOD2's electrostatic interaction with the negatively charged superoxide substrate. It is hypothesized that the activation of these sites serves as a molecular mechanism for regulating cellular oxidation levels and that the post-translational modification of these sites is regulated by SIRT3 - a member of the sirtuin family. Thus, the ability to detect acetylated SOD2 is of great interest – particularly if the acetylation measurement can be

quantitatively stated relative to the total abundance of SOD2. Antibody-based methods have been commonly used for the detection of protein acetylation sites, presenting a compelling opportunity for the implementation of a quantitative, microscale immunoassay towards acetylation analysis [90, 91].

Alternatively, isoelectric focusing can also be used to sort and identify target proteins based upon their isoelectric point while enabling characterization of subsequent protein modifications. The substitution of lysine's primary amine group with an acetyl group results in more negative charge conferred upon the entire biomolecule [92]. Thus, an acetylation event can be identified if the anticipated pI of the target protein is known and if the corresponding charge shift is detected. In a 1997 report from the Whitesides group [93], proteins less than 50 kDa in molecular weight were able to form resolved ladders of charge via capillary electrophoresis when modified with acetyl groups at regular increments.

The ability to differentiate acetylated SOD2 via isoelectric focusing and the possibility of combining this mechanism with acetylation specific immunodetection was validated by performing slab gel isoelectric focusing of acetylated SOD2. The resulting IEF gels were then immunoblotted separately against SOD2 and acetyl-lysine detection antibodies. To generate a model of acetylated SOD2, recombinant SOD2 was acetylated through incubation with acetic anhydride, as described in the work of Colton *et al.* [93].

Transfected SOD2, recombinant SOD2 and acetylated SOD2 samples were separated in four individual lanes in conjunction with a pI marker ladder mixture (Serva Electrophoresis) on a Novex pH 3-10 isoelectric focusing gel (Life Technologies) as illustrated in Figure 6.3. Each lane was set to contain 1 μg of SOD2. Two IEF gels with

identical samples constituents were run simultaneously, and the resulting focused

proteins were transferred to PVDF membranes that were blocked and incubated overnight

against acetylated-lysine or SOD2 specific primary antibody solutions. Following a one

hour incubation step with an HRP-linked secondary antibody, immunoblots were

developed using a HRP-reactive substrate for detection.
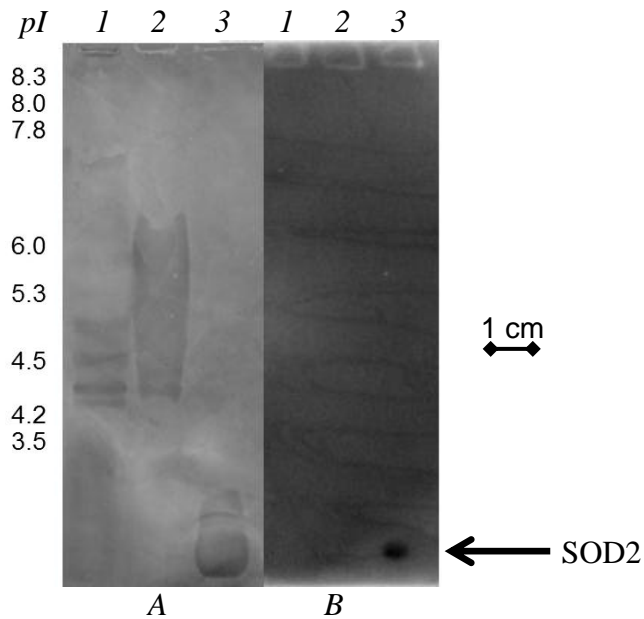
Figure 6.3: Anti-SOD2 (A) and anti-Acetylated lysine (B) immunoblots for acetylated SOD2 samples subjected to isoelectric focusing. Lanes 1, 2, and 3 correspond with transfected SOD2, recombinant SOD2 and acetylated SOD2, respectively. Reference pI marker values are shown at left.

Figure 6.3 demonstrates that the hyperacetylated SOD2 band was identified by both

anti-SOD2 and anti-acetylated lysine primary antibodies. Both antibodies produce a

blotted band which showed up prominently near the bottom of the gel. All forms of

SOD2 show up clearly when immunoblotting with the anti-SOD2 primary antibody (as

one would expect). However, only the acetylated SOD2 band indicates a strong affinity

for the acetylated-lysine antibody under these conditions. Both anti-SOD2 and anti-acetylated lysine blotting results consistently indicate a low pI value (~3) for the hyper-acetylated SOD2 sample. As we would expect, this value is charge shifted to a much more negative pI when compared against untreated, non-acetylated SOD2 bands. Taken together, these results suggest that isoelectric focusing can be used in conjunction with antibody-based techniques to provide separative power for identification of post-translational modifications upon specifically targeted proteins.

7. Demonstration of Single-Channel IEF Probing of Post-translational Modifications

The implementation of an on-chip strategy for isoelectric focusing and subsequent immunoanalysis of target proteins is described in this chapter. This technique is subsequently expanded towards the study of post-translational modifications (PTMs), which has emerged as a critical field for understanding proteomic regulatory mechanisms. Sample proteins are first separated through isoelectric focusing (IEF) before a combination of multispectral antibody probes is used to identify specific antigens bearing PTM residues. The co-localization of multiple fluorescent probes is interpreted to report and quantify PTM target proteins which exhibit a characteristic charge shift. As two examples, the microfluidic IEF-immunoassay is applied toward the analysis of phosphorylated heat shock protein 27 and acetylated SOD2.

The acetylation of SOD2 is just one practical example of how post-translational modifications (PTMs) are of critical importance to understanding proteomic regulatory and signaling mechanisms [94]. The diversity of the genome only accounts for a fraction of proteomic complexity and so the role of PTMs must be considered in order to describe the full range of protein function and relationships [1]. Many standard techniques for PTM analysis are resource intensive and may have difficulty dealing with complex or volume-limited samples. Results from mass spectrometry (MS) require sophisticated computer algorithms for interpretation, and signal-to-noise limits of the ion detection process can pose a challenge to the study of low abundance proteins [95]. MS is often

used in conjunction with antibody-based techniques which provide an enrichment step and further confidence in identifying a particular target [96]. In one experimental study alone, immunoaffinity enrichment was coupled with MS to identify over 6600 phosphorylation sites in ~2200 proteins [97]. However, these antibody-based techniques can require large amounts of starting material and sample prefractionation steps such as isoelectric focusing are often necessary.

In preparatory IEF for two-dimensional polyacrylamide gel electrophoresis (2D-PAGE), the focusing stage can require up to 12 hours if the process is allowed run overnight. However, a shift in charge alone may not be enough to conclusively identify a post-translationally modified protein target. In pan-specific Coomassie or silver-staining of a 2D-PAGE gel for a complex sample, the abundance of background proteins can obscure the observation of charge shifting for a single protein spot [98].

7.1 On-chip Isoelectric Focusing and Immunoprobing

A rapid on-chip isoelectric focusing technique was developed to integrate charge-based analyte separation with subsequent capture of all focused proteins to a polyacrylamide gel matrix [99]. The ability to immobilize all separated proteins onto a solid support provides the opportunity for combining the separative power of IEF with efficient immunoassay of targeted molecules. Operating the assay on a microscale format reduces sample volumes, opening up new opportunities for the analysis of biological samples which may be volume limited. Use of fluorescence immunoprobes for target detection provides measurement sensitivity comparable to existing techniques such as protein microarrays. Here, the basic operation of the IEF-immunoassay is

described, followed with an exploration of how the technique can be expanded towards the study of multiple targets in PTM analysis.

Assay Operation

The assay is carried out within a multifunctional polyacrylamide gel matrix in a glass microchannel (10.5 mm length × 70 μm width × 20 μm depth, Figure 7.1). Proteins are separated on the basis of isoelectric point (pI) and immediately immobilized to the gel matrix via UV photografting (Figure 7.2). Immobilized target proteins are then detected using fluorescent antibody probes. Subsequent fluorescence imaging provides a quantitative and spatially encoded data set where band position indicates the isoelectric point of the target protein relative to known pI markers.

1 mm

Figure 7.1: A glass chip housing three parallel microchannels forms the basic architecture for gel-based IEF immunoassay.

To begin the assay, a sample is first diluted in a loading buffer with UV-fluorescent pI ladder markers and titrated to pH 9.9 using sodium hydroxide. Approximately 2 μL of the diluted sample is required at the sample reservoir to perform the assay. Because target proteins are unlabeled, GFP is often included at a low concentration (~10 nM) as a surrogate protein to ensure effective protein loading, focusing and capture. The diluted

sample is electrophoretically introduced to throughout the microfluidic channel by applying an external electric field (200 V/cm) across the length of the device for five minutes. Electric fields are controlled using a programmable high voltage power supply, with platinum electrode tips placed at opposite reservoirs. Once the protein is loaded, channel wells are washed out thoroughly using a pipette, and solutions are exchanged with catholyte and anolyte buffers at opposite ends of the device. Isoelectric focusing proceeds through step-wise increases in field strength over the course of 17 minutes. The electric field is initiated at 50 V/cm, eventually reaching a maximum value of 300 V/cm.
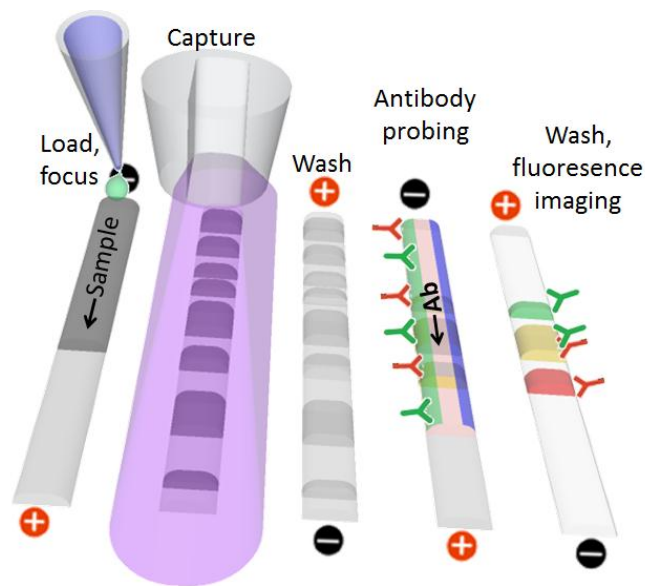
Figure 7.2: The stages of the microfluidic immunoassay include: sample loading (5 mins), sample focusing (17 mins), immobilization (<1 min), washout (35 mins) and fluorescent antibody probing/readout (60 mins).

When all proteins reach a focused equilibrium, the GFP and pI markers are imaged so that their positions can serve as a future reference for target pI measurements. An 11 second high intensity UV pulse from a Hamamatsu LC5 light source is used to initiate the

photoactive gel matrix. The key aspect of this gel is a benzephenone methacrylamide monomer (N-[3-[4-benzoylphenyl]formamido]propyl] methacrylamide, BPMAC) which is incorporated to the backbone of the polyacrylamide chain, forming a benzophenone polyacrylamide conjugate (BP-PA) gel. This monomer allows cross-linking of localized analytes when UV light excites the carbonyl groups of BPMAC into an electrophilic triplet state.

Following UV exposure and protein immobilization, an electrokinetic washout step (20 minutes at 150 V/cm, followed by 15 minutes at 200 V/cm) was performed to remove any proteins which were not captured by the BP-PA gel. Fluorescent probe antibodies are then electrophoretically introduced (200 V/cm for 5 minutes, then 100 V/cm for 20 minutes). After a brief incubation period, unbound probe molecules are removed by applying an electric field of 150 V/cm for 20 minutes, followed by 15 minutes at 200 V/cm. Subsequent fluorescent imaging of probed bands identifies targeted antigens through specific immunoaffinity interaction and provides quantitative measure of protein concentration, as well as a spatial position correlated to each target's characteristic isoelectric point.

The microscale format allows for streamlined control over reagent introduction, as well as rapid equilibration times for antigen-antibody binding so that the entire assay is complete within 120 minutes. Monitoring the focused GFP bands before and after UV capture suggests that approximately 1% of target proteins are effectively bound to the BP-PA gel. Although this degree of capture efficiency may seem low, the isoelectric focusing process enriches the sample by a factor of ~100 prior to target immobilization. This enrichment factor is geometrically determined, as the sample is initially loaded

through the full length of the channel (10 mm) before proteins are focused towards an equilibrium band position of approximately 100 μm width. Therefore, the amount of protein captured and localized to the BP-PA gel is roughly equivalent to the starting concentration of target protein within the bulk sample.

<u>Assay Reagents</u>

The BP-PA gel consists of BPMAC (synthesized in-house) at 5 mM in a 4%T polyacrylamide gel matrix. BPMAC monomer was synthesized via reaction of N- (3-aminopropyl)methacrylamide hydrochloride (APMA, MW: 178.7, Polysciences) with the succinimidyl ester of 4-benzoylbenzoic acid (BP-NHS, MW: 323.3, Invitrogen) in the presence of catalytic triethylamine (TEA) in dimethylformamide (DMF). The reactants and TEA (50 mM each in DMF) were incubated overnight at room temperature, then centrifuged at 18×10^3 g for 5 minutes. The supernatant was incubated on a tube inverter for 24 hours with 30 mg isothiocyanate-functionalized (primary amine reactive) polystyrene beads (Sigma-Aldrich) for every 100 μmol of APMA. The mixture was then spun at 18×10^3 g for 5 minutes and the supernatant was filtered through a 0.2 μm syringe filter. A 10-fold excess of acetone was added to the filtrate and the mixture was vacuum dried until the BPMAC product reached a white powder form.

Gel buffer components include CHAPS at 3% w/v, nondetergent sulfobetaine (NDSB) 256 at 200 mM and 10% sorbitol. A pH 3-10 Pharmalyte ampholyte mixture (GE Healthcare) in the BP-PA gel and loading buffer results in a linear gradient from pH 3 to 10 across the length of the channel. The antibody probe/washout buffer consists of 3% CHAPS, 15 mM glycine, 200 mM NDSB 256 and 10% sorbitol at pH 9.9. The

catholyte buffer consists of 20 nM arginine and 20 mM lysine at pH 10.1, while the anolyte consists of 70 mM phosphoric acid. Fluorescent pI markers ranging from pH 4.0 to 9.0 were purchased from Sigma Aldrich.

Device Fabrication

Photomasks to generate the glass channel network were designed in-house, and devices were fabricated at a microfluidic chip foundry (Caliper Life Sciences) using standard photolithography, wet-etch and glass bonding techniques. Prior to use, glass channels were flushed with sodium hydroxide and silanized to facilitate the adhesion of polyacrylamide to the channel surface. All polyacrylamide gels were made with dilutions starting from a 30%T, 2.6%C stock solution (37.5:1, acrylamide/bisacrylamide ratio) from Sigma Aldrich. Once the gel precursor solution was prepared, ammonium persulfate (APS) and tetramethylethylenediamine (TEMED) chemical initiators were mixed into the precursor at a final concentration of 0.08% w/v each. The precursor was then degassed for 60 seconds before being introduced to the reservoir wells and wicked through the microchannel structures. The catalytic activity of APS and TEMED resulted in complete polymerization of the gel matrix within 10 minutes.

7.2 Multispectral Antibody Probes for PTM Detection

Antibody probes specific to broad classes of post-translationally modified residues (e.g. phosphorylated tyrosine, acetylated lysine, etc.) are commercially available and have been well-characterized [100]. We investigated the ability to apply these modification-specific antibodies towards the quantitative measurement of immobilized

PTM proteins separated through microfluidic IEF. A multispectral detection approach determines the relative abundance of modified versus non-modified target proteins by comparing the signals arising from multiple colocalized fluorescent probes. This measurement strategy is analogous to how optical signals from red/green dye hybridization provide information regarding the up-regulation or down-regulation of gene expression relative to a control in DNA microarray experiments [101].

Rabbit polyclonal anti-phosphoserine (α-PhoS, AbCam) and mouse monoclonal anti-acetylated lysine (α-AceK, Biolegend) antibodies were labeled with AlexaFluor 568 according to manufacturer's instructions (α-PhoS*, α-AceK*, asterisk indicating a fluorescent conjugate). Fluorescence imaging was conducted on an Olympus IX71 inverted microscope equipped with an X-cite eXacte fluorescence light source (Lumen Dynamics) and a mechanical shutter (Sutter Instruments). Images were acquired through a 10$\times$ objective (Olympus UPlanFL) and Andor iXon3 885 Electron Multiplying CCD camera. Fluorescence bandpass filters employed in this work include the XF02-2 (Omega Optical), 49011 and 49008 (Chroma) filter sets for UV, green and red wavelength imaging, respectively.

The specificity and potential cross-reactivity of a two-color PTM measurement was assessed by testing an acetylated-lysine antibody against acetylated and non-acetylated forms of bovine serum albumin. Acetylated BSA (Life Technologies) was mixed with non-acetylated BSA (Sigma-Aldrich) at 1 μM each, and then loaded together into a BP-PA IEF microdevice. After isoelectric focusing, bands were immobilized via UV exposure and probed with green-labeled mouse monoclonal anti-BSA (AbCam) and red-labeled anti-Acetylated Lysine at 450 nM each.
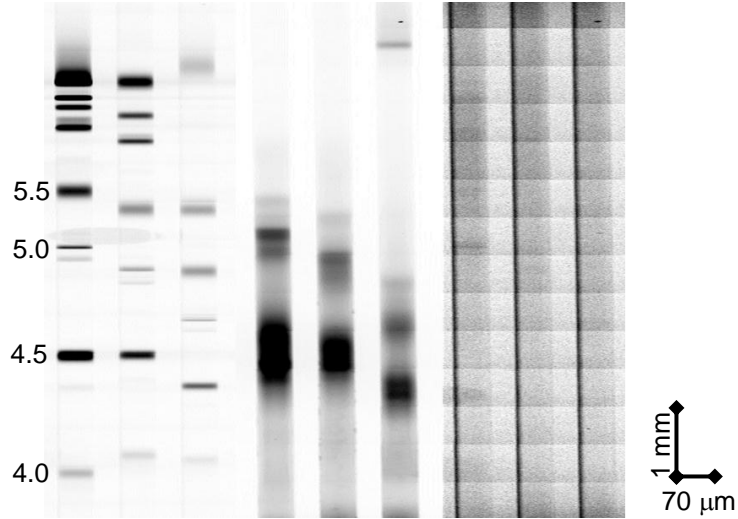
Figure 7.3: pI Ladder (left), anti-BSA blot (green, center), anti-Acetylated Lysine Blot (red, right)

After 25 minutes of loading and 35 minutes of washout, two resulting bands could be detected. The prominent band at pH 4.7 represented the standard isoelectric point of BSA, whereas the band at pH 5.3 may represent a degradation product [102]. No bands were observed in the red wavelength, suggesting that acetylated BSA falls outside the range of the on-chip pH gradient (as acetylated BSA has a reported isoelectric point below pH 4). Due to this mismatch in operating range, a mask-based approach was employed to photopattern protein plugs for use in antibody validation tests.

To selectively photopattern a region of BP-PA gel with antigenic material, a protein (acetylated-BSA in this case) was introduced at homogenous concentration across the channel by applying an electric field of 200 V/cm for 5 minutes. Once the electrophoretic filling of the channel was complete, a Mylar photomask with a 100 µm aperture was applied in conjunction with a high intensity UV pulse (11 seconds) to selectively expose a plug-like region of the gel for protein capture. Unbound protein

molecules were removed from the channel using a 35 minute electrophoretic washout step (200 V/cm). In the case of acetylated-BSA, a residual immobilized concentration of 450 nM was estimated within the BP-PA gel plug.
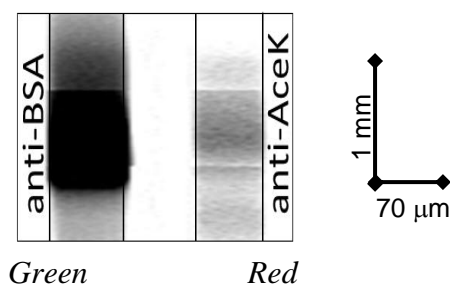
Figure 7.4: Anti-BSA (green channel, left) and anti-acetylated lysine (red channel, right) immunoblot experiments both confirm the presence of acetylated BSA within the photopatterned gel plug.

Figure 7.4 illustrates the fluorescence signal arising in two spectral channels following the washout step after anti-BSA and anti-acetylated lysine antibodies were applied to the photopatterned region at 500 nM each. The anti-BSA signal was detected at SNR = 130 ± 22.9 (n = 3), while fluorescence signal from anti-AceK was measured with a SNR of 20.5 ± 4.1 (n = 3). The antibody-to-antigen binding ratio was almost exactly the same between the photopatterned acetyl-BSA plug of Figure 7.4 and the nonacetylated BSA band immobilized after IEF in Figure 7.3 (0.71:1.0 compared to 0.68:1.0). This result suggests that little cross-reactivity exists between the BSA and acetyl-lysine specific antibodies, and that isoelectric focusing process does not reduce binding affinity for a matched detection antibody. Binding stoichiometries were calculated by correlating the initial concentration of the antigen to the calibrated fluorescence signal arising from the antibody probe.

As a negative control, a plug of cytochrome C (non-acetylated, Abcam) was also masked and immobilized through UV photopatterning at the center of a microfluidic channel. Following a washout step, the cytochrome C region (110 nM) was simultaneously probed with anti-acetylated lysine and mouse monoclonal anti-cytochrome C (α-CytC, AbCam), both at 500 nM. Results after dual-probe washout are shown in Figure 7.5 using identical exposure and contrast settings.
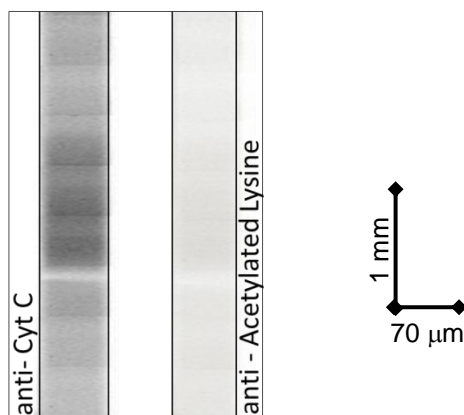
Figure 7.5: Anti-cytochrome C (left, green channel) displays a positive signal for the cytochrome C peptide, while anti-acetylated lysine does not indicate presence of acetylated lysine residues within this sample (right, red channel).

Results indicate that the non-acetylated cytochrome C plug produces a high signal (SNR = 21.3 ± 1.9, $n = 3$) when blotted against the cytochrome C specific antibody. However, little signal is observed (SNR = 3 ± 0.5) when this same region was blotted against the antibody for acetylated lysine. This result was anticipated, as the cytochrome C peptide was not known to bear an acetyl-modified lysine group.

7.3 IEF Probing for Post-Translational Modification Analysis

Next, the integrated workflow of the PTM immunoassay was validated through on-chip isoelectric focusing of a known PTM standard. A commercially available standard (Affymetrix) consisted of multiple forms of cytochrome C with varying numbers of acetylated lysine groups that result in "rungs" of distinct charge [103]. This cytochrome C ladder was first characterized with a Novex pH 3-10 IEF gradient slab gel, along with a reference pI ladder.
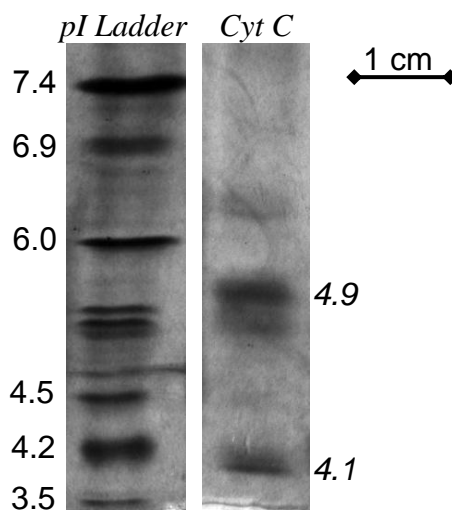
Figure 7.6: Two bands representing isoforms of cytochrome C are visible following slab gel IEF separation and subsequent Coomassie stain. Positions of the cytochrome C isoform bands (right) are compared against known pI values of a reference ladder (left).

The IEF gel was then subjected to a Coommassie stain to determine total protein content. The stained IEF gel of Figure 7.6 demonstrates two prominent bands of cytochrome C at pI 4.9 and 4.1, matching reported pIs from product literature [103]. A comparison of the intensities for these two bands also demonstrates that the concentration of cytochrome C isoforms within the ladder is not equally distributed.

103

This same cytochrome C ladder (460 nM) was then assayed via microfluidic IEF immunoblotting. After focusing and immobilization steps, the unlabeled sample was probed simultaneously with a green fluorescent antibody to cytochrome C (α-CytC, 500 nM) and a red fluorescent antibody to acetylated lysine (α-AceK, 500 nM). Results from this experiment are illustrated in Figure 7.7. The anti-cytochrome C detected a band at pI 4.9 ± 0.1 (SNR $= 82.6 \pm 14.8$, $n = 3$), whereas the acetylated lysine antibody was able to identify bands at pI 4.9 ± 0.1 (SNR $= 68.0 \pm 3.8$) and pI 4.1 ± 0.1 (SNR $= 47.4 \pm 2.4$).

The measured pI values agree with slab gel IEF and manufacturer reported pI, and correlation of pI from cytochrome C and acetyl-lysine immunoblotted bands suggests that both isoforms of cytochrome C are acetylated. Average separation resolution (*SR*) between consecutive "rungs" of the cytochrome C ladder was 1.31 ± 0.16 and the IEF gradient was linear ($y = 1.95x - 1.62$, $R^2 = 0.98$, where *y* represents pH and *x* represents the position of the band in mm). Based on the pI ladder distribution, the minimum resolvable pI difference was 0.1, with a peak capacity of 80 (assuming average bandwidth of 100 μm).

Protein concentrations for these two isoforms were determined by comparing the intensities of the two Coomassie stained bands. When fluorescence signals was normalized to relative protein concentration, the band at pI 4.1 exhibits an α-AceK* signal 22% higher than that of the cytochrome C band at pH 4.9. This result matches the anticipated difference in acetylation for the lower pI band – an expected 25% increase in PTM residues.
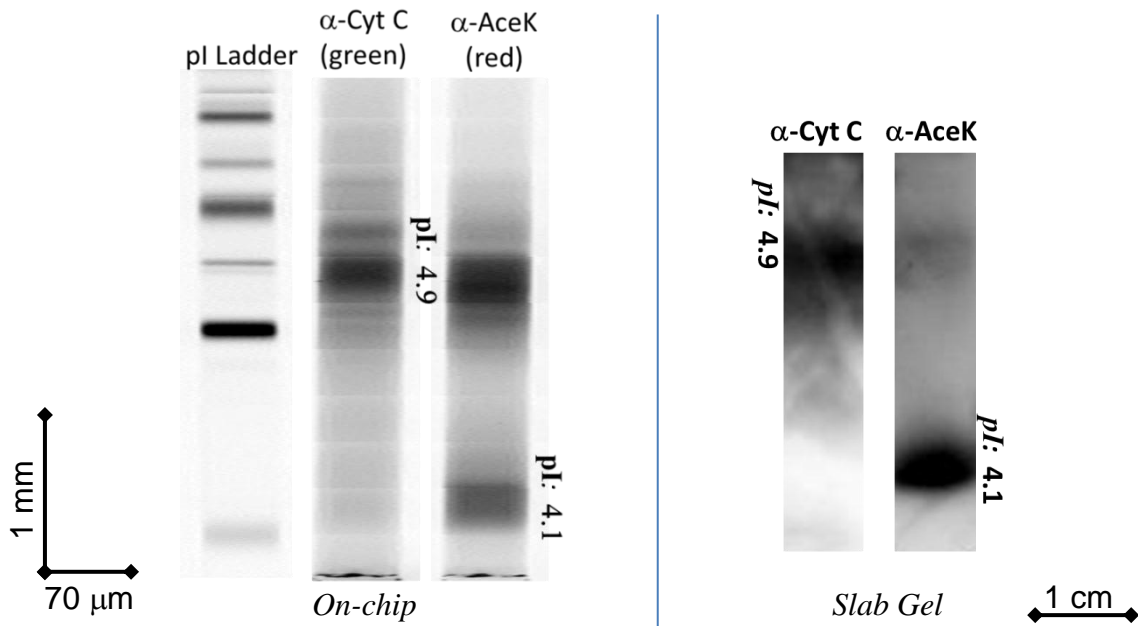
Figure 7.7: An acetylated cytochrome C sample is probed with antibodies to cytochrome C and acetylated lysine. Results from on-chip IEF-immunoassay display band patterns identical to separation and probing results obtained with the same antibodies through slab gel IEF and membrane based immunoblotting.

Results from on-chip blotting of cytochrome C were compared against analogous results from slab gel IEF immunoblotting. Cytochrome C ladder proteins separated upon a pH 3-10 IEF gel were transferred to a PVDF blotting membrane and detected using α-CytC and α-AceK. Targeted signals were then developed using HRP-linked secondary antibodies and chemiluminescent substrates, as illustrated on the right side of Figure 7.7. The band patterns observed in slab gel immunoblotting of the cytochrome C ladder are identical to band patterns observed from on-chip immunoassay. The anti-acetylated lysine probe demonstrates a stronger affinity for the cytochrome C band of lower pI, as these bands are expected to bear more acetylated residues. The cytochrome C antibody showed a stronger affinity for the band at higher pI, suggesting that the increased acetylation may obscure binding sites upon the cytochrome C epitope.

In comparison to slab gel IEF, the on-chip focusing process required only 17 minutes for completion (versus 150 minutes in the gel-based format) and consumed only 10 μL of anolyte/catholyte solution (versus 800 mL for a slab gel). Chip-based blotting of cytochrome C required 150 ng of probe antibody, whereas the slab gel/membrane blotting format required 50 μg of the same antibody. The consistent band patterns observed across slab gel and on-chip IEF immunoassays demonstrate the differential specificity of the two antibody approach, as well as the charge shifting of acetylated protein forms. Simultaneous multispectral detection allows one to visualize target protein PTMs based upon specific co-localized fluorescence signals.

7.4 IEF Phosphorylation Analysis

Phosphorylation is perhaps the most widely studied PTM, due to the ubiquitous nature of protein kinases which regulate cellular function [104-108]. It is estimated that one third of the human proteome becomes a targeted phosphorylation substrate at some point during the life cycle [109]. The versatility of the PTM-specific IEF immunoassay was tested by examining a recombinant phosphorylated form of heat shock protein 27 (pHSP27, AbCam), a chaperone protein bearing a known phosphorylated residue at serine 82 [110].

pHSP27 was spiked into loading buffer at 600 nM and then focused, immobilized and probed via on-chip IEF-immunoassay. Three different antibodies were tested against focused pHSP27 in separate experiments. These include: α-PhoS* (pan-specific for all phosphoserine), goat polyclonal α-HSP27* (specific for all forms of heat shock protein 27, Santa Cruz Biotechnology) and rabbit polyclonal α-pHSP27* (specific for the

phosphoserine 82 epitope of pHSP27, Santa Cruz Biotechnology). All antibodies were fluorescently labeled and utilized at 500 nM, with post-blotting results illustrated in Figure 7.8.
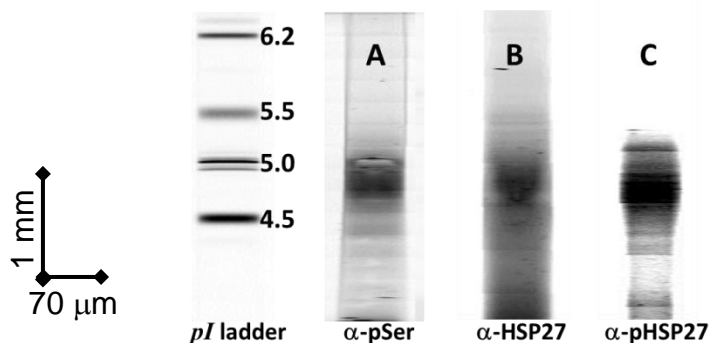
Figure 7.8: pHSP27 bears a phosphorylated serine residue and can be detected using (A) anti-phosphoserine, (B) anti-HSP27, and (C) anti-pHSP27 via on-chip IEF immunoassay. In all cases, the immunoprobed band is identified at pI 4.7.

Figure 7.8 demonstrates that the pHSP27 band was consistently identified by all three antibodies at pH 4.7 ± 0.1 ($n = 3$). Immunoprobing with α-HSP27* resulted in a SNR of 178.8 ± 29.5, while immunoprobing with α-PhoS* and α-pHSP27* resulted in SNRs of 80.3 ± 18.2 and 79.8 ± 8.4, respectively. The close correlation of the α-PhoS* and α-pHSP27* signals suggest that both antibodies are effective in binding the targeted phosphoserine residue of pHSP27.

In a negative control experiment, a non-phosphorylated HSP27 sample (AbCam) was analyzed by microfluidic IEF and immunoprobed with α-HSP27*, yielding a measured band at pI 5.1 ± 0.1 (n = 3). This observed pI difference suggests that the phosphoserine modifications of HSP27 results in a charge shift of -0.4 pH units, a result which is consistent with phosphorylation [111]. Immunoprobing the same sample with α-PhoS* and α-pHSP27* yielded no detectable signal, indicating no cross-reactivity. Intensity of

the α-HSP27* fluorescent signal was consistent (< 10% variation) in probing pHSP27 or HSP27, suggesting that the phosphorylation of pHSP27 does not alter the targeted epitope of α-HSP27*.

Top: pI ladder
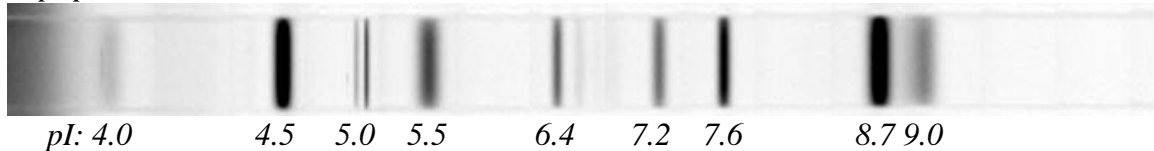
Middle: Anti-phosphoserine probe of phosphoenriched 3T3 lysate

Bottom: Anti-phosphoserine probe of control 3T3 lysate

Figure 7.9: Immunoprobing for phosphoserine within a phosphoenriched lysate indicates an abundance of phosphorylated serine residues when compared against a negative control (non-enriched) lysate sample.

To illustrate the pan-specific nature of the phosphoserine antibody, lysate from an NIH/3T3 cell line which was phosphoenriched through immobilized metal ion affinity chromatography (Santa Cruz Biotechnology) was assayed via on-chip IEF and anti-phosphoserine immunoprobing. As expected, the anti-phosphoserine generates a broad smear when tested against this phospho-enriched lysate sample. This smear pattern does not occur to the same extent when anti-phosphoserine is incubated against a normal (non-enriched) 3T3 cell lysate sample. Taken together, these results demonstrate that on-chip

immunoprobing can be designed to identify a broad class of modified residues (i.e. phosphoserine) or some highly specific target epitope (S82 in the case of α-pHSP27).

7.5 Isoelectric Focusing of SOD2

Moving towards on-chip IEF immunoanalysis of SOD2, we next characterized the isoelectric focusing behavior of SOD2 in a standard Novex pH 3-10 isoelectric focusing gel. Two forms of recombinant human SOD2 (rSOD2, labeled and unlabeled) were focused on an IEF slab gel, with each lane containing 1 μg of rSOD2 protein. The resulting slab gel was fixed and silver stained at the conclusion of isoelectric focusing, as illustrated in Figure 7.10.
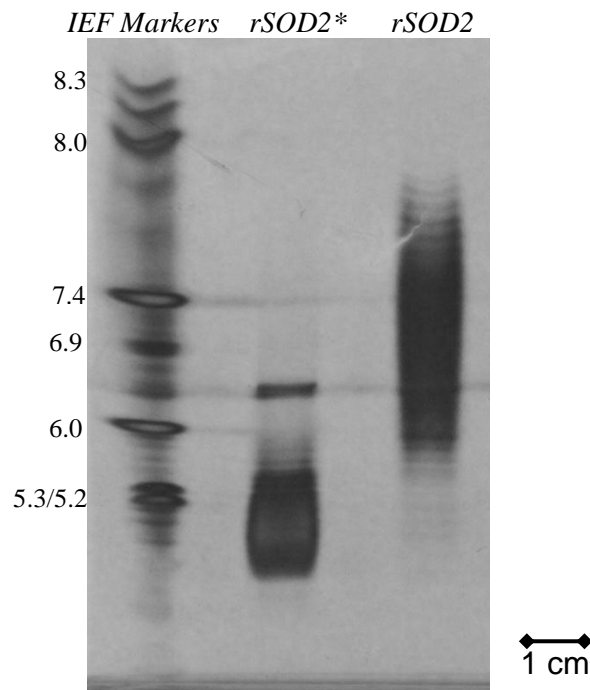
Figure 7.10: Slab gel isoelectric focusing of recombinant SOD2 reveals charge shifting of fluorescent conjugates.

The resulting rSOD2 peak exhibited a surprising degree of heterogeneity for a recombinant protein – with a scalloped band pattern ranging from pH 4.5-6.9, centered at pH ~6.0. The AlexaFluor dye conjugate dramatically alters the pI distribution of fluorescently labeled rSOD2*, bringing it to a pI (~3.5) lower than the previously reported pI of SOD2 at pH 7.7 [112]. This charge shift in response to a fluorescent conjugate was consistent with literature [113] as well as observed migration behavior of fluorescently labeled rSOD2 via native PAGE.
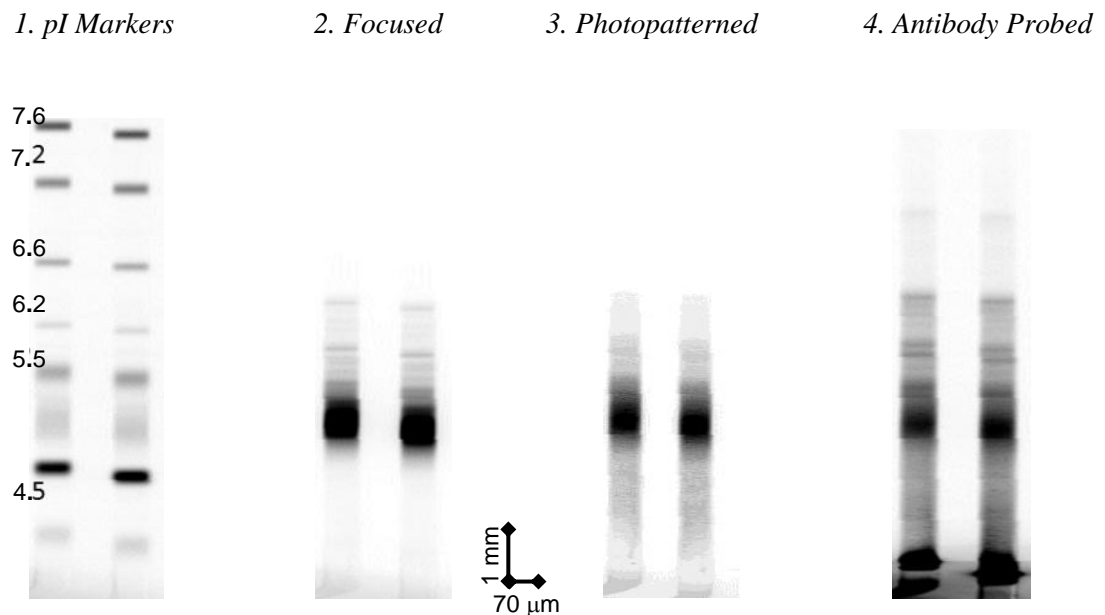
Figure 7.11: Immunodetection with fluorescent probes to SOD2 recovers the presence of SOD2 bands which were not visible after sample washout.

Given the ability to identify charge shifted forms of SOD2 on a slab gel, we then directed attention to the detection of SOD2 in an on-chip IEF immunoassay (Figure 7.11). Green fluorescent rSOD2* was introduced at 100 nM, then (2) focused, (3) photopatterned, and (4) probed with a red monoclonal antibody to SOD2 in a BP-PA IEF microdevice. The antibody probe step revealed several forms of SOD2 that were visible

after isoelectric focusing (2), but not visible directly following the UV-immobilization and washout stage (3). This result demonstrates that antibody probing can actually increase sensitivity for some protein forms when compared against direct antigen fluorescent labeling. The major protein band shows up at pH ~4.7 which falls below the reported pI value for SOD2 due to the Alexa Fluor dye conjugate. Taken together, these results demonstrate that direct target labeling is undesirable because optical measurements of the fluorescently labeled target molecules can be less sensitive than measurements arising from a matched fluorescent antibody probe. Furthermore, labeling of a complex sample can be practically impossible and dye conjugates would cause charge shifting to bias pI measurement.

IEF Probing of Transfected and Immunopurified SOD2

Looking forward, we sought to demonstrate measurement of an unlabeled SOD2 sample from immunopurified transfected 293T cells. Purified SOD2 from the transfected cell line was diluted into loading buffer, along with GFP loading control and reference pI markers. The mixture was introduced on-chip for isoelectric focusing, then immuno-probed with fluorescent anti-SOD2 (green label, 500 nM) and anti-acetyl-lysine (red label, 500 nM).
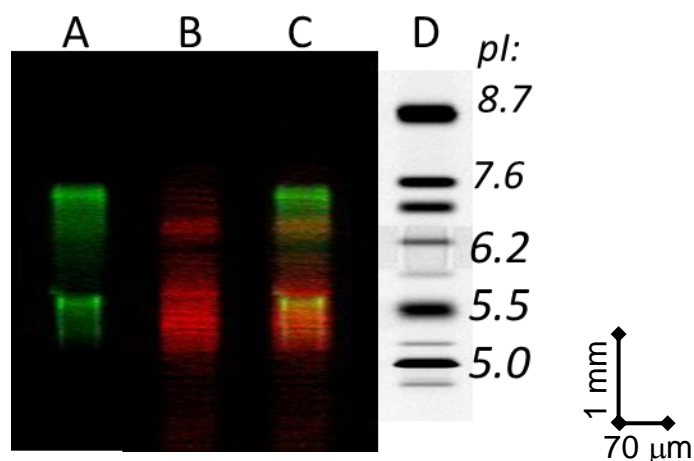
Figure 7.12: (A) SOD2 is revealed after immunoprobing the IEF separated sample with a green fluorescent antibody to SOD2. (B) Bands of immobilized SOD2 are identified using red anti-acetylated lysine. (C) Co-localized red and green bands in a merged color composite indicate the position of acetylated SOD2. (D) Focused UV-fluorescent pI markers serve as reference indicators for target pI.

Immunoprobing of SOD2 consistently revealed a band at pI 7.5, which agrees with previous reports of SOD2's isoelectric point [112]. Multispectral co-localization of dual antibody readouts indicate a major acetylated SOD2 identified by anti-acetylated lysine at pI = 5.6 ± 0.1 (SNR = 11.9 ± 3.9 n = 3) and another acetylated SOD2 band at pI 7.0 ± 0.1. The major band of SOD2 was identified by anti-SOD2 at pI = 7.5 ± 0.1 (average SNR = 103.1 ± 17.8).

The fluorescence generated by the primary acetylated lysine antibody is less than that of the anti-SOD2 green probe (by ~1 order of magnitude). These disparities may be due to differences in the dye labeling ratios of the antibodies or differences in binding affinities. Therefore, probe calibration experiments should be performed for each antigen-antibody pair prior to multi-probe comparison and analysis.

On-Chip IEF/Probing of SOD2 from Raw Cell Lysate

Applying probed IEF to a complex biospecimen, we performed a microfluidic immunoanalysis of raw, unlabeled lysate from a transfected 293T cell line expressing SOD2. After, 7.5× dilution of the sample into a loading buffer along with GFP and pI markers, the sample was electrophoresed into the microfluidic device. After focusing and immobilization, channels were washed out and the sample was probed with antibodies against SOD2 (green fluorescence) and acetylated lysine (red fluorescence) at 500 nM each. Results following 35 minutes of antibody washout are shown in Figure 7.13.
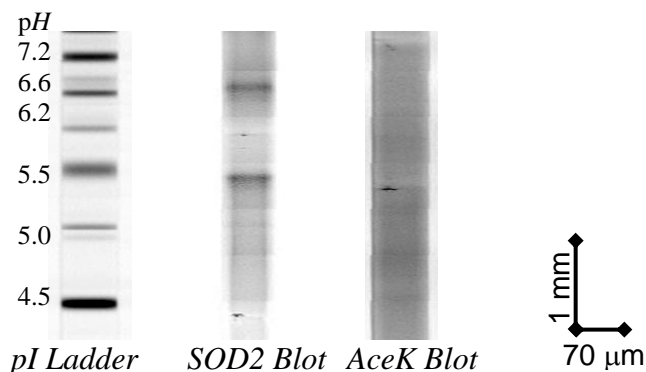
Figure 7.13: SOD2 can be detected from whole cell lysate via on-chip IEF-immunoassay, although the presence of other acetylated proteins within the cell lysate results in a background which obscures the fluorescence from acetylated SOD2.

Anti-SOD2 probing revealed two SOD2 bands at pH 7.5 ± 0.1 ($n = 3$) and 5.6 ± 0.1, at SNRs of 52.8 ± 8.5 and 12.6 ± 4.3, respectively. One can also observe gel defects within each channel corresponding to regions of protein precipitation. The 293T cell lysate was rich in acetylated proteins, which resulted in a high background arising from the anti-acetyl-lysine probe. However, the spatial distribution of the SOD2 antibody suggests charge-shifted isoforms below pH 7.5, indicating the presence of acetylated

SOD2. Area-under-the-curve measurement from anti-SOD2 fluorescence distribution plots allows estimation of concentration and relative abundance for constituent protein bands. Thus, it is estimated that an average of 15% ± 5% (n = 4) of total SOD2 content falls at pI lower than 7.5 - consistent with SOD2 isoforms bearing at least one acetylated lysine residue. When lysate from a non-transfected 293T cell line was probed via IEF immunoassay through the same protocol, the antibody washout was clean and the distinctive SOD2 bands do not appear in this negative control (shown in Figure 7.14, under identical contrast and exposure settings).
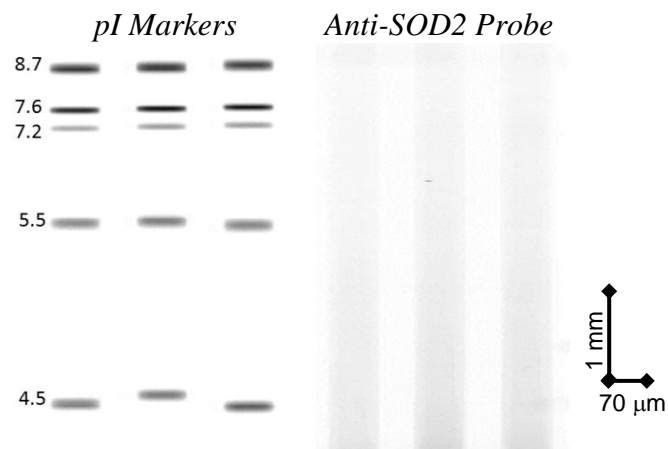
Figure 7.14: Non-transfected 293T cell lysate serves as a negative control and demonstrates no signal for SOD2 when red fluorescence primary antibody blotting (right).

A sandwich ELISA employing capture and detection antibodies specific for acetylation and SOD2 served as a benchmark measurement for the relative abundance of acetylated SOD2 within our samples. A sandwich ELISA was designed based upon the experimental design of Maloney *et al.* [114], where anti-acetylated lysine was used as a capture antibody and goat anti-SOD2 served as the detection antibody. This immunoassay captured lysate proteins bearing acetylated residues, and then reported the

presence of proteins from this acetylated population which were also specific for SOD2 detection (Figure 7.15).
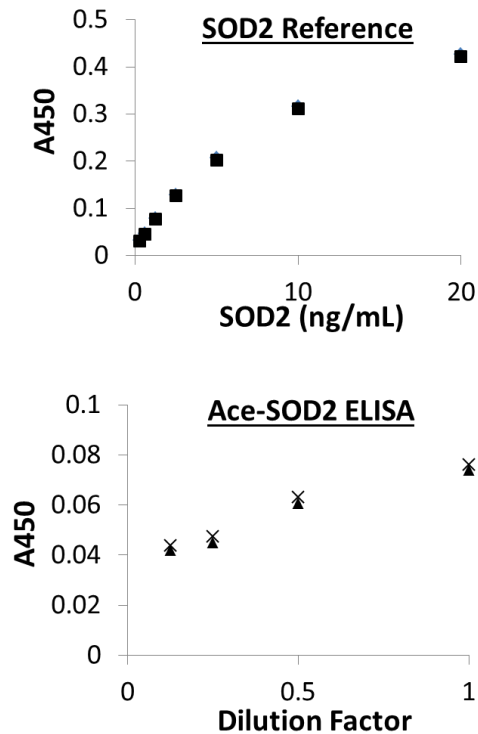
Figure 7.15: To validate results from IEF immunoprobing of acetylated SOD2, a sandwich ELISA was designed using anti-AceK as a capture antibody. ELISA absorbance readings for SOD2 detection are shown for the measurement of raw lysate and purified SOD2 (as reference).

An ELISA for measuring purified SOD2 to serve as a reference was carried out using a mouse anti-SOD2 capture antibody and the same SOD2 detection antibody as the acetylated lysate ELISA. When compared against reference SOD2 measurements, results from acetylated lysine capture suggest that the concentration of acetylated SOD2 is approximately 14% of the total SOD2 content, in close agreement with our on-chip immunoprobe estimate.

7.6 Quantitative Measurement of SOD2: Limits of Detection
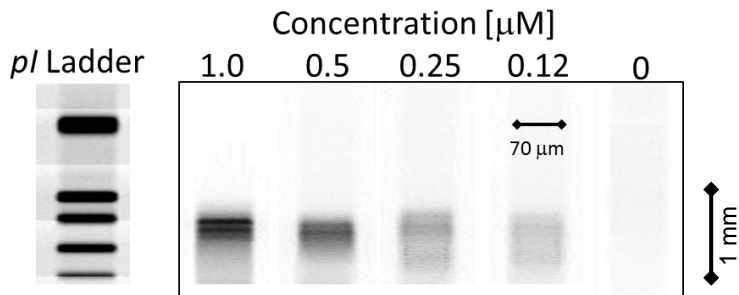
Figure 7.16: Following electrophoretic washout of unbound antibody probes, a linear relationship is observed between fluorescence blotting readouts and target concentrations across a recombinant SOD2 dilution series.

On-chip immunoprobed IEF was applied to a dilution series of recombinant SOD2 across a concentration range from 32-1000 nM. After IEF, immobilized SOD2 was probed with anti-SOD2 at 500 nM. Subsequently, we observed a highly linear relationship between fluorescence blotting readouts and corresponding target concentrations across the dilution series ($R^2 = 0.99$) with a lower limit of detection at approximately 3 nM. Recombinant SOD2 was also immunoprobed with anti-acetylated lysine, yielding no detectable signal. This result indicates that anti-acetylated lysine does not exhibit cross-reactivity for SOD2, and that recombinant SOD2 does not bear acetyl-lysine groups.
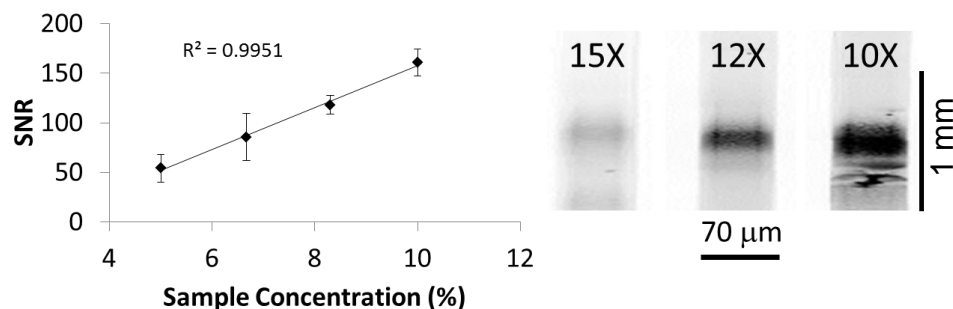
Figure 7.17: A linear calibration relationship was observed from an immunopurified SOD2 dilution series assayed via on-chip anti-SOD2 IEF immunoblotting.

Similarly, a dilution series of SOD2 purified from transfected 293T lysate was assayed using the microfluidic IEF immunoassay. Following the same protocol as the rSOD2 measurement, a linear calibration relationship could also be observed for immunopurified 293T cell lysate. Comparing the fluorescence signal from the immunopurified SOD2 dilution series (of unknown concentration) against fluorescence from the recombinant SOD2 series (of known concentration) allows an estimate of immunopurified SOD2 concentration at 3.3 μM. Thus, the recombinant SOD2 calibration curve provides a basis for quantitative measurement. This same calibration curve was also applied to previous measurements from raw transfected cell lysate to yield an estimated concentration of 3.0 μM for SOD2 overexpressed in 293T lysate.

Analysis of transfected 293T cells was performed on an estimated cell population of ~4000 (assuming an initial suspension at 1×10^7 cells/mL). This 4000 cell estimate was based on a typical sample reservoir of 3 μl. Raw lysates from the 293T cell line were prepared to 7.5× dilution in loading buffer, so each well contained 400 nL of lysate material. However, the actual volume of the microfluidic channel is estimated to be 14.5 nL - less than one percent of well volume. If only the volume of the microchannel was

considered, IEF immunoassay experiments would represent the analysis of about 20 cells. However, 2 to 3 μl serves as a more realistic lower limit for sample volume due to practical concerns of fluid handling and evaporation. If the magnitude of the fluorescent signal is assumed to scale linearly with lysate concentration, a threshold limit of detection of SNR ≈ 3 would correspond to a count of 1×10^3 cells for the SOD2-transfected 293T cells in question.

8. Understanding Single Channel IEF Probing Kinetics

In this chapter, we describe local effects on antibody probe loading and how the dynamics of probe loading are tied to measurement sensitivity. Empirical observations from BP-PA gel isoelectric focusing experiments demonstrate a directionally dependent bias in antibody mobility during electrophoretic probe loading. It is hypothesized that a residual pH gradient across the gel matrix is responsible for this behavior. Gel conjugates bearing fixed pH conditions are used to demonstrate how local pH conditions affect electrophoretic mobility, and a pH sensitive dye is used to map pH across BP-PA gel IEF microdevices. Finally, non-dimensional Damkohler analysis is now applied towards single channel target probing - an application where it becomes desirable to work within a reaction limited regime.

Measurement sensitivity for any immunoassay will be partially dependent upon the concentration of the antibody probe. The time course of development for a detected signal (C_{bound}) is described by the following differential equation where C corresponds to the local concentration of the free antibody:

$$\frac{dC_{bound}}{dt} = k_{on}C(b_m - C_{bound}) - k_{off}C_{bound}$$

In the case of our microfluidic IEF system, heterogeneity in the spatial distribution of the antibody probe can result in disparities in measurement. Setting an appropriate incubation point when the loaded antibody distribution is spatially homogenous is important for attaining repeatable and quantitative antibody probing results. Therefore, it

is useful to visually inspect the full length of the microfluidic channel before completing the antibody load process.

8.1 Directionally Dependent Loading Bias

As an example, the antibody introduction process was studied in Figure 8.1. Texas-Red labeled anti-GFP (500 nM) was electrophoretically loaded to the channel for 25 minutes at 200 V/cm, followed by full-channel imaging. In separate experiments, antibody migration was initiated from the cathodic reservoir (left side) and compared against results from the same loading protocol initiated from the anodic reservoir (right side). Results demonstrate a directionally dependent bias in the electrophoretic mobility of the antibody probe.

Figure 8.1: Antibody loading rates arising from the cathodic end of the device are slower than loading rates from anodic side. Identical imaging settings were maintained for both image sets.

Antibodies originating from the cathodic end of the device consistently exhibit a mass transport rate slower than the antibody probes from the anodic end. Figure 8.2 plots the final spatial distribution for observed probe fluorescence in these two cases. For a GFP band at the channel center, a uniform probe concentration which saturates most of the

channel results in a higher probed signal (SNR = 541) when compared against an antibody incubation exhibiting uneven probe distribution (SNR less than 3). GFP bands that result from the red anti-GFP probe are pictured in the inset of Figure 8.2.
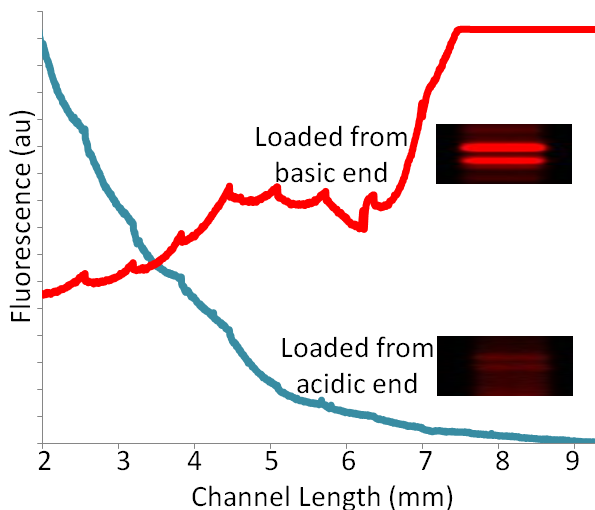
Figure 8.2: High antibody concentrations are favorable for target identification – shown here for GFP bands probed with Texas Red labeled anti-GFP* (inset). The red trace indicates the spatial distribution of probes loaded from the anodic side of the device, while the blue trace illustrates probe loading from the cathodic side.

8.2 Variations in Probe Loading Rates

In a similar experiment, fluorescent anti-GFP was introduced and then washed out of an IEF immunoassay microdevice. Antibodies were electrophoretically loaded into the channel for 25 minutes, followed by 30 minutes of washout time (both at 200 V/cm). Fluorescence distribution was monitored at 10 minute intervals and plotted for a typical experiment (Figure 8.3). Antibody probes were loaded from the cathodic (left) side of the gradient towards the anodic (right) side of the gradient. Figure 8.3 shows that although the probe antibody was continuously loaded for 25 minutes, the rate of mass transport seems to decrease over this same period. In this example (loading from the

cathodic end), antibody flux to the channel is non-linear, indicating diminishing returns
for probe loading over extended periods of time.
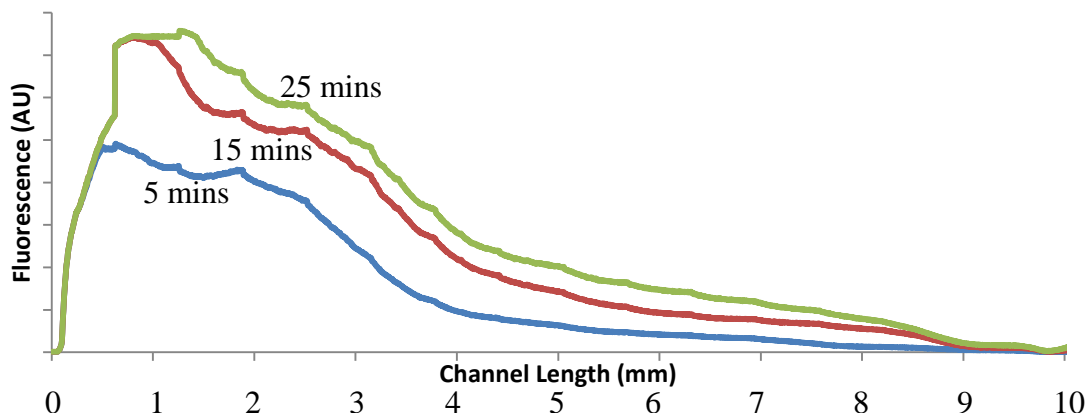
Figure 8.3: Antibody loading is observed over the course of 25 minutes. Probe introduction from the left (cathodic) reservoir results in heterogeneous spatial distribution and decreased mass transport rates over time.

In observing the antibody washout stage, it becomes clear that the majority of all unbound probes are washed out within the first 15 minutes of electric field application. Minimal changes in total fluorescence are observed after 20 minutes, indicating diminishing returns in washout efficiency. Therefore, washout timescales are set between 25-30 minutes because one would not expect a significant decrease in background levels beyond this point.
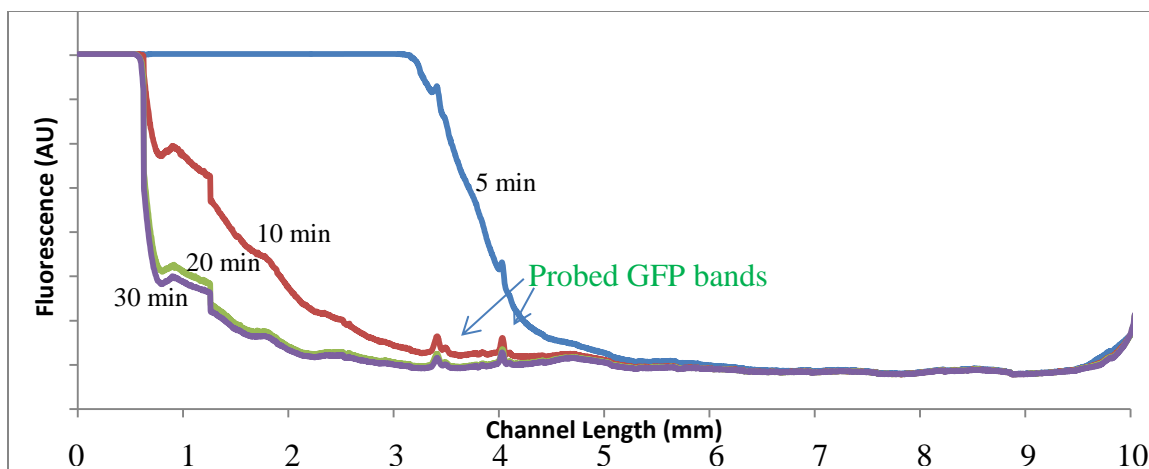
Figure 8.4: The antibody washout process (200 V/cm) results in little change to fluorescence intensity after the ~20 minute time point. Probed GFP bands emerge (3-4 mm) from the background at ~10 minutes (400 ms exposure).

8.3 Effects of Gel pH on Electrophoretic Mobility

The photo-blotting activity of the BP-PA gel is known to immobilize background ampholytes as well as focused proteins. Therefore, it was hypothesized that the IEF-UV exposure process capture focused ampholytes, resulting in a permanent and residual pH gradient affixed to the gel matrix. This residual pH gradient could, in turn, explain local differences in antibody mobility - as the local pH is known to affect protein charge density.

To verify this hypothesis, buffering acrylamido derivatives (Immobilines, GE Healthcare) were titrated to varying pH levels, and then added to a 4%T polyacrylamide BP-PA gel at a concentration of 20 mM. Immobiline gels serve as a comparative model for studying the influence of local pH on antibody electromigration and four gel pH conditions were employed: pH 3.6, 6.0, 7.7 and 9.8. FITC-labeled IgG (400 nM) was electrophoresed into the device for 30 minutes under a constant electric field of 150 V/cm. Progress of the antibody migration was monitored at 5 minute intervals.

123
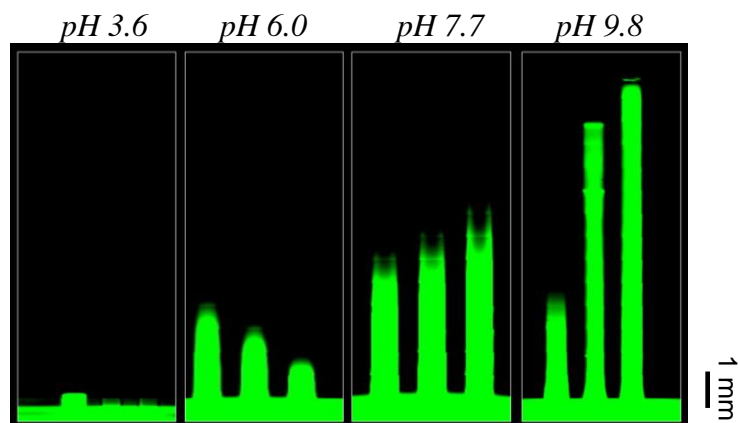
Figure 8.5: Fluorescent antibody migration was observed after 30 minutes for gels of varying pH.

Figure 8.5 illustrates the final distribution of the fluorescent IgG probe after 30 minutes of electrophoretic loading. pH immobilized gel conditions clearly demonstrate that electrophoretic mobility is decreased within lower pH gels. A plot of measured electrophoretic mobility as a function of local pH is given in Figure 8.6. Lower mobilities were attributed to a decrease in antibody charge when localized pH conditions approach the natural pI of the antibody probe.
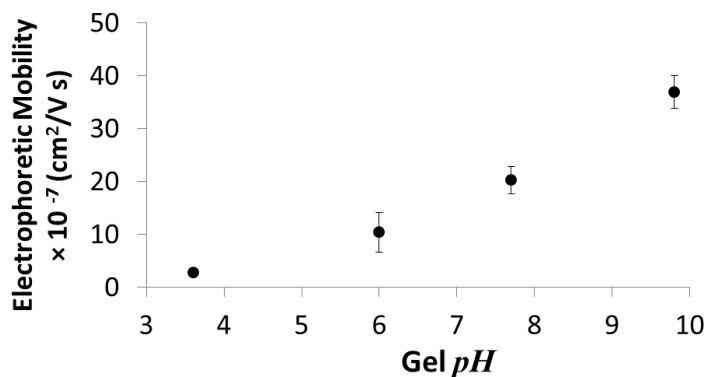
Figure 8.6: The electrophoretic mobility of an IgG molecule increases with local gel pH.

124

8.4 pH Mapping in Microfluidic Channels

To characterize the local conditions of BP-PA gels after photo-blotting, we studied local pH using 5-carboxy SNARF-1 dye (Life Technologies). SNARF is a long-wavelength pH dye indicator whose emission wavelength shifts in a pH dependent manner, depending on whether the molecule is in a protonated or unprotonated state [115, 116]. pH measurements were based on the ratio of SNARF fluorescence emission at multiple wavelengths when using a single wavelength excitation source [117]. SNARF dye was excited at 480 nm with fluorescence emission recorded at 535 nm, and then excited at 480 nm while fluorescence was monitored at 630 nm. This fluorescence emission ratio (*Em630/Em535*) was recorded for various pH condition to establish a calibration curve relating *Em630/Em535* to reference local pH. It was necessary to perform calibration experiments within the same buffer system and at a similar concentration range as the measurement application.

SNARF-1 was diluted to 40 μM in IEF Run Buffer A and introduced to microfluidic BP-PA IEF devices which had previously undergone isoelectric focusing/UV immobilization. The dye molecule was negatively charged and electrophoretically mobile within the gel. Because the pH measurement was based on the ratio of emission at two distinct wavelengths, the spatial distribution of the dye is not required to be homogenous to ensure accurate pH mapping. The average ratio of fluorescence intensities (*Em630/Em535*) is plotted as a function of channel distance in Figure 8.7:
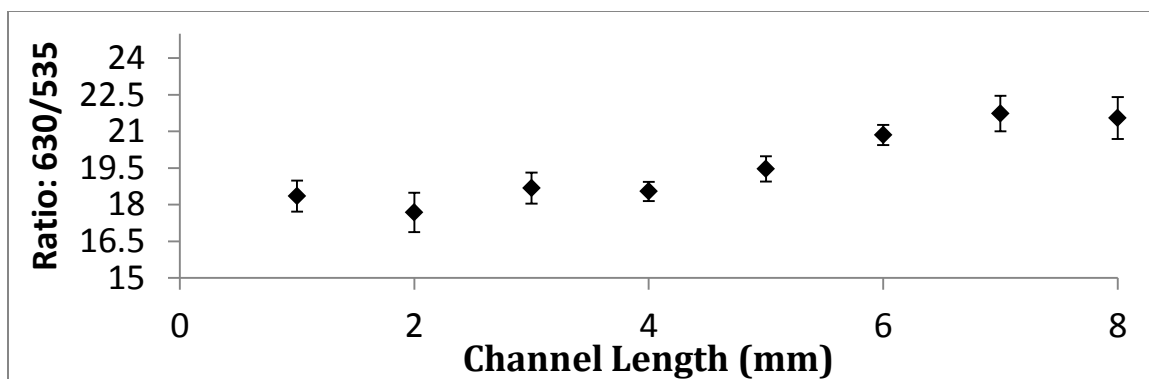
Figure 8.7: The emission ratio (Em630/Em535) increases when moving from left to right (cathodic to anodic) across the length of the channel.

From Figure 8.7, one can see that the *Em630/Em535* ratio increases as we move away from the cathodic reservoir. When we apply the calibration curve relating the *Em630/Em535* ratio to reference pH values, the following map of local gel pH is established:
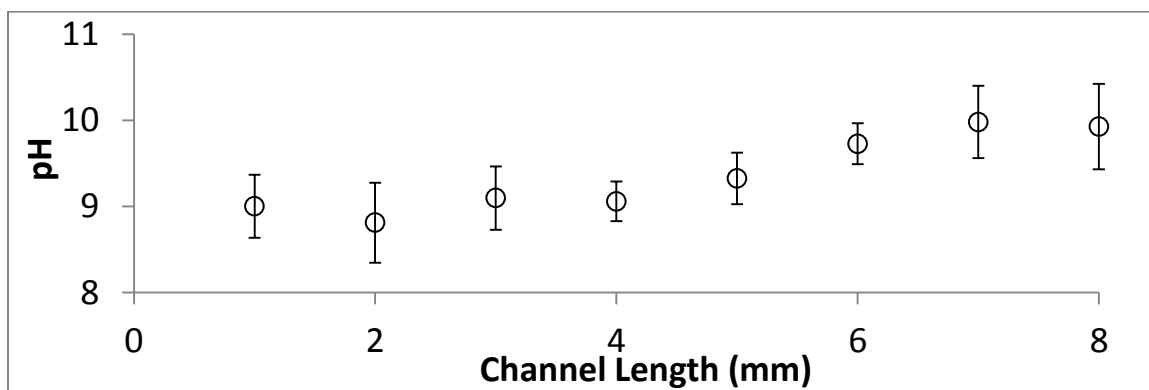
Figure 8.8: Local pH values throughout the gel range from 8.5 to 11.0.

Figure 8.8 demonstrates a pH gradient which becomes more basic near the anodic (right) side of the channel, suggesting that an immobilized pH gradient is present in the polyacrylamide gel. Higher gel pH on the anodic side of the device also explains why

126

electrophoretic migration was faster for probes moving away from the anodic terminal (consistent with our hypothesis). Once local gel pH conditions were established, mobility values from the introduction process in IEF immunoprobing could be mapped in correlation to local pH. When these experimental mobility values were superimposed upon Immobiline-derived data points, similar trends of decreased electrophoretic mobility at lower pH conditions could be observed.

8.5 Dynamics of Signal Development

Results from pH mapping demonstrate that a residual IEF gradient can inhibit antibody migration when the pH of the gel approaches the isoelectric point of the antibody probe. Therefore, it is advantageous to initiate probe migration from the more basic end of the device to expedite probe loading and achieve more spatially uniform immunoprobe coverage. Although a completely homogenous distribution of the antibody probe would be ideal, this result is difficult to achieve in reality. However, the probe loading step can be considered successful when the local probe concentration across the length of the microchannel exceeds the concentration of the antigen and the disassociation constant (K_d) of the antigen-antibody pair. Given a typical K_d of 1 nM (k_{on} = 1 $\times$ 10^6 s^{-1}, k_{off} = 1 $\times$ 10^{-3} M^{-1}s^{-1}), we introduce antibody probes at ~500 nM. Thus, we expect the binding reaction: $[Antigen][Probe] \overset{k_{on}}{\rightarrow} [Antigen - Probe]$ to rapidly reach a saturated equilibrium where: $[Antigen\text{-}Probe] >> [Antigen]$.

The immunoprobe loading step was designed so that probe-target binding interactions would be reaction limited rather than mass transport limited. The goal was to work at a Damkohler number < 1 (indicating a reaction limited regime). This design goal

127

differs from the 2D microfluidic blotting application where it was desirable to operate in a mass transport limited regime ($Da > 10$) for efficient target capture. For our system, $Da = (Lk_{on}b_m)/\mu E$, where L = 100 μm (immobilized band width), b_m = 100 nM and the antibody properties are assumed to be: k_{on} = 1 × 10^6 M^{-1} s^{-1}, μ = 5 × 10^{-6} cm^2 V^{-1} s^{-1}. Therefore, E was specified in the range of 200 V/cm to set a value of $Da < 1$. Operating under excess probe conditions and loading from the basic end of the pH gradient, we studied the development of a probed signal at the site of a focused and immobilized GFP antigen (Figure 8.9). Texas-red labeled anti-GFP (500 nM) was electrophoretically introduced to the microchannel over the course of 25 minutes (E = 200 V/cm) and then unbound probe molecules were flushed away over 35 minutes. Red probe fluorescence was consistently monitored at the site of the GFP band during loading and unloading steps.
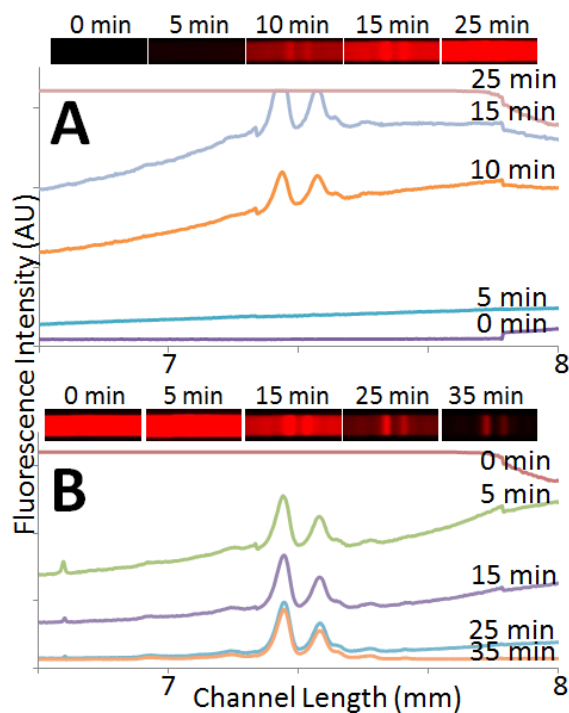
Figure 8.9: Fluorescence signals for the targeted bands begin to emerge (A) as the antibody probe is introduced throughout the target region, shown here over the course of 25 minutes. As excess antibodies are washed away (B), only the specifically bound probe remains upon the gel background, producing in a quantitative signal which contains spatially encoded pI and isoform information

The development of a probed signal at the site of the immobilized protein target was observed with a time constant of ~23 minutes. Background reduction and probe signal development was monitored as unbound antibodies were electrokinetically washed from the channel, leaving behind a probed target signal by $t = 35$ minutes. Some dissociation of the antibody probe from the antigen would be expected during the washout stage, but minimal changes in target signal intensity were observed. For a typical k_{off} of 1×10^{-3} s^{-1}, we would expect to see a 50% loss of the bound probe over 500 seconds. Persistence of the localized probe signal over a 35 minute time course suggests that disassociation kinetics may be slowed due to the porous structure and reduced diffusivity of the

polyacrylamide gel. Dissociated probes may rapidly bind to adjacent target proteins, as $k_{on} \gg k_{off}$.
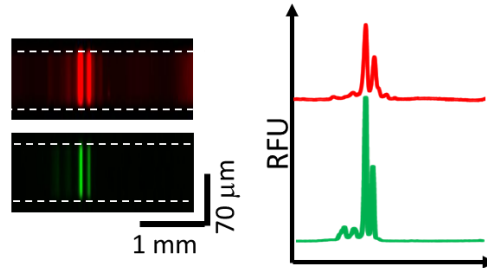
Figure 8.10: Immobilized target proteins are identified through a localized signal arising from a matched fluorescent antibody. The fidelity of the probe measurement is demonstrated here for focused GFP (bottom), subsequently probed with red-labeled fluorescent anti-GFP (top).

Spatial mapping of the focused target protein was consistent with the shape and position of the matched probe signal (Figure 8.10). Standard deviation of the resulting probe bandwidth was within 8% of the original target bandwidth. The center of mass of for each probed band lined up within $< 0.1\%$ of the original target band position (relative to the full channel length). Thus, the location of the bound probe serves as a high-fidelity technique for reporting spatially encoded isoform pI information.

9. **Towards High Sensitivity Detection Strategies for On-chip Immunoassay**

In this chapter, laser scanning and enzyme amplified detection strategies are described as potential methods for high sensitivity (sub-nM) microfluidic immunoassays. A commercial microarray laser scanner is adapted for compatibility with the microfluidic devices described in this work. Alternatively, enzyme-linked reporter antibodies can be applied in conjunction with ELF97 substrate molecules to generate a brightly fluorescent crystal product at the site of reaction. Optimal conditions for applying ELF97 detection in IEF immunoassays are explored through on-chip and off-chip characterization experiments.

9.1 Laser Microarray Scanning

Given that our limits of detection for fluorescent probes measured via microscopy tend to fall in the low nM range (Figure 7.16), we sought to improve the sensitivity of our microfluidic immunoassays by going beyond conventional microscope-based fluorescence imaging. The glass substrates used for microfluidic chip fabrication in this work demonstrate excellent optical transmission properties. Soda lime glass devices exhibit minimal photon scattering, serving as a good platform material for sensitive and linear fluorescence measurements. DNA microarrays are one other example of a fluorescent probe measurement performed upon a glass substrate. In DNA microarray experiments, laser scanners integrate powerful multispectral excitation sources with photomultiplier tube-based (PMT) photon detection [118]. The resulting full field images provide spatially encoded data sets which report probe binding with high sensitivity (~0.1

chromophores/μm^2) [119]. Although the footprint of the glass chips described in this work may differ from a standard microarray slide, commercial DNA microarray scanners can be adapted to work with microfluidic devices, providing a laser-based tool for high sensitivity protein detection.

Microarray imaging experiments were performed upon an Axon 4000B laser scanner, which employs two laser wavelengths at 532 and 635 nm. Alexa Fluor 568 dyes are compatible with the 532 laser. A full device scan (2.5 cm × 1.5 cm) requires approximately 5 minutes at 10 μm per pixel resolution or about 15 minutes at 5 μm per pixel. In early attempts, on-chip fluorescence could not be detected using the microarray scanner because the laser focus depth seemed to be incompatible with the depth of the embedded gel structures. The microarray scanner, which is normally used for imaging oligomer probes upon the surface of a glass slide, was only able to detect the access holes on the top face of the eBlot-2 microdevice.

This depth-of-focus obstacle can be circumvented by modifying the microarray slide holder to position chips at an offset, bringing the entire device closer to the optical scan head. A clearance of 1.9 mm is available between the surface of the sample holder and the laser scan head. The height of the microfluidic device is adjusted relative to the stage by mounting layers of glass which serve as spacing elements (Figure 9.1). Another method for solving the scan depth problem is to employ a microfluidic chip which is thinner than a standard device (1.9 mm). Here, a glass chip of 1 mm thickness (0.3 mm etched surface mated to a 0.7 mm reservoir face) was employed because its thin profile allowed embedded gel features to come into close proximity with the laser scan head.
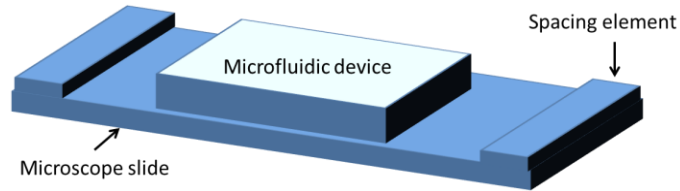
Figure 9.1: A glass slide with modified spacing elements serves as an adaptor for the microarray scanner, bringing the glass chip and integrated gel structures closer to the optical head.

Optimized Depth of Focus

The Axon 4000B scanning software interface (GenePix Pro) also allows users to adjust the focal plane from -50 μm to +200 μm relative to the zero position of the slide surface. Positive positions refer to focal planes above a standard microarray slide while negative positions are located below the slide surface. Modifying this depth-of-focus setting reveals that higher levels of fluorescence can observed when the scan depth is matched to the depth of the channel. Figure 9.2 illustrates the variations in measurement that can occur when the same dye-filled channels are imaged various scan depths. Thus, the major challenge is to mount the devices so the centerline of each microchannel falls within the middle of the laser scan range.
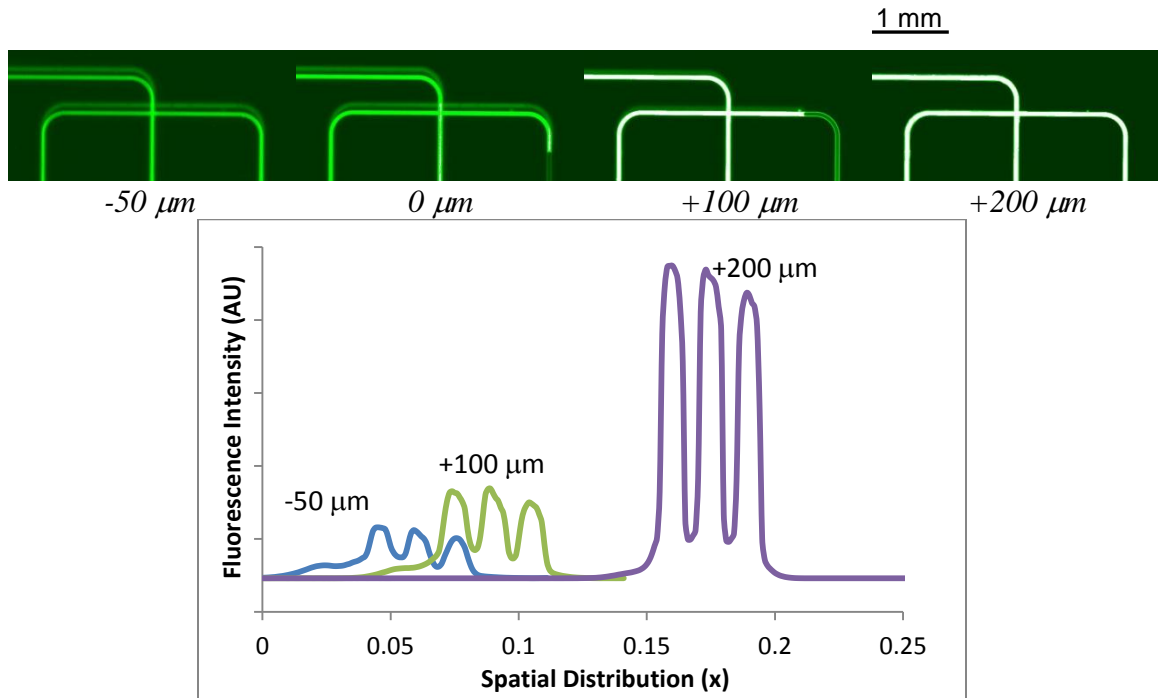
Figure 9.2: On-chip fluorescence measurements are most sensitive when the depth of laser scanning is matched to the depth of embedded gel structures within the glass device. The fluorescence distribution plot illustrates sets of channels as they are imaged across varying focus depths. +200 μm corresponds to a scan depth 200 μm above the anticipated surface of a microarray slide.

The intensity of the fluorescence signal can be also optimized by adjusting the gain of the PMT system. In Figure 9.3, microfluidic channels were filled with AlexaFluor 568 dye at 3.67 nM. Channel images were scanned at a spatial resolution of 5 μm per pixel, as the gain setting was varied from 650 to 890.
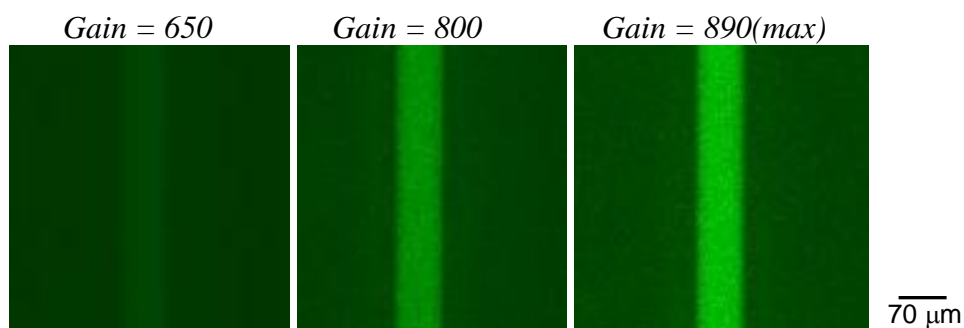
Figure 9.3: Adjustments to the PMT gain setting result in higher measured fluorescence values when imaging a microfluidic channel (532 nm scan at 5 µm per pixel).

At the maximum gain setting (Figure 9.3, right) the average SNR (observed channel fluorescence divided by glass substrate background) was 292. For purposes of comparison, the average SNR for this same channel was 72 when imaged upon the Andor/X-cite fluorescence microscopy system. Spatial resolution of the microarray scan corresponded to 5 µm per pixel in the *XY* plane (Figure 9.4), whereas 1 pixel ≈ 4 µm on the CCD camera when 4×4 pixel binning was employed.
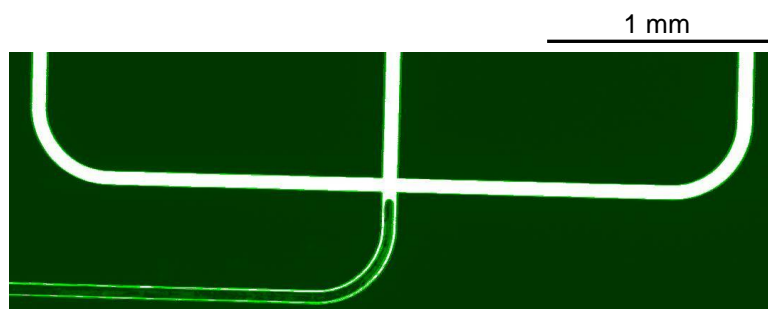
Figure 9.4: A high resolution scan of a partially filled device containing AlexaFluor 568 dye as imaged upon the Axon 4000B microarray scanner at 532 nm (1 pixel = 5 µm).

Some challenges to accurate and sensitive laser scanning include the ability to maintain a clean chip surface as well as a flat scanning plane. Unwanted residues upon

the surface of the glass such as tape, dust or fingerprints can result in light scattering, as illustrated in Figure 9.5 (scanned at 532 nm). If the microfluidic device does not sit perpendicular to the *z*-axis, refraction through the optical path can also result in spurious light scattering and "double channel" artifacts.

1 mm
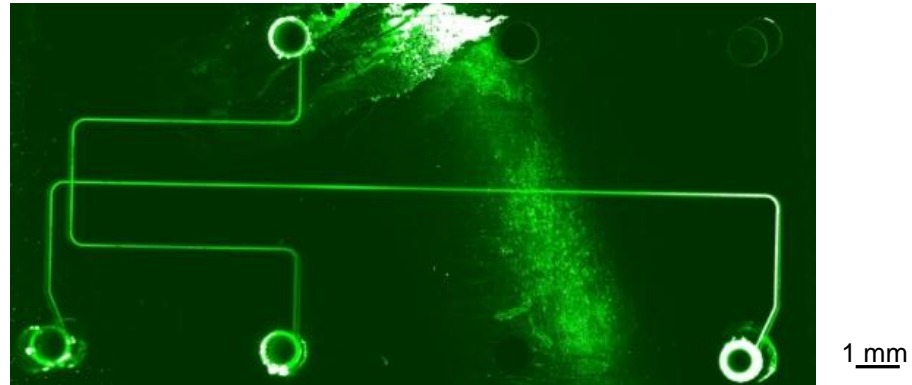
Figure 9.5: Imperfections upon the surface of the glass device (dust, residues, etc.) can result in light scattering which obscures on-chip fluorescence measurement.

9.2 Laser Scanning Detection of SOD2

SOD2 was assayed in an IEF-immunoassay chip at serial dilutions of 64 nM and 32 nM. After focusing, immobilization, and washout, a red fluorescent labeled polyclonal antibody to SOD2 (150 nM) was introduced into the device. Following incubation and antibody washout steps, the glass device was mounted upon an Axon 4000B instrument and scanned at 532 nm with a resolution of 5 µm/pixel and PMT gain setting of 600 (Figure 9.6).

70 μm

32 nM   *64 nM*
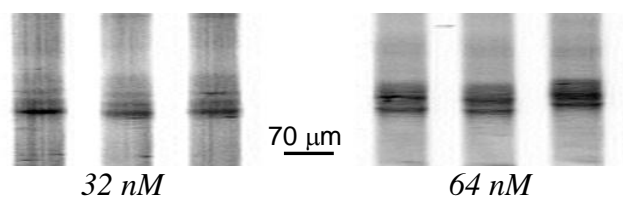
Figure 9.6: Superoxide dismutase 2 (32 and 64 nM) is probed with AlexaFluor 568 labeled anti-SOD2 and imaged upon a laser microarray scanning instrument.

For the sample at 32 nM, bands were detected at an average SNR of 31. This value represents a ~3× improvement in SNR compared to the same chip imaged on a standard fluorescence microscope (Figure 9.7). Bands at 64 nM are detected with an average SNR of 55.
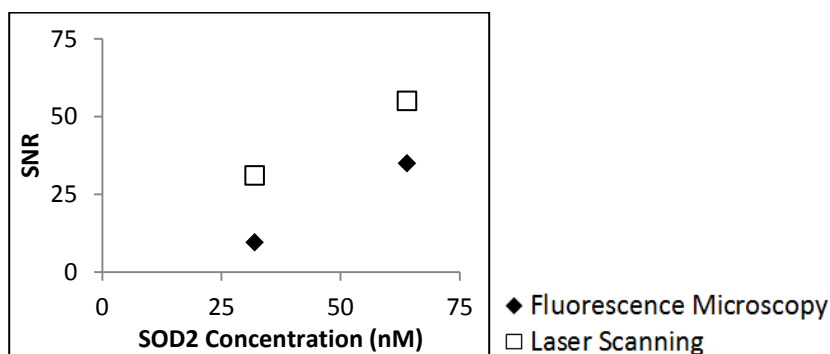
Figure 9.7: Results from SOD2 immunoassay imaging with a laser-based microarray scanner consistently demonstrate higher measurement sensitivity values (SNR) than corresponding images from traditional fluorescence microscopy.

9.3 Enzyme-Amplified Immunodetection: ELF97

Fluorescence based detection strategies are convenient for use within immunoassays, as these offer excellent measurement linearity and are compatible with well characterized optical systems. However, many high sensitivity measurements in molecular biology are able to go beyond fluorescence limits of detection by harnessing a powerful enzyme-linked signal amplification process [120]. Enzyme-conjugated antibodies are capable of

converting substrate molecules into a product yielding some detectable signal (e.g. colorimetric, chemiluminescent, etc.). As the substrate molecules are converted into products, new substrate molecules can be introduced - resulting in a continual conversion process known as enzymatic amplification. Enzymatic detection strategies have been employed in microfluidic devices, usually resulting in a chemiluminescent or electrochemical signal [121]. Most these are soluble products which are prone to dispersion and incompatible with the immunoassays presented here. Both the IEF immunoassay and 2D native blotting devices work on the basis of spatially encoded data visualizations which require a localized signal. Therefore, we explore the use of ELF97, a proprietary substrate which forms a brightly fluorescent precipitate (Figure 9.8). This insoluble product is localized to its reaction site upon cleavage of its phosphate group via alkaline phosphatase (AP).
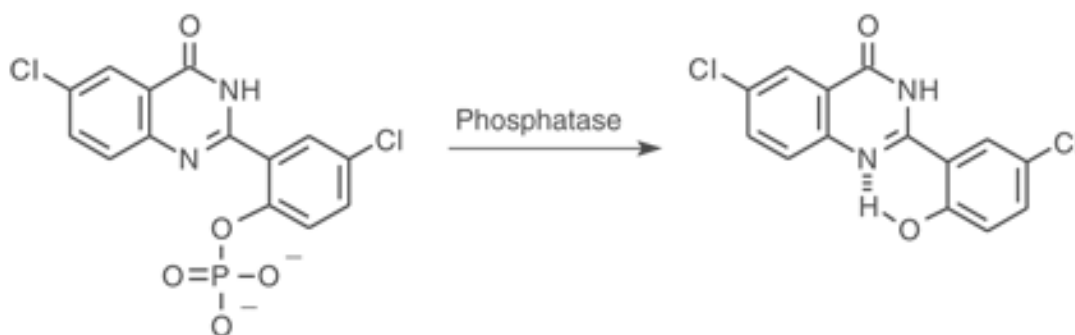
Water Soluble, Weak Blue Fluorescence   *Insoluble, Intense Green Fluorescence*

Figure 9.8: ELF97 forms a bright crystalline precipitate upon cleavage of its phosphate group, (adapted from Molecular Probes).

A dot blot experiment tested the ability of ELF-97 to identify an unlabeled protein target when used in conjunction with an enzyme-linked detection antibody. A glass slide was spotted with protein G at 1.5 μM, and spots were then incubated for one hour against AlexaFluor 568 labeled anti-protein G (α-PG*) or against alkaline phosphatase-conjugated IgG (AP-IgG) at concentrations of 1, 0.5 and 0.25 μM. After a washing step, the AP-IgG incubated spots were observed via fluorescence microscopy using a DAPI longpass filter. 0.25 mM ELF97 in a Tricine-NaOH buffer (100 mM, pH 8) was introduced to the AP-IgG incubated spots and formation of an insoluble, crystalline fluorescent product was observed. ELF97 product fluorescence increased over time, and was localized around the protein spots. α-PG* incubated spots were imaged using the 568 nm filter set and resulting fluorescence intensities for both AP-IgG and α-PG* incubated spots are shown in Figure 9.9.
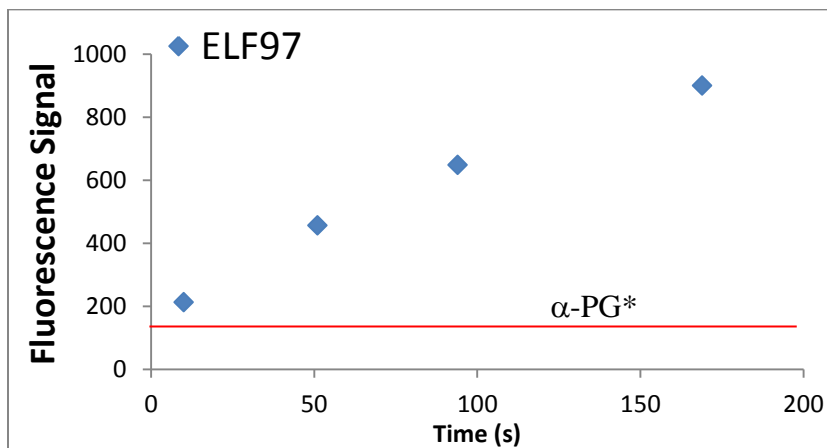
Figure 9.9: Fluorescence signal surrounding protein spots incubated against alkaline phosphatase-IgG increased as a function of time when these spots were developed using ELF97 substrate. In contrast, the signal arising from a fluorescent probe antibody (anti-protein G) remained static.

Figure 9.9 demonstrates the increase in local fluorescence for 1.5 µM protein spots as a function of time. Fluorescence arising from alkaline phosphatase activity on the ELF97 substrate appeared at protein spots within 10 seconds, and these signals were amplified over time. This signal was higher when compared against spots incubated with fluorescent α-PG under the same conditions. Over longer reaction time scales (> 15 minutes), the fluorescence product from the ELF97 substrate eventually saturated the CCD camera.

In translating this enzyme-linked matched pair to an electrophoretic on-chip immunoassay, it will be a challenge to control product formation and dispersion. The bright ELF97 crystals can result in high background for the surrounding gel. ELF97 crystal size will also be a factor in product dispersion, and crystal formation is known to be influenced by the constituents of the buffer medium. Enzyme linked amplification will need to be optimized for various application specific buffers.

ELF97 in Microfluidic Gel Electrophoresis

Applying the ELF97-linked detection strategy to a gel-based electrophoretic immunoassay requires that the all necessary reagents and antibodies must be electrophoretically mobile in the gel matrix. Furthermore, the enzyme-substrate pair must be able to form a detectable product crystal within the polyacrylamide gel and buffer context. Recent literature suggests these necessary conditions are possible. Kemper *et al.* [122] reported an in-gel enzymatic activity assay utilizing ELF97for the detection of beta-glucuronidase in a 4-20%T gradient gel, and a 7.5%T polyacrylamide

gel. In a report of AP-IgG capillary electrophoresis [123], AP-IgG was negatively charged and electrophoretically mobile within a 0.5% methylcellulose solution.

To better understand the process of enzyme/substrate conversion and ELF precipitate formation within microscale gel electrophoresis, a T-channel diffusion experiment was performed. The scheme shown in Figure 9.10 was used to evaluate the production of fluorescent ELF97 precipitate within a polyacrylamide gel under the influence of an electric field. Here, the ELF97 substrate concentration at the reservoir was 5 mM, and the alkaline phosphatase-IgG bulk concentration at the reservoir was maintained at 6 μM.
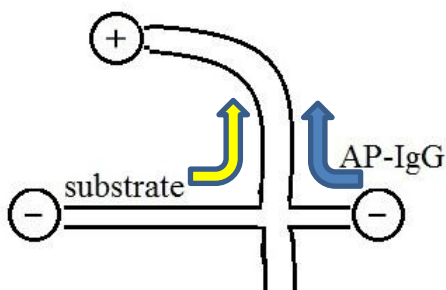
Figure 9.10: Cartoon of a t-junction experiment where negatively charged ELF97 and alkaline phosphatase conjugates flow towards a single electrode terminal. Diffusive enzyme-substrate mixing occurs at the channel intersection so that the dynamics of the AP-ELF97 conversion can be monitored.

A fluorescent signal that increased over time was observed at the channel junction (Figure 9.11). As the substrate/enzyme pair merges at the channel intersection, diffusive mixing occurs along the length of the uppermost channel. In the image sequence of Figure 9.11, the electrokinetic flow is continuous and crystal formation is shown to initiate at the far end of the uppermost channel.

555 sec	*735 sec*	*825 sec*
1005 sec	*1095 sec*	*1140 sec*

1 mm
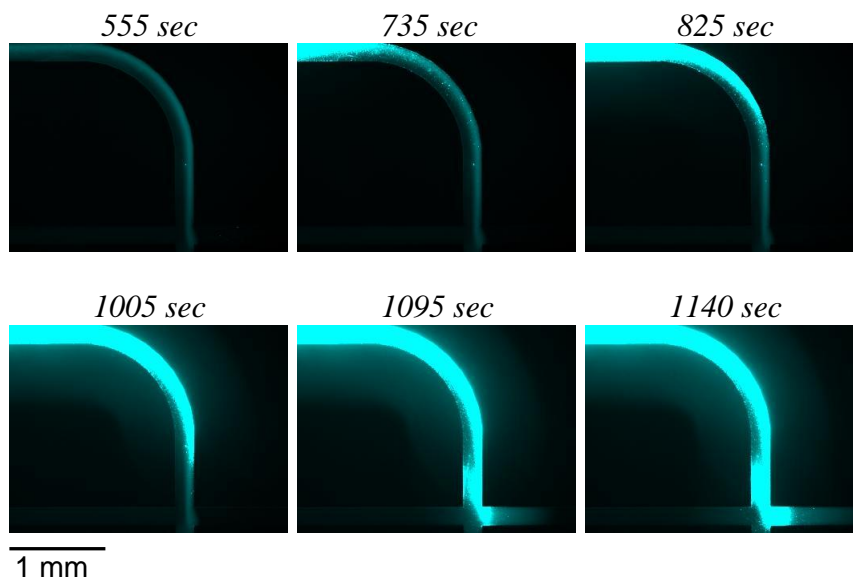
Figure 9.11: A fluorescent, crystalline product is first observed at the far end of the uppermost channel. Crystal formation eventually propagated back towards the intersection where the ELF97 substrate initially merged with an alkaline phosphatase conjugate. A time course is shown from 555 to 1140 seconds, using a DAPI fluorescence filter cube.

This experiment demonstrates that the formation of ELF97 product is possible within a microfluidic polyacrylamide gel under the influence of electrophoresis. As nucleation sites are formed downstream, crystal formation propagates back towards the channel intersection (Figure 9.11). Although diffusive mixing is higher downstream, the far end of the uppermost channel also represents a later time point when the localized product concentration is higher. When the electric field is shut off, fluorescence generation rapidly becomes uniform across the channel (Figure 9.12).

735 s   1 mm   *780 s*   *810 s*   *855 s*
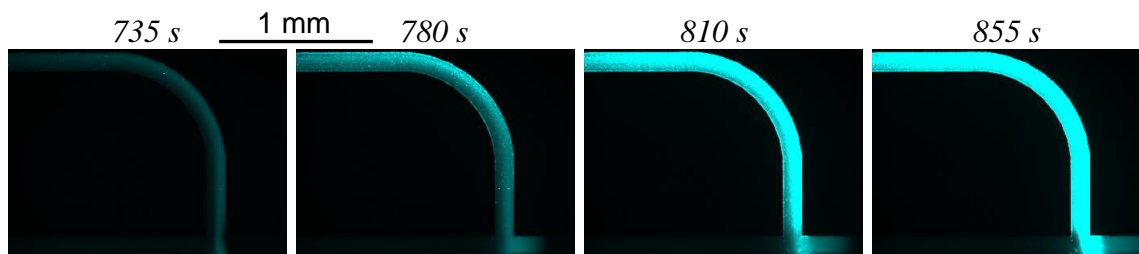
Figure 9.12:   ELF97 product formation is homogeneous across the length of the microchannel when the electric field is shut off at ~750 seconds.

The fluorescent signal resulting from the enzymatic cleavage of phosphate from ELF97 via alkaline phosphatase is extremely bright. This product is manifested in two forms − a crystalline precipitate appearing as bright specks within the gel, and a fine fluorescent product which is still electrophoretically mobile. This finer precipitate also diffuses within the gel, as evidenced when the electric field is switched off. Observing the ELF97-alkaline phosphatase reaction within this t-junction experiment suggests that the ELF97 product may require some critical local concentration before crystallization can occur. These preliminary results also indicated that both the ELF97 substrate and the 290 kDa AP-IgG conjugate are electrophoretically mobile under the conditions employed.

9.4 Enzyme Linked Detection of SOD2: Product Dispersion

We sought to apply this enzyme-linked detection strategy towards high sensitivity IEF-immunoassay of SOD2. Two forms of recombinant SOD2 (labeled and unlabeled) were assayed through on-chip isoelectric focusing and then immunoprobed with fluorescent antibodies to SOD2 (mouse monoclonal, 500 nM) using the standard protocol. An additional alkaline phosphatase-linked secondary antibody (goat anti-

143

mouse, 500 nM) was applied (200 V/cm for 5 minutes, then 100 V/cm for 20 minutes) and then unbound secondary antibodies were electrophoretically removed from the channel (150 V/cm for 20 minutes, then 15 minutes at 200 V/cm) following a brief incubation period. Finally, ELF97 substrate (0.67 mM) was introduced across the length of the microchannel for 10 minutes. The corresponding signal development was monitored at 2 minute intervals.

Sample	rSOD2* (Fluorescent)		rSOD2 (Unlabeled)	
Probe	None	ELF97/ AP-linked secondary	Fluorescent anti-SOD2	ELF97/ AP-linked secondary
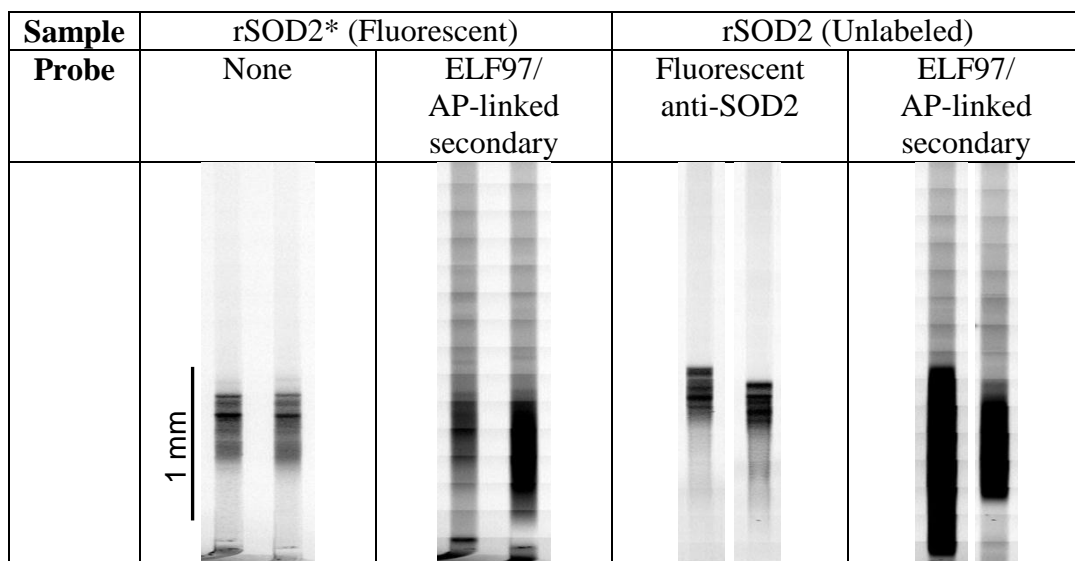
Figure 9.13: The position of immobilized target rSOD2* is compared against the distribution of corresponding product from secondary antibody/ELF97 probing. Similarly, unlabeled rSOD2 is revealed via a matched antibody probe and compared against the fluorescence distribution from a secondary antibody/ELF97 probe.

Figure 9.13 illustrates the spatial distribution of the ELF97 product as observed following 10 minutes of substrate introduction. Locations of the ELF97 product can be compared against the initial distribution of corresponding targets (labeled and unlabeled SOD2). In the case of unlabeled SOD2, initial target distribution was reported through a matched fluorescent primary antibody (anti-SOD2). Initial product formation coincides

with the front of the target bands and the relative positions of these "fronts" match the spatial positions of both labeled and unlabeled SOD2 targets. However, the enzymatic product zone is much broader than the protein bands observed via fluorescent probing. This result indicates that the large AP-IgG secondary conjugate is able to migrate through the 4%T BP-PA gel matrix. We can gain a further understanding of the trailing product zone through examining the dynamics of ELF97 product formation.
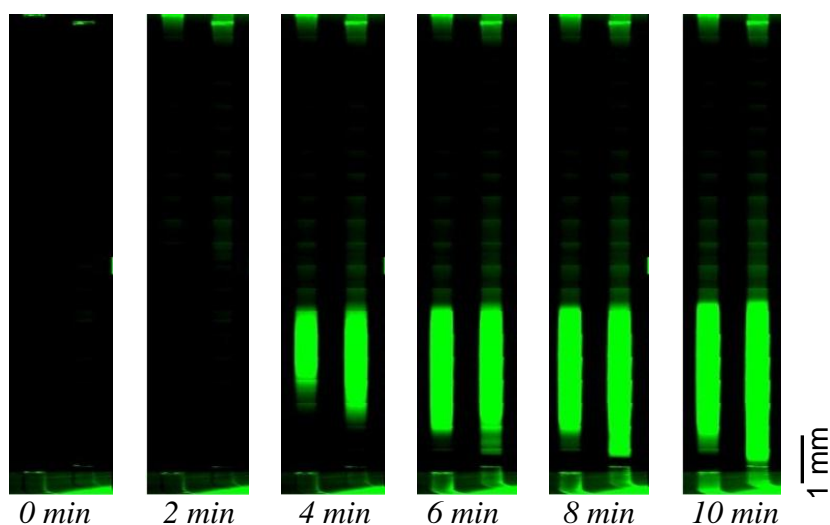
Figure 9.14: Continuous ELF97 crystal formation is observed over 10 minutes of substrate loading. Fluorescent crystals are first produced between 2 and 4 minutes.

Figure 9.14 illustrates the rate of product formation, which can occur quickly. In this example, the most important stages of fluorescent product development occur between 2 minutes and 4 minutes of substrate loading. These early stages of product conversion represent time points which would provide the highest degree of spatial resolution, as some measurement resolution is subsequently lost due to product dispersion. The time dependent nature of ELF97 crystal formation (observed in Figure 9.11) helps to explain

the trailing distribution of fluorescent crystals downstream of the targeted sample bands. Dispersion of this fluorescent product could undermine probe signal analysis, especially if the sample contains more than one immobilized band of interest. Thus, it becomes critical to understand factors which influence the process of ELF97 crystal formation in the specific gel and buffer conditions.

9.5 ELF97 Product Conversion and Solubility: Buffer Dependence

Crystallization occurs when it becomes thermodynamically favorable for solute molecules to adopt a regular lattice structure [124], the formation of which is characterized by primary nucleation, secondary nucleation and crystal growth phases. The thermodynamic favorability of crystal formation will be determined by factors such as temperature and, solute concentration. The presence of amphiphilic surfactant molecules within a system is also known to affect the intermolecular forces which determine crystal solubility. Therefore, it is important to understand how components of the various isoelectric focusing and electrophoresis buffers may affect ELF97 crystal solubility in our microfluidic system. The two major buffer solutions employed in BP-PA isoelectric focusing are:

- Run Buffer A (RbA, used for introducing and washout of antibody probes): 3% CHAPS (w/v), 200 mM NDSB 256, 10% Sorbitol (v/v), 15 mM Glycine NaOH (pH 10.4), 4.5% DMSO (v/v).

- Run Buffer B (RbB, gel buffer used in sample loading): 3% CHAPS (w/v), 200 mM NDSB 256, 10% Sorbitol (v/v), 2% Pharmalytes 3-10 pH 9.7 (w/v), 4.5% DMSO (v/v)

A 1 mM stock solution of ELF97 product in DMSO was diluted into four separate aliquots of RbA, RbB, Tris-glycine (25 mM Tris, 192 mM glycine, pH 8.3) and a 50/50

mixture of Tris-glycine/RbA. All ELF97 products were diluted into buffer solutions at a 1:1 ratio and crystals were imaged using fluorescence microscopy (DAPI filter, 20× objective). The solubility of the ELF97 product varied widely across different buffer solutions, as apparent from visible changes in crystal density and aggregate size. Figure 9.15 illustrates that the largest and most visible crystals were generated within Tris-glycine buffer. ELF97 product in the Tris-glycine/RbA mixture exhibited intensity values lower fluorescence readings within Tris-glycine buffer but higher than those of RbA.

500 μm

Run Buffer A	Run Buffer B	Tris Glycine Buffer	50% mix: TG + RbA
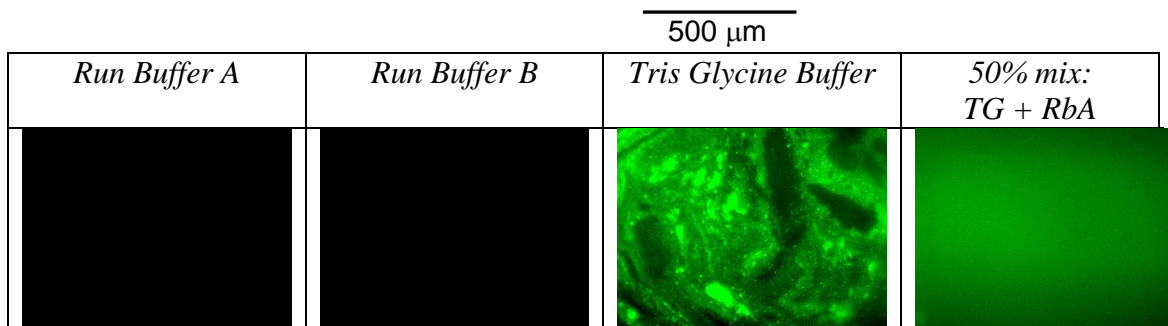
Figure 9.15: ELF97 product crystals (125 μM) dissolved within various buffer solutions are displayed under identical imaging conditions.

Non-fluorescent ELF97 product molecules in RbA and RbB were rearranged into bright crystals of diverse size and shape when these were diluted 20× in water. This result suggests that the addition of excess H₂O was able to dilute buffer components from RbA and RbB which affect product solubility. The crystal size and the solubility of the ELF97 product are also observed to be time dependent. A time sequence montage for a crystal mixture from RbB diluted 20× is shown in Figure 9.16. Over time, large crystals shrank and "congealed" into a single mass.

500 μm

Time →
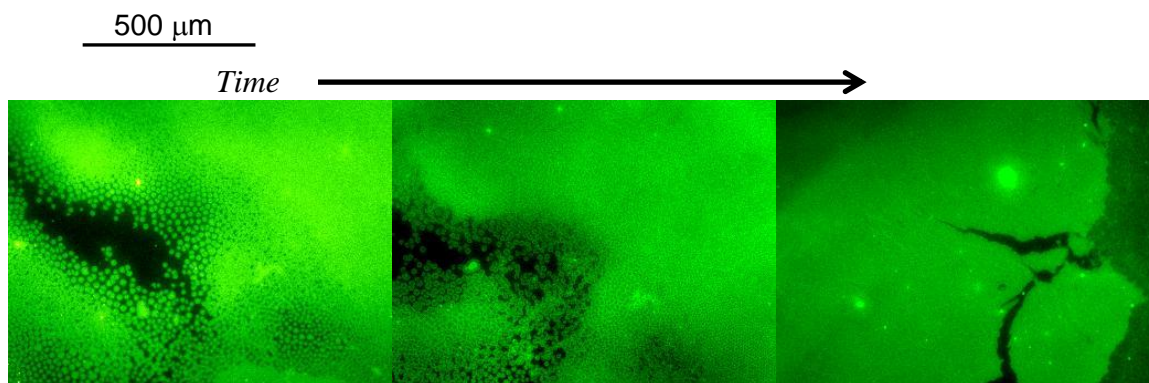
Figure 9.16: ELF97 crystals change size and aggregate dynamically when run buffers are diluted with H$_2$O.

This "transient solubility" effect was also observed in the diluted RbA mixture. Localized crystal regions transitioned in and out of the solid phase - a phenomenon which may reflect convective and diffusive effects on local solvent concentration gradients. The product displays an extremely bright green fluorescence in the form of a solid crystal precipitate but exhibits a low level blue fluorescence when it becomes solubilized.

From these results, we can conclude that the solubility of the ELF97 product is strongly influenced by the buffer, as some component of RbA and RbB inhibits crystal formation. Physical properties of the ELF97 crystal (such as size and shape) demonstrate a strong effect on its corresponding fluorescence signal. Therefore, higher substrate or higher product concentrations will not necessarily result in stronger detection signals if local gel conditions are not conducive to crystal growth.

Differences in the ELF97 product within RbA versus RbB suggest that buffer pH plays an important role in crystal formation. The composition of RbA is almost identical to that of RbB, with one exception being that there is a 1M glycine NaOH titration step for RbA. Local pH was suggested as a major factor because it was known to affect the

activity of alkaline phosphatase. To investigate pH effects upon ELF97 fluorescence production, a microplate experiment was performed in which alkaline phosphatase-linked IgG was combined with ELF97 substrate in buffer solutions of varying pH. Enzymatic interactions were screened on a 96 well plate to determine the optimal pH for producing a fluorescent crystalline precipitate. A range of conditions from pH 6.9 to pH 9.3 were tested in Tris-glycine buffer (titrated via NaOH or HCl). Product measurements were taken every 10 seconds, over a period of 12 minutes using a fluorescence plate reader (Figure 9.17).
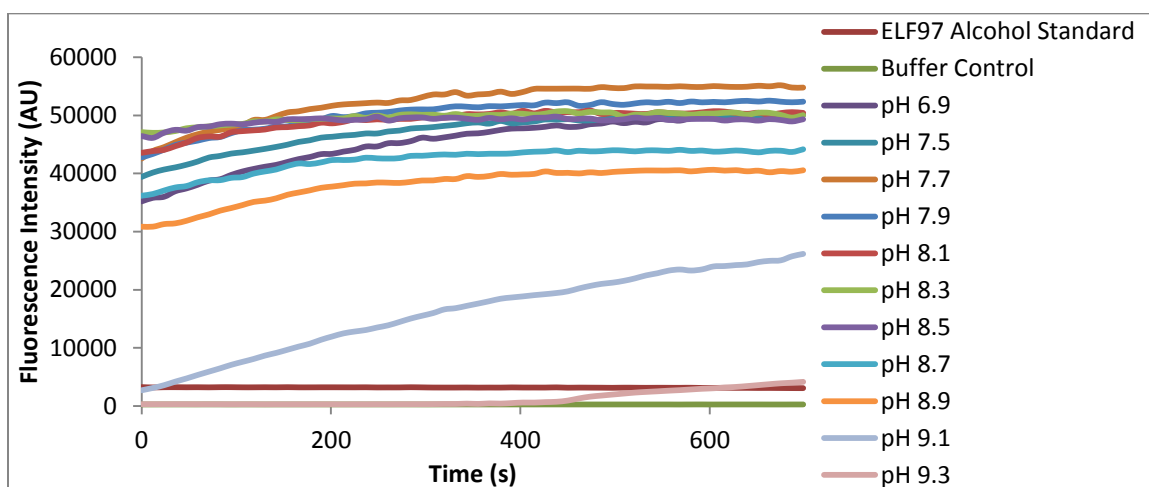
Figure 9.17: The conversion of ELF97 substrate into a fluorescent product was observed as a function of time across buffers of varying pH.

Results indicate that the initial rate of fluorescence production was highest between buffer pH 8.3-8.5, which corresponds to the buffering range and nominal pH of standard Tris-glycine. The highest increase in fluorescent production occurred within the first 60 seconds after the enzyme and substrate solutions were mixed together. Figure 9.18 plots the fluorescence produced during this initial period of substrate conversion (measured at

~ 1 minute) as a function of buffer pH. Again, the highest conversion rates were observed at pH 8.3, and so this value serves as a target pH point for subsequent work with on-chip immunodetection via ELF97.
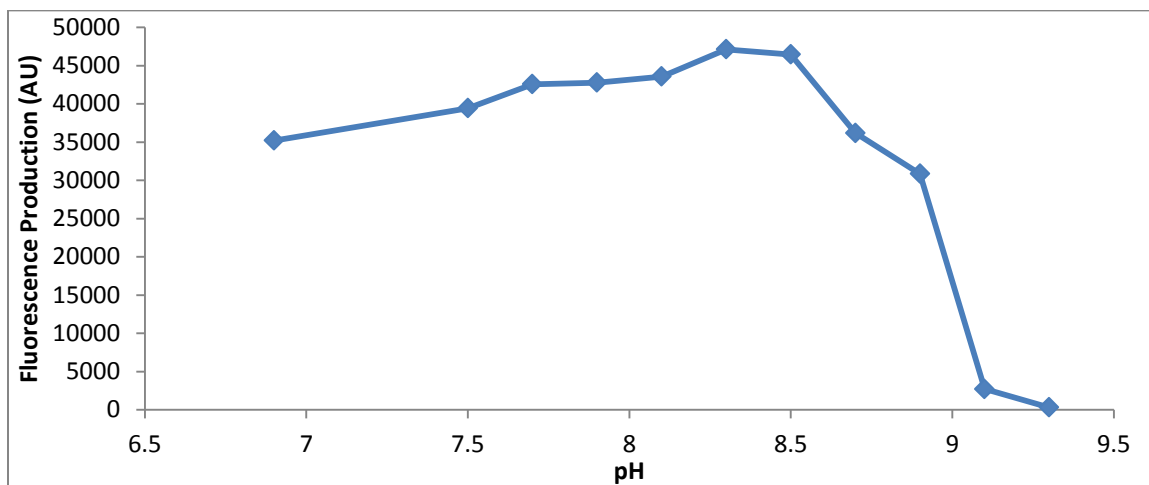
Figure 9.18: Initial rates of ELF97 substrate conversion via alkaline phosphatase are highest within a buffer pH range of 8 to 8.5 (measured at 60 seconds).

It is also possible that non-ionic detergents (such as CHAPS) may interfere with the intermolecular forces that which are responsible for crystal nucleation. To determine which buffer components might be responsible for the inhibition of ELF97 production, four different run buffers were formulated without CHAPS, NDSB, sorbitol and DMSO, respectively. In each case, all other constituents of the run buffer were kept the same. Alkaline phosphatase-linked IgG was then combined with ELF97 substrate (125 μM) within these buffers. 200 μL of each reaction volume was then observed over time using a 96 well microplate reader. Figure 9.19 clearly demonstrates that the inclusion of 3% CHAPS has a dramatic effects upon ELF97 fluorescence by altering the solubility of the product crystal solubility. A closer examination of the product via fluorescence

microscopy showed that the magnitude of the brightness could be correlated to crystal size and density.
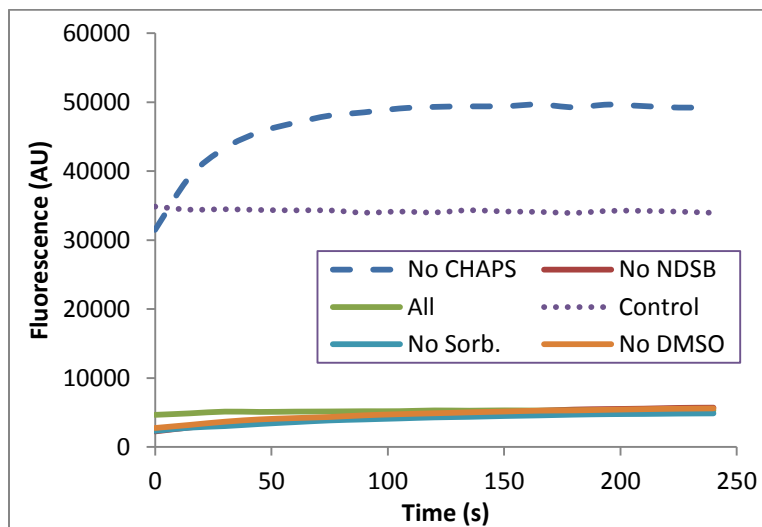
Figure 9.19: The rate of alkaline phosphatase/ELF97 fluorescence production was highest for the run buffer in the absence of CHAPS.

A microplate experiment was designed to assess the effects of varying CHAPS concentration upon ELF97 fluorescence activity. Run buffers were formulated from 3% CHAPS down to 0% CHAPS in increments of 0.5%. Fluorescence production from an ELF97 substrate (125 µM) and AP-IgG reaction mixture was monitored in these different buffers over time. Results plotted in Figure 9.20 illustrate the maximum fluorescence observed at the endpoint (t = 7 minutes) as a function of CHAPS concentration.
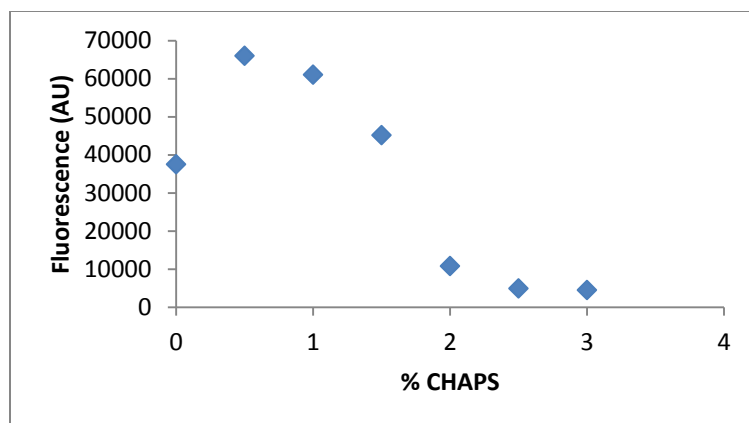
Figure 9.20: Fluorescence production rates for the alkaline phosphatase/ELF97 enzyme-substrate pair were shown to be highest in run buffers containing 0.5% CHAPS.

The maximal fluorescence intensity was obtained at a CHAPS concentration of 0.5%, rather than the CHAPS-free buffer (0%). Crystalline products formed from enzyme-substrate reactions in 0.5% CHAPS were then examined under fluorescence microscopy, as illustrated in Figure 9.21.
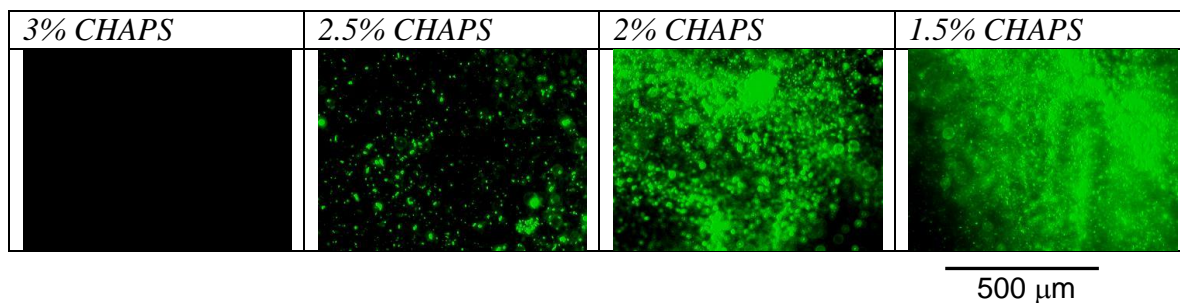
Figure 9.21: ELF97 product solubility and fluorescence varies in response to the concentration of CHAPS detergent within the reaction buffer.

Again, we see that the physical properties of the insoluble ELF97 crystal have a strong effect upon the magnitude of the corresponding fluorescent signal. A subsequent experiment examining the effects of CHAPS concentration on alkaline phosphatase-

ELF97 fluorescence kinetics in Tris-glycine also revealed the same trend, with a maximal reading in 0.5% CHAPS.

9.6 GFP Probing via ELF97

Off-chip characterization of the ELF97 crystallization process helped identify critical factors for enzymatic signal production including optimal pH levels and detergent concentrations. One important question which remained was whether these components would be essential for maintaining effective isoelectric focusing and BP-PA gel capture. For example, altering the concentration of CHAPS to allow for efficient fluorescent crystal formation may be counterproductive to the prevention of protein precipitation during isoelectric focusing. A 1997 paper from Conti and Righetti [125] suggests that different formulations of solubilizing agents will be optimal for different proteins in IEF. Therefore, optimized conditions for crystal growth were validated in an on-chip IEF immunoassay system.

IEF gel and buffer solutions were formulated at a reduced CHAPS concentration of 0.5%. Recombinant GFP (600 nM) was then focused and immobilized on-chip. The GFP was probed with a red labeled goat polyclonal antibody to GFP, followed by an alkaline phosphatase-conjugated anti-goat IgG secondary antibody. ELF97 substrate (0.67 mM) was introduced for 5 minutes before the electric field was shut off and bands were allowed to develop over time. Figure 9.22 demonstrates that the ELF97 could be converted to a bright insoluble crystalline form which precipitated at the site of the GFP band.
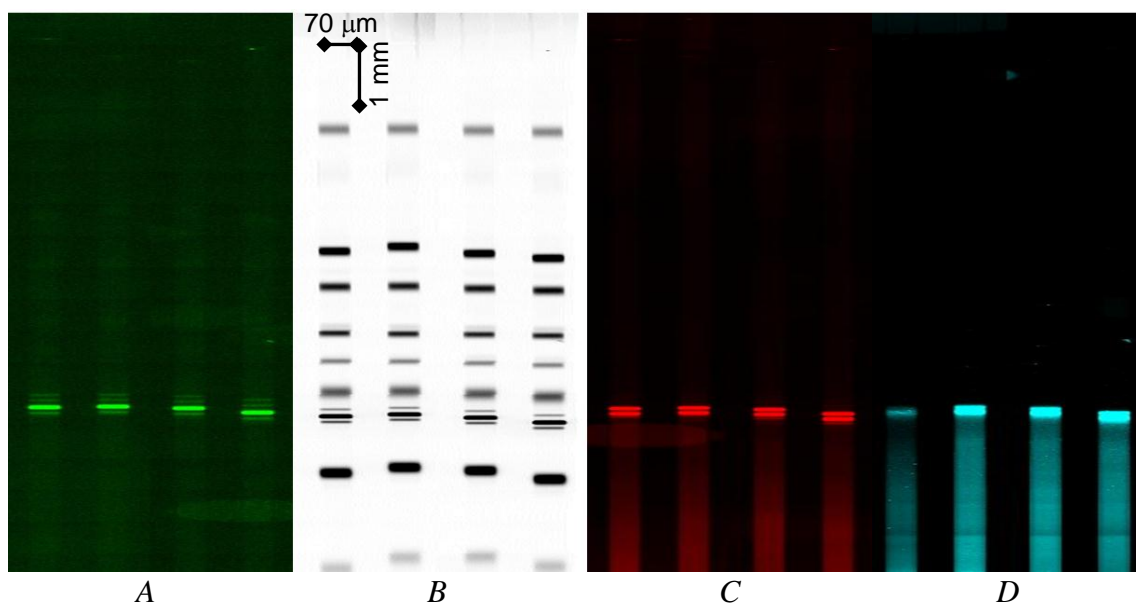
Figure 9.22: Results from focusing, probing and following ELF97 development

A) *Captured and focused GFP*
B) *Isoelectric focusing marker proteins*
C) *Red polyclonal primary antibody probing of GFP*
D) *ELF97 crystal bands following secondary Ab and substrate introduction*

Even at an exposure time of 10 ms, the signal from the ELF97 crystal band saturated the CCD camera. The maximum signal intensity was $16.3\times$ higher than the band signal from the fluorescent primary antibody and $77\times$ higher than the signal from the target GFP band itself. However, the degree of signal amplification arising from the enzymatic conversion process was actually much higher, due to the limitations of pixel saturation.

Although the substrate was continuously introduced, fluorescent crystal formation did not become apparent until six minutes of substrate loading. The ELF97 crystal clearly formed a front which was co-localized to the GFP band. However, crystal formation occurs behind this front, as product formation first becomes apparent in the region behind the target band. Two bands were visible during the initial stages of precipitate formation, but the fluorescent product eventually accumulated to obscure GFP isoforms so that only

a single band could be observed. A reduction of CHAPS concentration from 3.0 to 0.5%

(w/v) resulted in a 60% increase in target capture efficiency (from 1.7% to 2.8%, n=8)

indicating that higher CHAPS concentrations interfere with the ability of local proteins to

covalently attach with benzophenone in the BP-PA gel.

9.7 Enzyme Linked Detection of SOD2 in Transfected Lysate

Next, the application of an enzyme-linked probe detected via ELF97 was tested using

a target protein (SOD2) within a complex sample background. Lysate from a 293T

transfected cell line expressing SOD2 was diluted 6× and electrophoretically loaded into

a BP-PA microgel for isoelectric focusing. IEF gel and buffer solutions were formulated

at a CHAPS concentration of 1% (w/v). Mouse monoclonal antibodies to SOD2 were

conjugated to alkaline phosphatase via a kit based upon a bisaryl hydrazone bond and an

amine-coupled S-HyNic Linker.

After focusing and immobilization, microchannels were washed out and the alkaline

phosphatase conjugated anti-SOD2 primary antibody was introduced at 400 nM.

Following removal of the enzyme conjugate primary, ELF97 substrate (2.5 mM) was

introduced to the microchannels via application of an electric field (200 V/cm for 6

minutes). The electric field was then shut off, and substrate development was observed

for 20 minutes (exposure time = 20 ms). Results from ELF97 development at $t = 20$

minutes are shown in Figure 9.23. All of the channels were able to convert ELF97 into a

soluble fluorescent product (Figure 9.23C). However, it was only in the far right channel

that the soluble product was able to coalesce into a crystal precipitate, resulting in a

single ELF97 crystal band centered at pH 5.5.
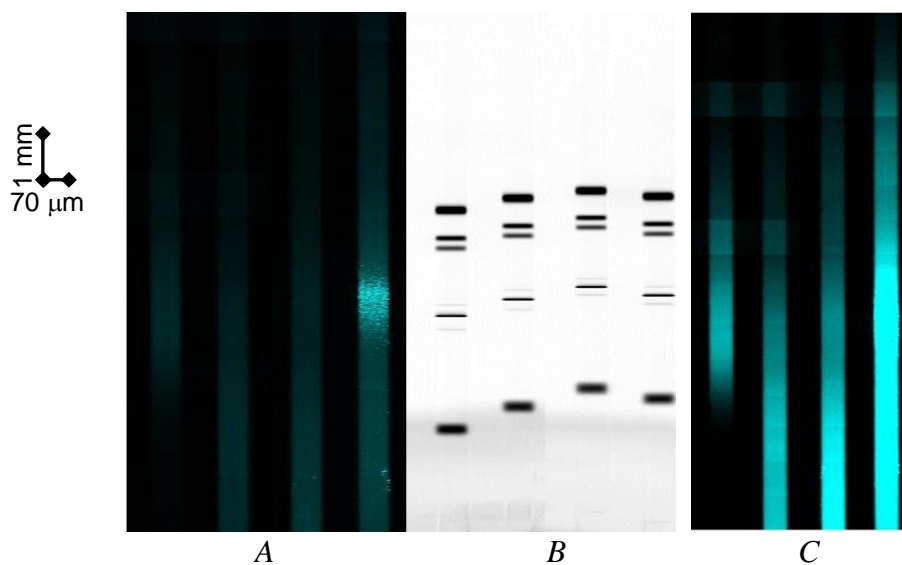
Figure 9.23: A) ELF97 development at t=20 minutes. B) UV fluorescent pI ladder. C) ELF97 development at t=20 minutes is shown at lower fluorescence contrast.

The onset of crystallization generates a saturating fluorescence response at the reaction site which dwarfs the previously observed background. Figure 9.24 depicts the emergence of this ELF crystal product as it emerges from a dimly fluorescent background. This results suggest that high sensitivity target detection is possible if fluorescent crystals are allowed to form at the antigenic site and if the signal background can be controlled through optimization of the enzyme/substrate development process.
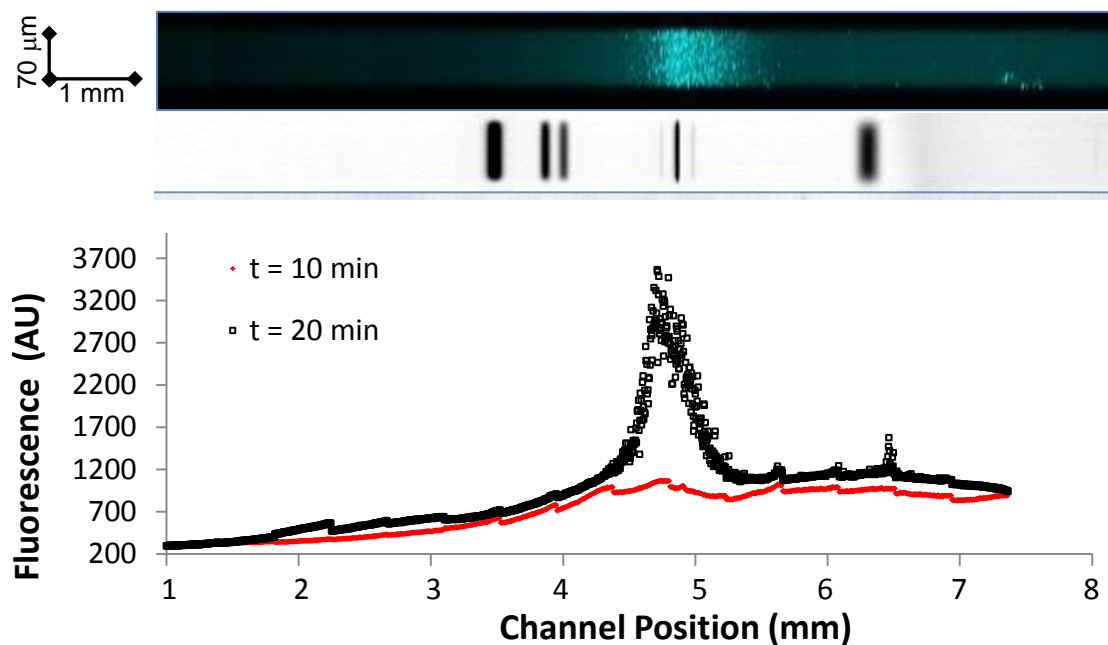
Figure 9.24: A band of fluorescent product crystallizes, to emerge from the channel background between t = 10 mins and t = 20 mins.

Alternatively, one can generate a plot of localized enzyme activity by plotting fluorescence production as a function of time at a single point along the axis, and then taking the first derivative with respect to time to eliminate background artifacts. The maximum slope can then be correlated to the rate of substrate turnover and in turn, the number of enzyme linked probe molecules.

9.8 ELF97 Crystal Development: Effects of Substrate Distribution

To explore optimal conditions for enzyme linked signal development, a variety of substrate concentrations and electrokinetic loading processes were explored. These included substrate concentrations of 5 mM, 3.3mM, 2.2 mM and 1.1 mM. The strength of the loading field was gradually increased from 200 to 400 V/cm and correspondingly, the timescale of loading was decreased from 6 minutes to as little as 75 seconds.

At higher field strength (400 V/cm), fluorescence development usually occurred within the first minute of loading, whereas other experiments (200 V/cm) typically required 4 to 5 minutes prior to the onset of crystallization. Fluorescent crystallization proceeded from the anodic end of the device, eventually growing to the point where the background signal overwhelmed the antigen band. ELF97 crystals were able to form at a faster rate under high field strength conditions. However, the rapid development of target bands was complicated by the simultaneous emergence of high background signals. Resulting channel images could be difficult to interpret when crystals were fully developed, although distinct peaks could be identified by rigorously monitoring fluorescence distribution during the early stages of crystal growth.

Based upon these results, we conclude that faster crystallization rates are achieved through higher loading field strengths, longer substrate loading times and higher substrate concentrations. The initial approach was to saturate the channel with as much substrate in as short of a timeframe as possible. However, the high background in these situations suggests that it would be advantageous to decrease the substrate concentration so that specific target bands are allowed to develop slowly and preferentially.

9.9 Limits of Alkaline Phosphatase-Linked ELF97 Detection

Alkaline phosphatase at varying concentrations (700 nM to 700 fM) was directly loaded, focused and immobilized within BP-PA isoelectric focusing devices. Following a washout step, ELF97 substrate (2.5 mM) was electrophoretically loaded into the channels at 250 V/cm for 2.5 minutes. Results across a range of concentrations – imaged at $t = 45$ minutes are shown in Figure 9.25 at identical exposure and contrast settings:
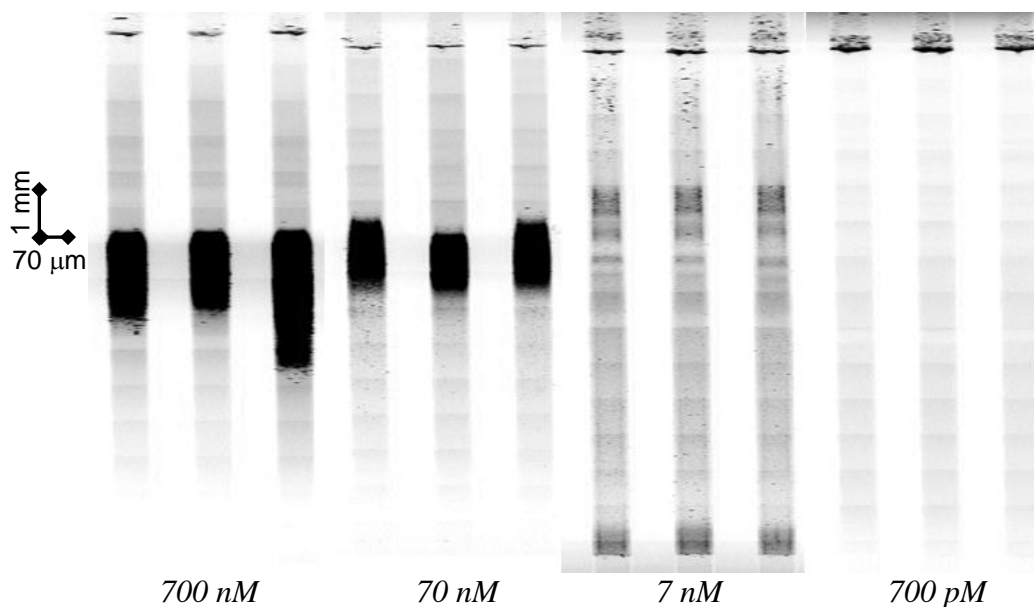
Figure 9.25: ELF97 signals arising from direct alkaline phosphatase immobilization indicate limits of detection in the low nM range.

Figure 9.25 demonstrates that the lower limit of detection for pure immobilized alkaline phosphatase lies in the low nM range, as no crystal signal could be observed at values of 700 pM and below. From the final band distribution (assuming 1% capture efficiency), we estimate 1.5×10^6 alkaline phosphatase molecules are distributed across a span of 300 μm, corresponding to a local alkaline phosphatase concentration of about 100 pM at the point of signal generation.

In a similar experiment, AP plugs of 10 nM, 1 nM and 100 pM were immobilized in BP-PA gels containing 0% CHAPS. CHAPS was completely removed from the buffer to see if the absence of this detergent could encourage ELF crystal formation at lower enzyme concentrations. As ELF97 substrate was introduced under identical conditions, scans were performed across a time span of 12 minutes. However, only the 10 nM experiment was able to generate fluorescent crystals within the first 20 minutes of

incubation. This result suggests that CHAPS alone is not completely responsible for the inability to form fluorescent crystals in the BP-PA gel at alkaline phosphatase concentrations ≤ 1 nM.

10. Conclusion

This chapter describes conclusions and contributions drawn from this work towards high efficiency immunoanalysis of multiple protein targets. Advances in multianalytical protein blotting and post-translational modification analysis are summarized. We outline key similarities and differences in operational objectives for microfluidic two-dimensional blotting and probed IEF immunoassays. Damkohler analyses of antigen-antibody interactions within the two electrophoretic systems are used to model system performance and inform device design, and some directions for the future development of high sensitivity microfluidic immunoassay are proposed.

Immunoassays described in this work apply antigen-antibody binding interactions within a microscale format for rapid and efficient detection of multiple targets in a single sample. The two dimensional immunoblotting device is able to separate constituent analytes based upon charge-to-mass ratio and identifies multiple targets through specific immunoaffinity binding interactions. Similarly, immunoprobed isoelectric focusing separates analytes on the basis of isoelectric point, allowing for subsequent analysis of target proteins and post-translationally modified residues.

A multistage gel photopatterning process was integrated with traditional mask-based photolithography and UV-initiated polymerization chemistry to allow multiple polyacrylamide gels with different physical and functional properties to be integrated into a planar central chamber ($\approx$ 1mm $\times$ 1mm) with no dead volume. The placement of disparate gel microstructures in close proximity with one another resulted in a

161

streamlined assay process that could be completed within 5 minutes. After electrophoretic separation through a sieving matrix, target proteins were directly transferred to adjacent blotting regions (containing matched pair antibodies) through automated and spatially uniform electric field control. Discretized protein blotting zones captured all target molecules at high efficiency, which enabled comparison of relative protein expression levels. Fluorescence readings from immobilized targets yielded quantitative measurements of protein concentration and a "label free" detection strategy was demonstrated to eliminate the need for fluorophore conjugation to the sample. The two-dimensional blotting format presented in this work improves upon standard slab-gel blotting through an integrated workflow that enables simultaneous detection of multiple analytes. Immunoblotted target proteins are rapidly isolated from a sample and subsequent analyses occur in the absence of a complex background.

Operation of the 2D multianalytical blotting device was demonstrated for several model proteins simultaneously, providing a multiplexed protein measurement platform to obviate the need for laborious cycles of slab gel PAGE and membrane reblotting. This two-dimensional immunoassay platform was then applied towards the study of acetylated superoxide dismutase 2, a mitochondrial enzyme which catalyzes the conversion of damaging superoxide into hydrogen peroxide and O_2. The charge shifting behavior of acetylated SOD2 and the need to screen multiple antibodies motivated the development of an isoelectric focusing immunoassay with pan-specific protein capture for the analysis of post-translationally modified SOD2.

A microfluidic device for immunoprobed isoelectric focusing combined the power of charge-based protein separation with the specificity imparted by antibody mediated target

identification. IEF was carried out in a single microchannel containing a polyacrylamide gel, followed by covalent immobilization of proteins to the gel matrix. Two types of antibody probes were applied to analyze PTMs upon a specified protein target. Antibodies in one spectral channel were specific for broad classes of post-translationally modified residues, while antibodies labeled in another spectral channel were specific for the protein of interest. Therefore, the co-localization of multi-spectral probe signals provided layered information regarding protein identity and corresponding degrees of PTM. Observations of varying antibody mobility in polyacrylamide gels of different pH were correlated with pH gradient maps to suggest conditions for optimal fluorescent probe coverage.

Antibody-mediated target recognition was coupled with observation of characteristic charge shifting behavior to provide further confidence in identifying post-translational modifications. Imaging probed target bands along the length of the microchannel allowed for intuitive data visualization and analysis so that quantitative PTM measurements could obtained through a single workflow. The assay can be completed within 2 hours and was demonstrated for analysis of phosphorylated and acetylated proteins in buffers and complex samples.

Non-dimensional Damkohler analysis was applied to inform microfluidic system design for both the 2D native blotting and the probed IEF immunoassays. It is instructive to consider similarities and differences in assay operation which underlie these two applications. In both cases, there exists some finite amount of some protein target whose concentration will be determined by the biological sample of interest.

In two dimensional planar immunoblotting, the target antigen is electrophoretically mobile while a capture antibody is immobilized. Here, the goal is to capture all of the targeted antigen molecules as they move through the antibody functionalized blotting region. Thus, we design the system to be mass transport limited ($Da > 10$), and parameters such as binding site density, and the magnitude of the electric field are tuned to enable efficient blotting performance. A numerical simulation based upon known device physics and a Langmuir binding model is developed as a tool to describe the efficiency of protein capture in relationship to operating parameters and characteristic Da.

	2D Immunoblotting	Probed Isoelectric Focusing
Separation Mechanism	Charge-to-mass ratio	Isoelectric point
Targets Detected	Multiple proteins within the same sample	Target proteins and matching post-translational modifications
Operating Regime	Mass transport limited ($Da > 10$)	Reaction limited ($Da < 1$)
Assay Time	5 minutes	2 hours

Table 10.1: A comparison of 2D immunoblotting and probed isoelectric focusing immunoassays. Each strategy employs a different separation mechanism and Damkohler operating regimes are tuned to achieve multi-target detection goals.

In immunoprobing proteins separated after isoelectric focusing, the antigen targets are immobilized (via covalent attachment to BP-PA) while the antibody probe is electrophoretically mobile. In this case, we now design the system to be reaction limited ($Da < 1$) because the goal is to achieve a high degree of antigen-antibody complex formation within a short amount of time. Antibody probes which remain unbound do not negatively impact system performance, because these can be removed from the gel and therefore may be specified in excess.

164

These microscale immunoassay formats result in decreased reagent volume requirements over four orders of magnitude. An order of magnitude decrease is also observed for sample volume (and hence, cell population) requirements, opening up new possibilities in the range of biological questions that can be explored through immunoassay. Looking forward, IEF reagent compositions can be optimized to increase the efficiency of the UV-immobilization process (as only ~1% of target antigens are currently captured through the benzophenone conjugate).

Promising results from laser scanning have been presented as another method to increase measurement sensitivity. However, further improvements to sensitivity (beyond the limits of fluorescence detection) are likely to be possible through the use of enzyme-linked signal amplification. Obtaining quantitative measurements from enzymatic techniques can be challenging in an on-chip immunoassay - even when examining an insoluble fluorescent product. Localized product signals, observed at a single time point, cannot be directly or linearly correlated to target protein concentration. Other relevant factors affecting Michaelis-Menten reaction kinetics include local substrate concentrations and calibrated enzyme activity. These factors must be characterized to enable high sensitivity, quantitative target measurements via on-chip enzymatic immunoassay and multiple measurements will be necessary to establish a time course of reaction.

11. References

1. Dunham, I. and E. Consortium, *An integrated encyclopedia of DNA elements in the human genome.* Nature, 2012. **489**(7414): p. 57-74.
2. Khoury, G.A., R.C. Baliban, and C.A. Floudas, *Proteome-wide post-translational modification statistics: frequency analysis and curation of the swiss-prot database.* Sci Rep, 2011. **1**.
3. Braden, B.C. and R.J. Poljak, *Structural features of the reactions between antibodies and protein antigens.* FASEB J, 1995. **9**(1): p. 9-16.
4. Wan, X.S., et al., *Three immunoassays based on monoclonal antibodies specific for prostate specific antigen (PSA), alpha-1-antichymotrypsin (ACT), and the PSA-ACT complex.* Prostate, 2003. **56**(2): p. 131-41.
5. Hattori, T., et al., *High affinity anti-inorganic material antibody generation by integrating graft and evolution technologies: potential of antibodies as biointerface molecules.* J Biol Chem, 2010. **285**(10): p. 7784-93.
6. Teale, J.D., et al., *Production of antibodies to tetrahydrocannabinol as the basis for its radioimmunoassay.* Nature, 1974. **249**(453): p. 154-5.
7. Zeck, A., M.G. Weller, and R. Niessner, *Characterization of a monoclonal TNT-antibody by measurement of the cross-reactivities of nitroaromatic compounds.* Fresenius Journal of Analytical Chemistry, 1999. **364**(1-2): p. 113-120.
8. Kurien, B.T. and R.H. Scofield, *A brief review of other notable protein detection methods on blots.* Methods Mol Biol, 2009. **536**: p. 557-71.
9. Fido, R.J., A.S. Tatham, and P.R. Shewry, *Western blotting analysis.* Methods Mol Biol, 1995. **49**: p. 423-37.
10. Towbin, H., T. Staehelin, and J. Gordon, *Electrophoretic transfer of proteins from polyacrylamide gels to nitrocellulose sheets: procedure and some applications.* Proc Natl Acad Sci U S A, 1979. **76**(9): p. 4350-4.
11. Giddings, J.C., *Unified Separation Science.* 1991: Wiley-Interscience.
12. Bousse, L., et al., *Protein sizing on a microchip.* Anal Chem, 2001. **73**(6): p. 1207-12.
13. Vergeles, M., et al., *Stokes drag at the molecular level.* Phys Rev Lett, 1995. **75**(2): p. 232-235.
14. Stryer, L., *Biochemistry.* 4th edition ed. 1995, New York, NY: W.H. Freeman & Company.
15. Yao, S., et al., *SDS capillary gel electrophoresis of proteins in microfabricated channels.* Proc Natl Acad Sci U S A, 1999. **96**(10): p. 5372-7.
16. Tsai, S.W., et al., *Native and sodium dodecyl sulfate-capillary gel electrophoresis of proteins on a single microchip.* Electrophoresis, 2004. **25**(3): p. 494-501.
17. Herr, A.E. and A.K. Singh, *Photopolymerized cross-linked polyacrylamide gels for on-chip protein sizing.* Anal Chem, 2004. **76**(16): p. 4727-33.
18. Krajewski, S., X. Huang, and M. Krajewska, *Multiple antigen detection (MAD) western blotting.* Methods Mol Biol, 2009. **536**: p. 473-81.
19. Pan, W., W. Chen, and X. Jiang, *Microfluidic Western blot.* Anal Chem, 2010. **82**(10): p. 3974-6.

20. Liu, J., et al., *Polyacrylamide gel plugs enabling 2-D microfluidic protein separations via isoelectric focusing and multiplexed sodium dodecyl sulfate gel electrophoresis.* Electrophoresis, 2008. **29**(11): p. 2241-50.

21. Das, C., et al., *Integration of isoelectric focusing with multi-channel gel electrophoresis by using microfluidic pseudo-valves.* Lab Chip, 2007. **7**(12): p. 1806-12.

22. Bjellqvist, B., et al., *Isoelectric focusing in immobilized pH gradients: principle, methodology and some applications.* J Biochem Biophys Methods, 1982. **6**(4): p. 317-39.

23. Laas, T., I. Olsson, and L. Soderberg, *High-voltage isoelectric focusing with pharmalyte: field strength and temperature distribution, zone sharpening, isoelectric spectra, and pI determinations.* Anal Biochem, 1980. **101**(2): p. 449-61.

24. Dinasarapu, A.R., et al., *Signaling gateway molecule pages--a data model perspective.* Bioinformatics, 2011. **27**(12): p. 1736-8.

25. Sennepin, A.D., et al., *Multiple reprobing of Western blots after inactivation of peroxidase activity by its substrate, hydrogen peroxide.* Anal Biochem, 2009. **393**(1): p. 129-31.

26. Gallagher, S., et al., *Immunoblotting and immunodetection.* Curr Protoc Immunol, 2008. **Chapter 8**: p. Unit 8 10.

27. Arenkov, P., et al., *Protein microchips: use for immunoassay and enzymatic reactions.* Anal Biochem, 2000. **278**(2): p. 123-31.

28. Noya, O. and B. Alarcon de Noya, *The multiple antigen blot assay (MABA): a simple immunoenzymatic technique for simultaneous screening of multiple antigens.* Immunol Lett, 1998. **63**(1): p. 53-6.

29. Fritzler, M.J., *Advances and applications of multiplexed diagnostic technologies in autoimmune diseases.* Lupus, 2006. **15**(7): p. 422-7.

30. Pelech, S., C. Sutter, and H. Zhang, *Kinetworks protein kinase multiblot analysis.* Methods Mol Biol, 2003. **218**: p. 99-111.

31. Aebersold, R., et al., *Towards an integrated analytical technology for the generation of multidimensional protein expression maps.* J Protein Chem, 1998. **17**(6): p. 533-5.

32. Hille, J.M., A.L. Freed, and H. Watzig, *Possibilities to improve automation, speed and precision of proteome analysis: a comparison of two-dimensional electrophoresis and alternatives.* Electrophoresis, 2001. **22**(19): p. 4035-52.

33. Lee, K.H., *Proteomics: a technology-driven and technology-limited discovery science.* Trends Biotechnol, 2001. **19**(6): p. 217-22.

34. Hierlemann, A., et al., *Microfabrication Techniques for Chemical/Biosensors.* Proc. IEEE, 2003. **91**(6): p. 839-863.

35. Unger, M.A., et al., *Monolithic microfabricated valves and pumps by multilayer soft lithography.* Science, 2000. **288**(5463): p. 113-6.

36. Lion, N., et al., *Microfluidic systems in proteomics.* Electrophoresis, 2003. **24**(21): p. 3533-62.

37. Melin, J. and S.R. Quake, *Microfluidic large-scale integration: the evolution of design rules for biological automation.* Annu Rev Biophys Biomol Struct, 2007. **36**: p. 213-31.

38. Tia, S. and A.E. Herr, *On-chip technologies for multidimensional separations.* Lab Chip, 2009. **9**(17): p. 2524-36.

39. Thorsen, T., S.J. Maerkl, and S.R. Quake, *Microfluidic large-scale integration.* Science, 2002. **298**(5593): p. 580-4.

40. Ramsey, J.D., et al., *High-efficiency, two-dimensional separations of protein digests on microfluidic devices.* Anal Chem, 2003. **75**(15): p. 3758-64.

41. Culbertson, C.T., S.C. Jacobson, and J.M. Ramsey, *Microchip devices for high-efficiency separations.* Anal Chem, 2000. **72**(23): p. 5814-9.

42. Apori, A.A. and A.E. Herr, *Chip-based immunoassays.* Methods Mol Biol, 2012. **919**: p. 233-48.

43. Anderson, G.J., M.C. C, and R.T. Kennedy, *Western Blotting Using Capillary Electrophoresis.* Anal Chem, 2011.

44. Herr, A.E., et al., *Microfluidic immunoassays as rapid saliva-based clinical diagnostics.* Proc Natl Acad Sci U S A, 2007. **104**(13): p. 5268-73.

45. Fan, R., et al., *Integrated barcode chips for rapid, multiplexed analysis of proteins in microliter quantities of blood.* Nat Biotechnol, 2008. **26**(12): p. 1373-8.

46. Berry, S.M., E.T. Alarid, and D.J. Beebe, *One-step purification of nucleic acid for gene expression analysis via Immiscible Filtration Assisted by Surface Tension (IFAST).* Lab Chip, 2011. **11**(10): p. 1747-53.

47. Fordyce, P.M., et al., *De novo identification and biophysical characterization of transcription-factor binding sites with microfluidic affinity analysis.* Nat Biotechnol, 2010. **28**(9): p. 970-5.

48. Becker, H., Lowack, K., Manz, A., *Planar quartz chips with submicron channels for two-dimensional capillary electrophoresis applications.* J. Micromech. Microeng., 1998. **8**: p. 24-28.

49. Kaniansky, D., et al., *Capillary electrophoresis separations on a planar chip with the column-coupling configuration of the separation channels.* Anal Chem, 2000. **72**(15): p. 3596-604.

50. Huang, L.R., et al., *A DNA prism for high-speed continuous fractionation of large DNA molecules.* Nature Biotechnology, 2002. **20**(10): p. 1048-1051.

51. Lao, A.I. and I.M. Hsing, *Flow-based and sieving matrix-free DNA differentiation by a miniaturized field flow fractionation device.* Lab Chip, 2005. **5**(6): p. 687-90.

52. Yang, S., J. Liu, and D.L. DeVoe, *Optimization of sample transfer in two-dimensional microfluidic separation systems.* Lab Chip, 2008. **8**(7): p. 1145-52.

53. He, M. and A.E. Herr, *Polyacrylamide gel photopatterning enables automated protein immunoblotting in a two-dimensional microdevice.* J Am Chem Soc, 2010. **132**(8): p. 2512-3.

54. Tovey, E.R. and B.A. Baldo, *Protein binding to nitrocellulose, nylon and PVDF membranes in immunoassays and electroblotting.* J Biochem Biophys Methods, 1989. **19**(2-3): p. 169-83.

55. Emmett, M. and A.J. Crowle, *Crossed immunoelectrophoresis: qualitative and quantitative considerations.* J Immunol Methods, 1982. **50**(2): p. R65-83.

56. Laine, A., M.P. Ducourouble, and M.H. Hannothiaux, *Identification of proteins by crossed immunoelectrophoresis with a trap-gel.* Anal Biochem, 1987. **161**(1): p. 39-44.

57. Gale, D.S., J.M. Versey, and J.R. Hobbs, *Rocket immunoselection for detection of heavy-chain diseases.* Clin Chem, 1974. **20**(10): p. 1292-4.

58. He, M. and A.E. Herr, *Automated microfluidic protein immunoblotting.* Nat Protoc, 2010. **5**(11): p. 1844-1856.

59. Squires, T.M., R.J. Messinger, and S.R. Manalis, *Making it stick: convection, reaction and diffusion in surface-based biosensors.* Nat Biotechnol, 2008. **26**(4): p. 417-26.

60. Benes, K., P. Tong, and B.J. Ackerson, *Sedimentation, Peclet number, and hydrodynamic screening.* Phys Rev E Stat Nonlin Soft Matter Phys, 2007. **76**(5 Pt 2): p. 056302.

61. Sadana, A. and T. Vo-Dinh, *Antibody-antigen binding kinetics. A model for multivalency antibodies for large antigen systems.* Appl Biochem Biotechnol, 1997. **67**(1-2): p. 1-22.

62. Buchanan, D.D., et al., *Effect of buffer, electric field, and separation time on detection of aptamer-ligand complexes for affinity probe capillary electrophoresis.* Electrophoresis, 2003. **24**(9): p. 1375-82.

63. Zhuang, G., et al., *Measurement of association rate constant of antibody-antigen interaction in solution based on enzyme-linked immunosorbent assay.* J Biosci Bioeng, 2001. **92**(4): p. 330-6.

64. Inger, G.R., *Scaling nonequilibrium-reacting flows: The legacy of Gerhard Damkohler.* Journal of Spacecraft and Rockets, 2001. **38**(2): p. 185-190.

65. Bharadwaj, R., et al., *Analysis and optimization of nonequilibrium capillary electrophoresis of alpha-fetoprotein isoforms.* Anal Chem, 2008. **80**(1): p. 129-34.

66. Wei, Y., et al., *Measurement of Protein-Ligand Binding Constants from Reaction-Diffusion Concentration Profiles.* Anal Chem, 2010.

67. O'Neill, R.A., et al., *Isoelectric focusing technology quantifies protein signaling in 25 cells.* Proc Natl Acad Sci U S A, 2006. **103**(44): p. 16153-8.

68. Gallagher, S.R., *One-dimensional SDS gel electrophoresis of proteins.* Curr Protoc Cell Biol, 2007. **Chapter 6**: p. Unit 6 1.

69. Qiu, X., et al., *Calorie restriction reduces oxidative stress by SIRT3-mediated SOD2 activation.* Cell Metab, 2010. **12**(6): p. 662-7.

70. Tia, S.Q., et al., *Multianalyte on-chip native Western blotting.* Anal Chem, 2011. **83**(9): p. 3581-8.

71. Schagger, H. and G. von Jagow, *Blue native electrophoresis for isolation of membrane protein complexes in enzymatically active form.* Anal Biochem, 1991. **199**(2): p. 223-31.

72. Maalouf, A., M. Gadonna, and D. Bosc, *An improvement in standard photolithography resolution based on Kirchhoff diffraction studies.* Journal of Physics D-Applied Physics, 2009. **42**(1).

73. Righetti, P.G. and C. Gelfi, *Electrophoresis gel media: the state of the art.* J Chromatogr B Biomed Sci Appl, 1997. **699**(1-2): p. 63-75.

74. Hou, C. and A.E. Herr, *Ultrashort separation length homogeneous electrophoretic immunoassays using on-chip discontinuous polyacrylamide gels.* Anal Chem, 2010. **82**(8): p. 3343-51.

75. He, M. and A.E. Herr, *Microfluidic polyacrylamide gel electrophoresis with in situ immunoblotting for native protein analysis.* Anal Chem, 2009. **81**(19): p. 8177-84.

76. Diamandis, E.P. and T.K. Christopoulos, *The biotin-(strept)avidin system: principles and applications in biotechnology.* Clin Chem, 1991. **37**(5): p. 625-36.

77. Wilbur, D.S., et al., *Development of new biotin/streptavidin reagents for pretargeting.* Biomol Eng, 1999. **16**(1-4): p. 113-8.

78. Glass, N.R., et al., *Organosilane deposition for microfluidic applications.* Biomicrofluidics, 2011. **5**(3): p. 36501-365017.

79. Lerch, M.A. and S.C. Jacobson, *Electrokinetic fluid control in two-dimensional planar microfluidic devices.* Anal Chem, 2007. **79**(19): p. 7485-91.

80. Giancoli, D., *Physics for Scientists & Engineers with Modern Physics*. 4th ed. 2008, Boston, MA: Addison-Wesley.

81. Fu, L.M., et al., *Electrokinetic injection techniques in microfluidic chips.* Anal Chem, 2002. **74**(19): p. 5084-91.

82. Alarie, J.P., S.C. Jacobson, and J.M. Ramsey, *Electrophoretic injection bias in a microchip valving scheme.* Electrophoresis, 2001. **22**(2): p. 312-7.

83. Fuxman, A.M., K.B. McAuley, and L.J. Schreiner, *Modelling of polyacrylamide gel dosimeters with spatially non-uniform radiation dose distributions.* Chemical Engineering Science, 2005. **60**(5): p. 1277-1293.

84. Hatch, A.V., et al., *Integrated preconcentration SDS-PAGE of proteins in microchips using photopatterned cross-linked polyacrylamide gels.* Anal Chem, 2006. **78**(14): p. 4976-84.

85. Apori, A.A. and A.E. Herr, *Homogeneous immunosubtraction integrated with sample preparation enabled by a microfluidic format.* Anal Chem, 2011. **83**(7): p. 2691-8.

86. Song, S., A.K. Singh, and B.J. Kirby, *Electrophoretic concentration of proteins at laser-patterned nanoporous membranes in microchips.* Anal Chem, 2004. **76**(15): p. 4589-92.

87. Ozden, O., et al., *Acetylation of MnSOD directs enzymatic activity responding to cellular nutrient status or oxidative stress.* Aging (Albany NY), 2011. **3**(2): p. 102-7.

88. Gems, D. and L. Partridge, *Genetics of Longevity in Model Organisms: Debates and Paradigm Shifts.* Annu Rev Physiol, 2012.

89. Greaves, M., et al., *Mapping cell surface antigen expression of haemopoietic progenitor cells using monoclonal antibodies.* Ciba Found Symp, 1981. **84**: p. 109-29.

90. Choudhary, C., et al., *Lysine acetylation targets protein complexes and co-regulates major cellular functions.* Science, 2009. **325**(5942): p. 834-40.

91. Cohen, H.Y., et al., *Acetylation of the C terminus of Ku70 by CBP and PCAF controls Bax-mediated apoptosis.* Mol Cell, 2004. **13**(5): p. 627-38.

92. Gauci, S., et al., *A versatile peptide pI calculator for phosphorylated and N-terminal acetylated peptides experimentally tested using peptide isoelectric focusing.* Proteomics, 2008. **8**(23-24): p. 4898-906.

93. Colton, I.J., et al., *Formation of protein charge ladders by acylation of amino groups on proteins.* Journal of the American Chemical Society, 1997. **119**(52): p. 12701-12709.

94. Norris, K.L., J.Y. Lee, and T.P. Yao, *Acetylation goes global: the emergence of acetylation biology.* Sci Signal, 2009. **2**(97): p. pe76.

95. Roepstorff, P., *Mass spectrometry in protein studies from genome to function.* Curr Opin Biotechnol, 1997. **8**(1): p. 6-13.

96. Aebersold, R. and M. Mann, *Mass spectrometry-based proteomics.* Nature, 2003. **422**(6928): p. 198-207.

97. Olsen, J.V., et al., *Global, in vivo, and site-specific phosphorylation dynamics in signaling networks.* Cell, 2006. **127**(3): p. 635-48.

98. Minden, J.S., *Two-dimensional difference gel electrophoresis.* Methods Mol Biol, 2012. **869**: p. 287-304.

99. Hughes, A.J., et al., *Microfluidic integration for automated targeted proteomic assays.* Proc Natl Acad Sci U S A, 2012. **109**(16): p. 5972-7.

100. Kehoe, J.W., et al., *Using phage display to select antibodies recognizing post-translational modifications independently of sequence context.* Mol Cell Proteomics, 2006. **5**(12): p. 2350-63.

101. DeRisi, J.L., V.R. Iyer, and P.O. Brown, *Exploring the metabolic and genetic control of gene expression on a genomic scale.* Science, 1997. **278**(5338): p. 680-6.

102. Ehrenpreis, S., P.H. Maurer, and J. Sri Ram, *Modified bovine serum albumin. I. Preparation and physicochemical studies of some derivatives.* Arch Biochem Biophys, 1957. **67**(1): p. 178-95.

103. Saito, H., et al., *Isoelectric Point Marker*, U.S. PTO, Editor. 1982, Oriental Yeast Company, Tokyo, Japan.

104. Blume-Jensen, P. and T. Hunter, *Oncogenic kinase signalling.* Nature, 2001. **411**(6835): p. 355-65.

105. Watanabe, N. and H. Osada, *Phosphorylation-dependent protein-protein interaction modules as potential molecular targets for cancer therapy.* Curr Drug Targets, 2012.

106. Ullrich, A. and J. Schlessinger, *Signal transduction by receptors with tyrosine kinase activity.* Cell, 1990. **61**(2): p. 203-12.

107. Rush, J., et al., *Immunoaffinity profiling of tyrosine phosphorylation in cancer cells.* Nat Biotechnol, 2005. **23**(1): p. 94-101.

108. Ferrell, J.E., Jr., *Tripping the switch fantastic: how a protein kinase cascade can convert graded inputs into switch-like outputs.* Trends Biochem Sci, 1996. **21**(12): p. 460-6.

109. Cohen, P., *The role of protein phosphorylation in human health and disease. The Sir Hans Krebs Medal Lecture.* Eur J Biochem, 2001. **268**(19): p. 5001-10.

110. Zhang, D., L.L. Wong, and E.S. Koay, *Phosphorylation of Ser78 of Hsp27 correlated with HER-2/neu status and lymph node positivity in breast cancer.* Mol Cancer, 2007. **6**: p. 52.

111. During, R.L., et al., *Anthrax lethal toxin paralyzes actin-based motility by blocking Hsp27 phosphorylation.* EMBO J, 2007. **26**(9): p. 2240-50.

112. Bloor, J.H., et al., *Characterization of superoxide dismutase (SOD-1 and SOD-2) activities in inbred mice: evidence for quantitative variability and possible nonallelic SOD-1 polymorphism.* Biochem Genet, 1983. **21**(3-4): p. 349-64.

113. Bingaman, S., V.H. Huxley, and R.E. Rumbaut, *Fluorescent dyes modify properties of proteins used in microvascular research.* Microcirculation, 2003. **10**(2): p. 221-31.

114. Maloney, A., et al., *Gene and protein expression profiling of human ovarian cancer cells treated with the heat shock protein 90 inhibitor 17-allylamino-17-demethoxygeldanamycin.* Cancer Res, 2007. **67**(7): p. 3239-53.

115. Hight, M.R., et al., *Multispectral fluorescence imaging to assess pH in biological specimens.* J Biomed Opt, 2011. **16**(1): p. 016007.

116. Xu, Z., et al., *A novel fiber-optic pH sensor incorporating carboxy SNAFL-2 and fluorescent wavelength-ratiometric detection.* J Biomed Mater Res, 1998. **39**(1): p. 9-15.

117. Bassnett, S., L. Reinisch, and D.C. Beebe, *Intracellular pH measurement using single excitation-dual emission fluorescence ratios.* Am J Physiol, 1990. **258**(1 Pt 1): p. C171-8.

118. Ramdas, L. and W. Zhang, *Microarray image scanning.* Methods Mol Biol, 2006. **319**: p. 261-73.

119. Korn, E.L., et al., *Objective method of comparing DNA microarray image analysis systems.* Biotechniques, 2004. **36**(6): p. 960-7.

120. Breininger, J.F. and D.G. Baskin, *Fluorescence in situ hybridization of scarce leptin receptor mRNA using the enzyme-labeled fluorescent substrate method and tyramide signal amplification.* J Histochem Cytochem, 2000. **48**(12): p. 1593-99.

121. Wang, J., *On-chip enzymatic assays.* Electrophoresis, 2002. **23**(5): p. 713-8.

122. Kemper, C., et al., *Simultaneous, two-color fluorescence detection of total protein profiles and beta-glucuronidase activity in polyacrylamide gel.* Electrophoresis, 2001. **22**(5): p. 970-6.

123. Harrington, S.J., R. Varro, and T.M. Li, *High-Performance Capillary Electrophoresis as a Fast in-Process Control Method for Enzyme-Labeled Monoclonal-Antibody Conjugates.* Journal of Chromatography, 1991. **559**(1-2): p. 385-390.

124. Erdemir, D., A.Y. Lee, and A.S. Myerson, *Nucleation of crystals from solution: classical and two-step models.* Acc Chem Res, 2009. **42**(5): p. 621-9.

125. Conti, M., et al., *Capillary isoelectric focusing: the problem of protein solubility.* J Chrom A, 1997. **757**: p. 237-245.

126. Mendoza, L.G., et al., *High-throughput microarray-based enzyme-linked immunosorbent assay (ELISA).* Biotechniques, 1999. **27**(4): p. 778-80, 782-6, 788.

127. Wiese, R., et al., *Simultaneous multianalyte ELISA performed on a microarray platform.* Clin Chem, 2001. **47**(8): p. 1451-7.

128. Speel, E.J., et al., *A novel fluorescence detection method for in situ hybridization, based on the alkaline phosphatase-fast red reaction.* J Histochem Cytochem, 1992. **40**(9): p. 1299-308.

12. Appendices

Appendix A: Loading Control Measurements

When the target concentration of the sample may be in question, it can be useful to employ an internal standard for normalization of subsequent measurements or to determine if there is some failure with sample loading and transfer. Internal standards proteins are products of so-called "housekeeping genes" that are stably and constitutively expressed at high levels within most cells. The expression level of an internal standard is assumed to be constant. Thus, immunodetection of the internal standard serves as a control which allows normalization of the target signal, as well as an indicator for troubleshooting problems with the assay workflow.

GAPDH is a 37 kDa enzyme located in the cytosol which catalyzes the conversion of glyceraldehyde 3-phosphate and a common housekeeping gene whose expression is frequently utilized as an internal standard during qPCR. Therefore, GAPDH was utilized as a model protein to assess the ability to perform concurrent internal standard measurements on a microfluidic device. Biotinylated anti-GAPDH was obtained from a commercial source and used to fabricate a microfluidic device with a 6%T blotting gel specific for GAPDH immobilization. Fluorescent GAPDH was assayed upon an anti-GADPH device with a 6%T separation gel. Target binding and immobilization was observed when the GAPDH band was transferred laterally to the blotting gel. The capture efficiency here was not as strong as observations of other

binding targets. Figure 12.1 displays an image sequence as a GAPDH band is transferred across the central chamber from right to left.
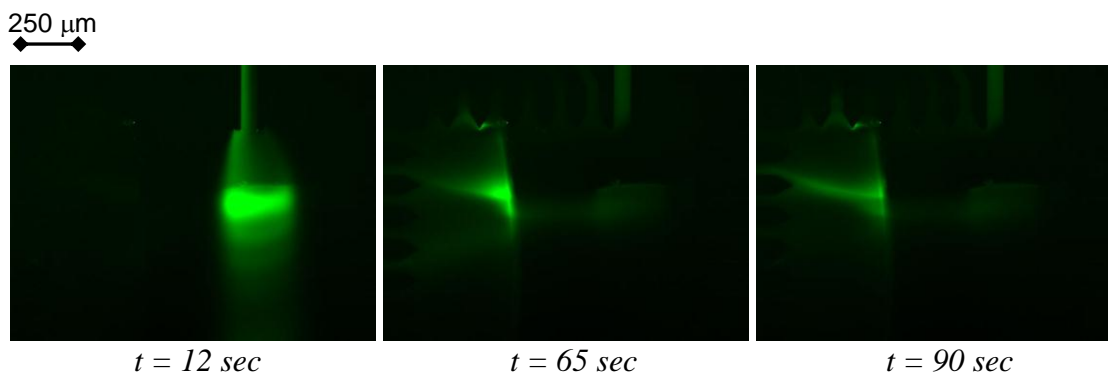

250 μm

| t = 12 sec | t = 65 sec | t = 90 sec |

Figure 12.1: GAPDH band immobilization into an anti-GAPDH blotting region over 90 seconds.

The lower capture efficiency may be due to the fact that this blotting gel precursor contained a lower concentration of capture antibody (0.5 μM versus the typical 1.6 μM), as these antibodies were provided at a low concentration by the commercial supplier. Nevertheless, the anti-GAPDH blotting gel shows a marked affinity for the GAPDH sample.

Validation of GAPDH IEF-Immunoprobing in Lysate

IEF gel and buffer solutions were formulated at a CHAPS concentration of 1%. Regular 293T cell lysate was then spiked with purified GAPDH and diluted 6× into loading buffer (along with pI markers and GFP loading control). The final concentration of GAPDH in the lysate/loading buffer mixture was 1.8 μM. After focusing and immobilization, the channels were washed out and a red fluorescent anti-GAPDH (650

nM) was introduced. The channels are shown below, following probe washout (Figure 12.2).
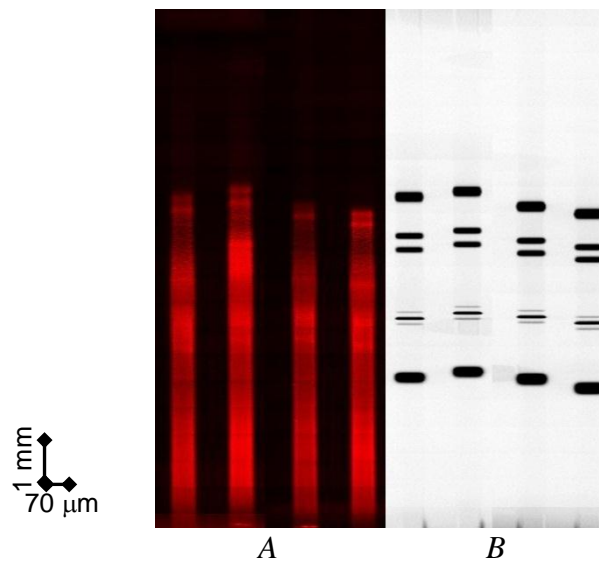
Figure 12.2: Red α-GAPDH, probing (A, after washout) and UV fluorescent pI ladder (B)

Under these conditions, two prominent bands were observed at pH 7.8 and 8.0 (*A*). These high pI points agree with anticipated values. Other possibly non-specific bands also occur at pH 6.6 and 4.9. If possible, the GAPDH control should be imaged using primary antibody fluorescence to avoid obfuscating the ELF97 signal arising from the target antigen.

Appendix B: Alternative Fluorescence Substrates

Papers from Mendoza *et al.* [126] and Wiese et al. [127] which employ ELF97 as a detection mechanism (enzyme linked protein arrays coupled with CCD scanning) have demonstrated crystal growth and LLOD at antigen concentrations between 90-170 pM. It may be possible that even a small amount of zwitterionic detergent (CHAPS @ 0.5%) inhibits crystal formation at low enzyme concentrations – when product conversion falls within the range of the detergent concentration. However – other alkaline phosphatase substrate pairs should be identified and considered simultaneously. A brief review of three potential enzyme/substrate pairs is given below:

Substrate	Ex/Em wavelength	Notes
Fluorescein Diphosphate	490/514 nm	One of the most sensitive fluorogenic substrates. Sensitivity ~ 0.1 pg AP
MUP	360/449 nm	Previous lab experience (zymography). Sensitivity: 0.3 pg AP
AttoPhos	435/555	Promega, Sensitivity: 0.05 milliunits AP
VectorRed	595/615	Yields red fluorescent precipitate.
FastRed/Napthol Phosphate	553/565-620 (584 max)	Yields red fluorescent precipitate with broad emission spectra.

Relevant parameters towards the analysis of enzyme/substrate fluorescence production include:

- Substrate introduction rate and local substrate concentration
- Imaging conditions such as exposure time
- Spectral properties: excitation/emission wavelengths for each substrate
- Solubility and diffusivity of the product molecule
- Buffer conditions (i.e. detergent concentration)
- Immobilized enzyme concentrations (sensitivity)

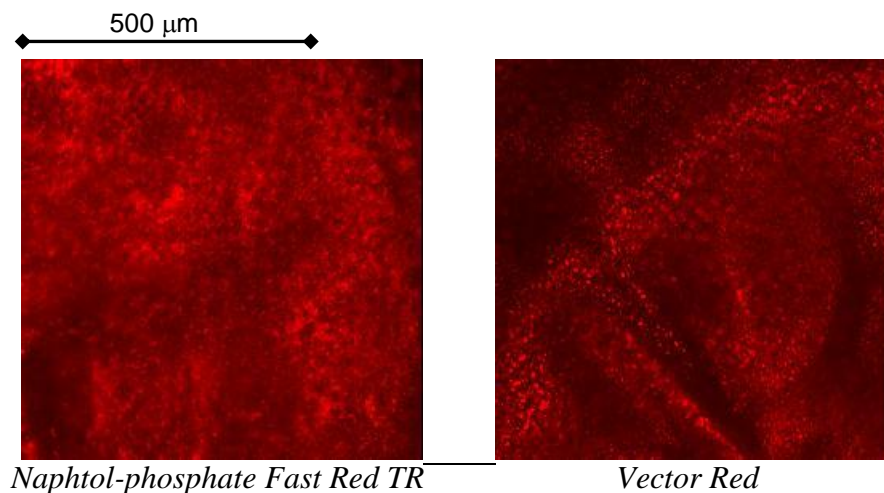*Naphtol-phosphate Fast Red TR*   *Vector Red*

Figure 12.3: Naphtol-phosphate Fast Red and Vector Red substrates for alkaline phosphatase linked enzymatic fluorescence detection.

A Vector Red Alkaline Phosphatase substrate kit (Vector Labs) was prepared according to manufacturer's instructions, while a different "Alkaline Phosphatase Fast Red" substrate was prepared according to Speel *et al.* [128]. The Fast Red technique employs a Naphol-ASMX-phosphate substrate along with a Fast Red TR diazonium salt as a trapping agent. Substrates were tested on a glass surface and both were found to yield a red fluorescent precipitate with broad emission spectra when incubated with Alkaline Phosphatase (Figure 12.3).

Because the rate of fluorescence production was higher with the AP Fast Red substrate, this reagent was electrophoretically introduced on-chip to assess its turnover rate and local precipitation characteristics. Photo-immobilized plugs of alkaline phosphatase with concentrations ranging from 10 pM - 10 nM (assuming 1% BP-PA gel capture) were used for faster screening (Figure 12.4).
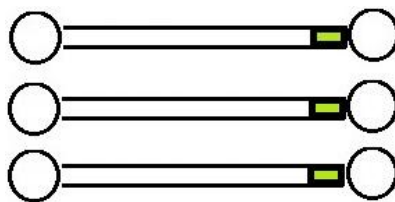
Figure 12.4: Photo-immobilized enzyme plugs for fluorescence substrate screening experiments.

AP-Fast Red substrate was contained at the left reservoir and a driving electric field was established from left to right at 300 V/cm for 8 minutes. Scans were performed at 1 minute intervals across a total time span of 16 minutes. However – no red precipitate crystallization could be observed at any AP concentration < 1 nM. This result suggests that the Naphol-ASMX-phosphate substrate might not be charged, despite its phosphate group, or that the local buffer conditions may not be conducive to crystal formation.

The 10 nM channels were able to generate localized soluble fluorescence activity at the AP plug – which could only be observed at the UV wavelength (shown below). This result did not occur at AP concentrations ≤ 1 nM.
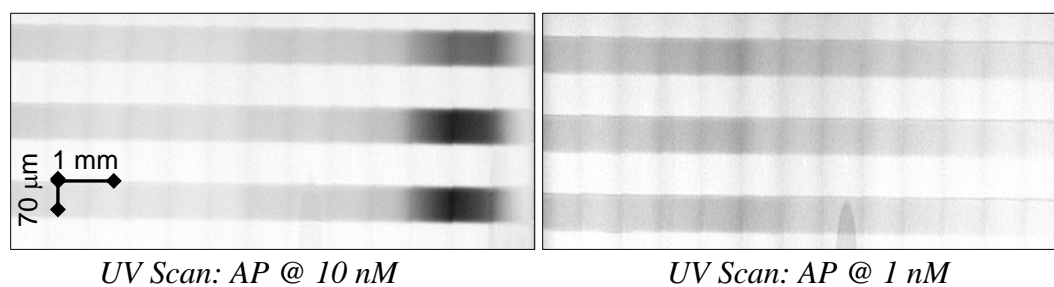

UV Scan: AP @ 10 nM   *UV Scan: AP @ 1 nM*

Figure 12.5: Fluorescent product visualization using a Fast Red substrate across alkaline phosphatase gel plugs at 1 and 10 nM.

Appendix C: pH Gradient Compression

pI Marker Distribution: Ionic Concentration Dependence

When lysates from Santa Cruz Biotechnology were assayed at two different concentrations, the 5× and the 10× dilutions resulted in different pH gradient distributions:
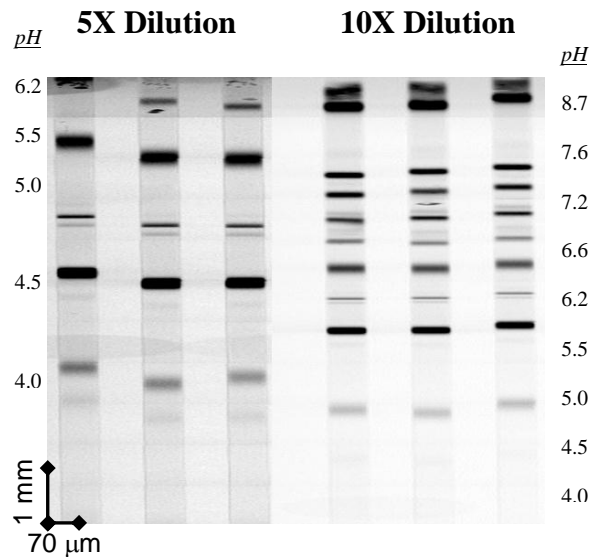

Figure 12.6: Varying sample dilution ratios can result in differences in isoelectric point distribution.

In the case of the lower dilution factor (Figure 12.6, left), the pI ladder is heavily skewed towards the cathodic end, with a maximum pH of 6.2 at the upper limit of the gradient. When the dilution factor is increased to 10×, the gradient is well spaced, ranging from pH 4 to pH 9 with a skew that is still towards the cathode, but less prominent. These tests were performed on the same chip, in the same day using identical gel and buffer solutions. Results demonstrate that sample concentration can have a dramatic result upon pH gradient distribution. The Santa Cruz lysate comes in a RIPA buffer which contains 50 mM NaCl. It is hypothesized that differences in ionic strength

between the 5× and 10× dilutions are reflected in an increased degree of cathodic drift for high conductivity samples.

A different batch of 293T lysate from Santa Cruz biotechnology was evaluated within the BP-PA isoelectric focusing gel format. This new aliquot of lysate was special-ordered within a buffer containing no NaCl. Unlike previous experiments with lysates from Santa Cruz, this sample did not affect the distribution of the pI ladder. The behavior can be attributed to the low salt content – which results in rapid antibody introduction and allows us to utilize a higher sample concentration in the loading buffer.

Alternative Ampholyte Systems for Modified pH Gradient Distribution

IEF reagents were assembled with modified ampholyte and anolyte solutions to generate a pH gradient ranging from 3-7. Results from ladder focusing are illustrated below using identical imaging conditions:

Modified pH Gradient 3-7

4.0   4.5   5.0   5.5   6.2 6.6

Typical pH Gradient 3-10
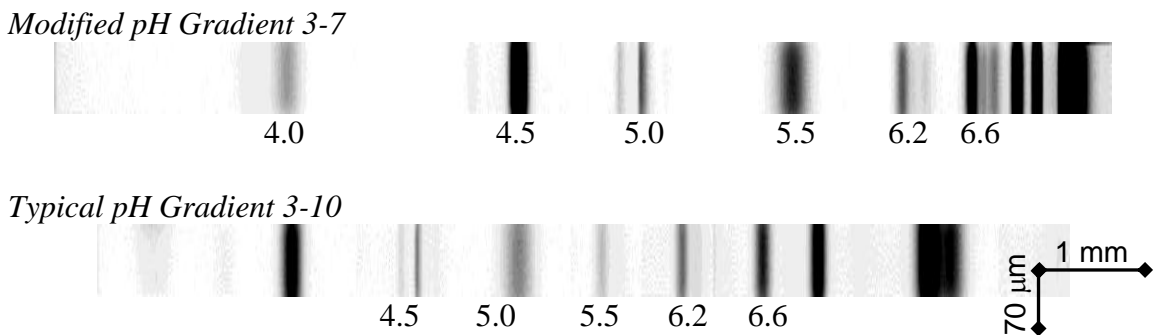

4.5   5.0   5.5   6.2   6.6

Figure 12.7: Altering the composition of the ampholytes used in IEF gel buffers will result in spatial variations in isoelectric point distribution.

In the modified pH gradient, basic ladder components of pI > 7 are pushed out towards the cathodic periphery of the channel. The pI 4.0 marker is visible in the modified gradient while this cannot be seen in the ladder below it. Based upon the broader distribution, the pH 3-7 gradient is able to generate an average improvement in separation resolution of 24% for analytes whose isoelectric point is located between *pH* 3 and pH 7.

Appendix D: MATLAB Code for 1D Electrophoretic Blotting Simulation

```matlab
clear all
close all

% band properties
n=161  %INPUT: # segments in the band - MUST BE AN ODD NUMBER
sig=80 %INPUT: width protein band (gauss distribution, units = um)
bw= 4*sig; % full bandwidth = 4*sigma (units = um)

% migration properties
uepcm=6.63e-5;  % INPUT: EP mobility of antigen (units = cm^2 / V*s)
E=50;           % INPUT: field strength (units: V/cm)
uocm= uepcm*E;  % calculate migration speed (units: cm/s)
uo= uocm * 1e4; % convert speed to microns/sec

% gel properties
gw=335     %INPUT: gel width (units = microns)
dx= bw/n  % specify segment width: defined by the band(units = microns)
dt=dx/uo; % calculate step time (units = sec)

p=floor(gw/dx) % specify number of gel segments
ttotal=dt*p    % calculate total time of binding assay

bm = 1.6e-6;  %INPUT: no. of binding sites (units = M)

co = zeros(n,1);   % initial concentration distribution
bo = ones(p,1)*bm; % define initial gel array
so = zeros(n,1);   % define spatial distribution array
% values of initial protein sample band, units = microns)

bmid = ceil(n/2);  % define central band element
% the spatial array is symmetric w.r.t. band center
for i=1:bmid-1
    so(bmid-i)=i*dx;
    so(bmid+i)=so(bmid-i);
end

% define initial concentration distribution
for i=1:n
    co(i)=c(so(i),sig);
end

nosteps = n + p; % calculate total number of reaction steps
nopos = 2*n + p; % calculate the total # of positions in band array
cband = zeros (nopos, nosteps); % define band array
bgel = zeros (p, nosteps);      % define gel array
bbound=zeros(p,nosteps);        % array describing # of bound molecules

bgel(:,1)=bm; % set binding sites in the gel to initial bmgel value

% define initial band distribution
for i=1:n
```

```matlab
cband(i,1)=co(i);
end

% bind migration through blotting gel
for j=2:nosteps

if j<=p+1 % if the band has not yet reached the end of the gel

    for i=2:n % band that hasn't entered the gel just moves along
    cband(i,j)=cband(i-1,j-1);
    end

    for i=n+1:n+p % binding within gel
    dc=lang(cband(i-1,j-1),bgel(i-n,j-1),bm,dt);
    cband(i,j)=cband(i-1,j-1)-dc;
    bgel(i-n,j)=bgel(i-n,j-1)-dc;
    bbound(i-n,j)=bm-bgel(i-n,j);

     if bgel(i-n,j)<0 % check physical limits
     bgel(i-n,j)=0;
     bbound(i-n,j)=bm-bgel(i-n,j);
     end

    end

else % j>p+1% the band has started to move out of the gel

    for i=2:n % band that hasn't entered the gel
    cband(i,j)=cband(i-1,j-1);
    end

    for i=n+1:n+p % band within the gel
    dc=lang(cband(i-1,j-1),bgel(i-n,j-1),bm,dt);
    cband(i,j)=cband(i-1,j-1)-dc;
    bgel(i-n,j)=bgel(i-n,j-1)-dc;
    bbound(i-n,j)=bm-bgel(i-n,j);

     if bgel(i-n,j)<0 % check physical limits
     bgel(i-n,j)=0;
     bbound(i-n,j)=bm-bgel(i-n,j);
     end

    end

    for i=n+p+1:nopos% band out of gel
    cband(i,j)=cband(i-1,j-1);
    end

end

end

efficiency=1-(sum(cband(:,j))/sum(cband(:,1))) %capture efficiency
sumband = sum(cband(:,1))
```

```matlab
kon = 5.75e5;
da=(gw*kon*bm)/uo % report Da number


function [cvalue] = c(y,t)
% inputs: y = position (units = microns), t = time (units = sec)
% output: concentration value

n=900; % number of molecules
D=40; %units = um^2 / sec

cvalue=(n/(4*pi*D*t)^0.5)*exp(-(y^2)/(4*D*t));


function [dc] = lang(c,b,bm,dt)

% accepts three inputs:
% c = free antigen concentration from the band element (units = M)
% b = free binding site concentration at the gel element (units = M)
% bm = original binding site concentration (units = M)
% dt = time step (units = sec)

% specify on and off rates
kon = 1.8e6; % on rate [units = (M*s)^-1]
koff = 1e-1; % off rate [units = s^-1]

dcdt = kon*c*b - koff*(bm-b); % bm-b = # bound complexes per unit time

dc = dcdt*dt; % calculate total # of bound complexes
```

Publishing Agreement

It is the policy of the University to encourage the distribution of all theses, dissertations, and manuscripts. Copies of all UCSF theses, dissertations, and manuscripts will be routed to the library via the Graduate Division. The library will make all theses, dissertations, and manuscripts accessible to the public and will preserve these to the best of their abilities, in perpetuity.

I hereby grant permission to the Graduate Division of the University of California, San Francisco to release copies of my thesis, dissertation, or manuscript to the Campus Library to provide access and preservation, in whole or in part, in perpetuity.

_____   1/9/13
Author Signature   Date

(This page must be signed and dated by the author and include the correct pagination – as the last numbered page number of your document.)

185